Two decades of Martini: Better beads, broader scope

Siewert Marrink, Luca Monticelli, Manuel Melo, Riccardo Alessandri, D. Peter Tieleman, Paulo Souza

▶ **To cite this version:**

Siewert Marrink, Luca Monticelli, Manuel Melo, Riccardo Alessandri, D. Peter Tieleman, et al.. Two decades of Martini: Better beads, broader scope. WIREs Computational Molecular Science, 2022, 10.1002/wcms.1620 . hal-03864638

HAL Id: hal-03864638
https://cnrs.hal.science/hal-03864638

Submitted on 24 Nov 2022

HAL is a multi-disciplinary open access archive for the deposit and dissemination of scientific research documents, whether they are published or not. The documents may come from teaching and research institutions in France or abroad, or from public or private research centers.

L'archive ouverte pluridisciplinaire **HAL**, est destinée au dépôt et à la diffusion de documents scientifiques de niveau recherche, publiés ou non, émanant des établissements d'enseignement et de recherche français ou étrangers, des laboratoires publics ou privés.

Check for updates

Received: 16 February 2022 | Revised: 15 April 2022 | Accepted: 19 April 2022

DOI: 10.1002/wcms.1620

ADVANCED REVIEW

WIREs COMPUTATIONAL MOLECULAR SCIENCE WILEY

Two decades of Martini: Better beads, broader scope

Siewert J. Marrink[1] | **Luca Monticelli**[2] | **Manuel N. Melo**[3] | **Riccardo Alessandri**[4] | **D. Peter Tieleman**[5] | **Paulo C. T. Souza**[2]

[1]Groningen Biomolecular Sciences and Biotechnology Institute & Zernike Institute for Advanced Materials, University of Groningen, Groningen, The Netherlands

[2]Molecular Microbiology and Structural Biochemistry (MMSB - UMR 5086), CNRS & University of Lyon, Lyon, France

[3]Instituto de Tecnologia Química e Biológica António Xavier, Universidade Nova de Lisboa, Oeiras, Portugal

[4]Pritzker School of Molecular Engineering, University of Chicago, Chicago, Illinois, USA

[5]Centre for Molecular Simulation and Department of Biological Sciences, University of Calgary, Alberta, Canada

Correspondence
Siewert J. Marrink, Groningen Biomolecular Sciences and Biotechnology Institute & Zernike Institute for Advanced Materials, University of Groningen, Nijenborgh 7, Groningen, 9747 AG, The Netherlands.
Email: s.j.marrink@rug.nl

Edited by: Modesto Orozco, Associate Editor and Peter R. Schreiner, Editor-in-Chief

Abstract

The Martini model, a coarse-grained force field for molecular dynamics simulations, has been around for nearly two decades. Originally developed for lipid-based systems by the groups of Marrink and Tieleman, the Martini model has over the years been extended as a community effort to the current level of a general-purpose force field. Apart from the obvious benefit of a reduction in computational cost, the popularity of the model is largely due to the systematic yet intuitive building-block approach that underlies the model, as well as the open nature of the development and its continuous validation. The easy implementation in the widely used Gromacs software suite has also been instrumental. Since its conception in 2002, the Martini model underwent a gradual refinement of the bead interactions and a widening scope of applications. In this review, we look back at this development, culminating with the release of the Martini 3 version in 2021. The power of the model is illustrated with key examples of recent important findings in biological and material sciences enabled with Martini, as well as examples from areas where coarse-grained resolution is essential, namely high-throughput applications, systems with large complexity, and simulations approaching the scale of whole cells.

This article is categorized under:

Software > Molecular Modeling

Molecular and Statistical Mechanics > Molecular Dynamics and Monte-Carlo Methods

Structure and Mechanism > Computational Materials Science

Structure and Mechanism > Computational Biochemistry and Biophysics

KEYWORDS

coarse graining, Martini force field, molecular dynamics

1 | INTRODUCTION

The need to reduce the level of detail in the description of a system of interacting particles, that is, to coarse-grain (CG), dates back to the very beginning of the field of molecular dynamics (MD) simulations. The first protein models in the

This is an open access article under the terms of the Creative Commons Attribution License, which permits use, distribution and reproduction in any medium, provided the original work is properly cited.
© 2022 The Authors. *WIREs Computational Molecular Science* published by Wiley Periodicals LLC.

17590884, 0, Downloaded from https://wires.onlinelibrary.wiley.com/doi/10.1002/wcms.1620 by Cochrane France, Wiley Online Library on [24/11/2022]. See the Terms and Conditions (https://onlinelibrary.wiley.com/terms-and-conditions) on Wiley Online Library for rules of use; OA articles are governed by the applicable Creative Commons License

70s represented each residue with two particles located on Cα and the center of the side chain, a simplification necessary to enable pioneering simulations of protein dynamics.[1] Similarly, simulations of polymers relied on CG representations, going back to the freely jointed chain models of Binder and coworkers in the early 80s.[2] With increasing computational power and software optimization, more detailed all-atom simulations became the standard in the field of biomolecular simulations during the 80s and 90s. However, the hope that, with a continuing increase in capacity, all processes could be captured with such detailed models turned out to be idle. Even today, with access to exascale computing power, all-atom simulations are still limited to spatiotemporal scales less than 100 nm and typically covering few microseconds.[3–5] Considering the gap with processes in real life, the need for a CG description is still as urgent as in the early days.[5–11] The requirement of more sampling speed became (re)apparent in the late 90s, and caused a surge in the development of numerous enhanced sampling methods as well as the re-valuation of the principle of coarse-graining. In this context, the Martini model was conceptualized and evolved over the years to the current "Martinidome" (Figure 1).

The major assumption underlying the Martini model is that small chemical fragments can be represented by specific CG bead types (the building blocks), irrespective of the molecule to which the fragment belongs, and independent of the state conditions. The interactions between the different bead types are modeled with Lennard–Jones (LJ) potentials, calibrated with experimental thermodynamic data, such as partitioning free energies, as major target. Effective bonded interactions are obtained through optimization of bond distributions with respect to all-atom simulations. The Martini

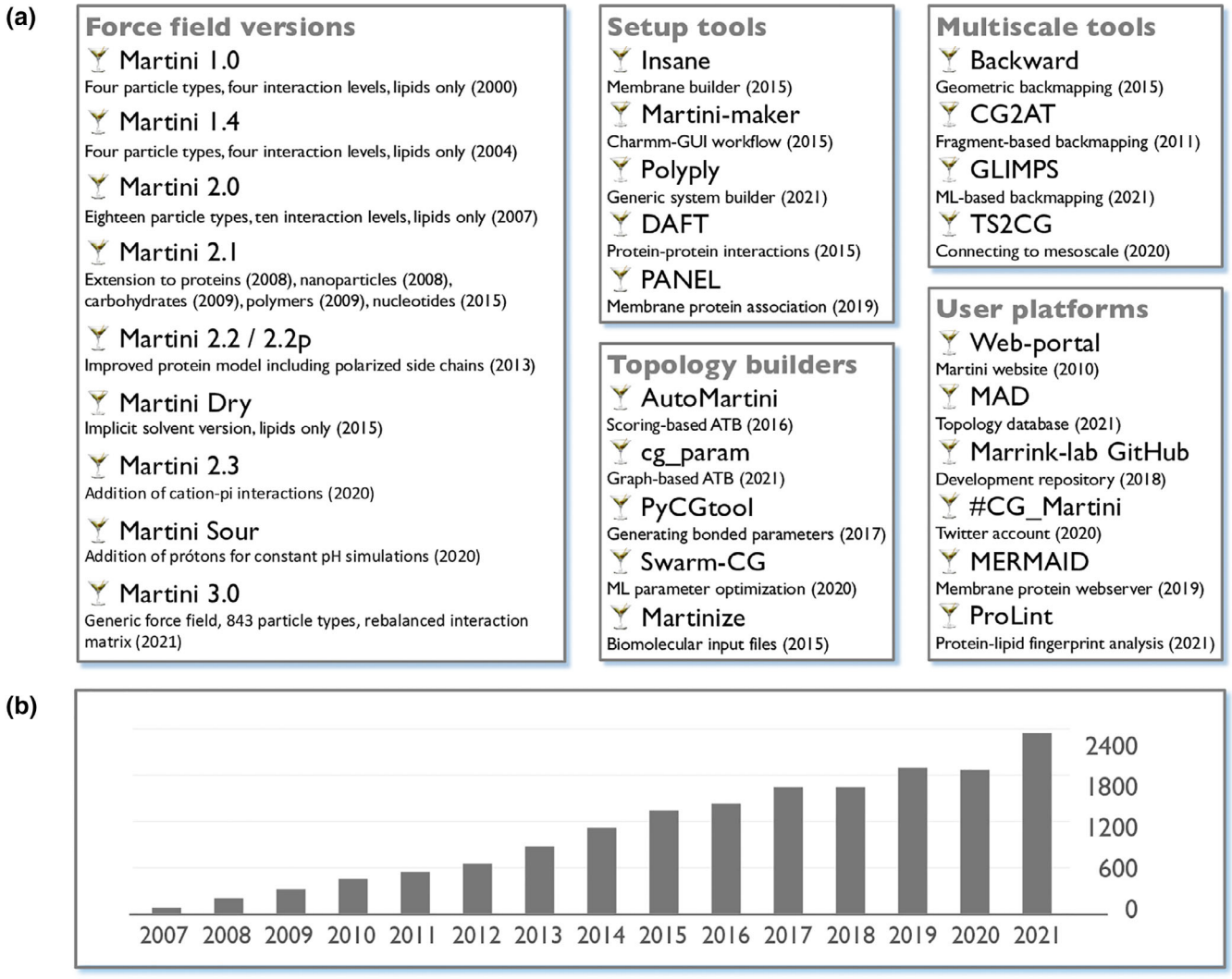

FIGURE 1 Historical overview of the Martinidome. (a) The different force field versions are listed in the leftmost box, a selection of popular auxiliary tools for the setup of starting structures, building of topologies, converting to other resolutions, and user platforms are shown in the other boxes. (b) Growing citation numbers for the basic Martini papers, taken from the Martini google scholar profile.[26]

17590884, 0, Downloaded from https://wires.onlinelibrary.wiley.com/doi/10.1002/wcms.1620 by Cochrane France, Wiley Online Library on [24/11/2022]. See the Terms and Conditions (https://onlinelibrary.wiley.com/terms-and-conditions) on Wiley Online Library for rules of use; OA articles are governed by the applicable Creative Commons License

model thus combines top-down and bottom-up parameterization strategies. It is important to realize this coarse-graining philosophy of the Martini model is shared with other CG force fields (e.g., SPICA[12,13] and SIRAH[14,15]), but is distinctly different from bottom-up models that aim at reproducing structural features of higher resolution models with high accuracy.[16,17] The Martini model, in being a generic force field, also sets itself apart from CG models that are dedicated to specific (bio)molecular classes (e.g., oxDNA,[18] UNRES[19]), or to coarser (supra-CG) models that do not aim to capture chemical specificity. Despite the more limited structural accuracy of Martini models as compared to structure-based CG models, the model compatibility provided by Martini allows for complex systems to be set up more easily. Moreover, structure-based CG models often require complex potential forms for nonbonded interactions, which may result in lower computational performance than LJ-based CG models. With respect to supra-CG models, the fact that they represent effectively all chemical species as beads connected by springs makes them suitable to describe a wide range of physics, but much less suitable to describe specific chemical systems. Hence, Martini has an edge with respect to coarser CG models when aiming to simulate systems that require chemically specific predictive CG modeling.

Looking back over the past two decades, we have seen many exciting developments around the Martini force field, which has slowly matured during these years. Remarkably, different communities appreciate the model for different reasons: Biologists use it to study cellular processes at length and time scales inaccessible with all-atom models[20,21]; Chemists appreciate the building-block principle and use Martini to cover the vast chemical space in high-throughput applications in material science[22]; Physicists take the opportunity to test predictions based on mean-field assumptions and other mesoscale models with a molecularly detailed model,[23] and finally, nonscientists use Martini for illustrative purposes in education[24] and even as a basis for creation of art objects.[25] The still increasing citation numbers (Fig 1b) are further proof of the high demand for a CG model such as Martini in modern integrative research.

The remainder of this review is structured as follows. In the next section, we provide a historical overview of the major developments underlying the Martinidome. Subsequently, we review the latest Martini 3 model, highlighting the major strategic choices underlying the model as well as current best practices of using it. Then, we provide key examples from the recent literature to illustrate the use of Martini, divided into six categories that benefit from the power of Martini: (i) applications in the field of biophysics and structural biology, (ii) applications in the bio–nano interface, (iii) applications in materials sciences, (iv) high-throughput applications, (v) systems with high complexity, and (vi) applications connecting to the full-cell scale.

2 | A BRIEF HISTORY OF MARTINI

In this section, we will guide the reader through a historical perspective on Martini, from the very first lipid models to the current Martinidome, depicted in Figure 1.

2.1 | Lipids only

Originally, the Martini force field was developed to simulate lipid systems only. A prototype model (version 1.0) was ready in 2002, now 20 years ago, and applied to simulate lipid vesicle formation and fusion,[27,28] something that was not feasible with atomistic resolution at the time. The completed version of the first Martini model, version 1.4, was published in 2004,[29] building on pioneering work from Smit et al.[30,31] and the group of Lipowsky,[32,33] who already showed that simplistic CG models of surfactants and lipids can be used to simulate their self-assembly into a variety of aggregation states. However, contrary to these models which are physics based, expressed in reduced units, the Martini model is a chemistry-based model with CG beads representing chemical fragments with realistic units of size and energy.

In this first model, four different bead types were considered to distinguish between apolar, intermediately polar, polar, and charged fragments. The basic idea, which was also adopted by the Klein group around the same time to model surfactant systems,[34] was to use Lennard–Jones potentials to capture the effective nonbonded interactions between CG beads, calibrated to reproduce thermodynamic data, together with standard harmonic bonded potentials parametrized to match the conformational flexibility of reference atomistic simulations. This basic underlying philosophy combining top-down and bottom-up approaches has not changed. Using this concept, the Martini model mapped to real lipids, and was able to distinguish, for example, saturated lipids from unsaturated ones, and a phosphatidylcholine (PC) from a phosphatidyl-ethanolamine (PE) headgroup, with structural and thermodynamic membrane properties "semi-quantitatively" matching experimental data. Note that, from the very beginning, the Martini model used a

17590884, 0, Downloaded from https://wires.onlinelibrary.wiley.com/doi/10.1002/wcms.1620 by Cochrane France, Wiley Online Library on [24/11/2022]. See the Terms and Conditions (https://onlinelibrary.wiley.com/terms-and-conditions) on Wiley Online Library for rules of use; OA articles are governed by the applicable Creative Commons License

screened Coulombic potential to capture the interaction between charged particles, including those of zwitterionic lipid heads.

In 2007, the name Martini was coined for version 2.0.[35] The model was still limited to lipid-based systems, but with the increased number of bead types (18) and interaction levels, many more lipids could be realistically represented. Labels were introduced to differentiate between hydrogen bond donor and acceptor groups. This more sophisticated version allowed further pioneering studies, for instance on membranes showing liquid-ordered/liquid-disordered coexistence.[36] More recently, the lipid model has also been reparametrized as an implicit solvent model, appropriately called Dry Martini,[37] and coupled to either stochastic rotational dynamics[38] or lattice Boltzmann[39] to capture hydrodynamics. In the meantime, the Martini 2 lipid library has been steadily increasing, with CG models generated for different classes of more specialized lipids, including glycolipids,[40,41] cardiolipins,[42] polymer-modified lipids,[43,44] lipopolysaccharides,[45–47] sterols, and hopanoids.[48]

2.2 | Extensions to other (bio)molecules

With the apparent success of Martini to simulate lipid dynamics, the natural next step was to extend the force field toward (membrane) proteins, resulting in version 2.1 in 2008,[49] which was later improved to version 2.2 in 2013.[50] To model peptides and proteins we faced an obvious limitation of the use of isotropic beads: capturing the directionality of H-bonds, and hence protein folding, would be out of scope. To keep the secondary structural elements in place, specific bonded parameters were calibrated for helices, β-strands, coil, turns, and bends.[49,50] Additionally, an elastic network approach, coined "ElNeDyn," was introduced to keep tertiary structures folded and stable in relation to a specific reference structure.[51] Early successes of the Martini protein model included the oligomerization of G-protein-coupled receptors (GPCRs), showing a membrane-thickness depending aggregation propensity in accordance with experimental data,[52] and the tension-induced gating of the mechanosensitive channel of large conductance (MscL).[53] Note that the groups of Sansom and Schulten developed their own initial protein models compatible with Martini.[54,55]

Extension of the model to other major classes of biomolecules followed over the years: carbohydrates in 2009,[56] DNA in 2015,[57] and RNA in 2017.[58] More specific biomolecules were also added to the Martini library, such as protein posttranslational modifications[59,60] and a variety of cofactors and metabolites.[61,62] In the meantime, Martini had found its first applications outside the field of biomolecular sciences, with models for polymers (PEG) dating back to 2009,[63] and nanoparticles (fullerenes) in 2008.[64] One of the strengths of Martini is that, due to the building block approach, Martini models can be combined allowing researchers from the very beginning to study how different classes of biomolecules interact with each other, and with other materials. A pioneering example is the solvation of fullerenes in a lipid membrane environment.[64]

2.3 | Polarizable versions and other developments

With the increasing number of applications, also shortcomings of the model became apparent. A number of those are inherent to the process of coarse-graining, such as entropy/enthalpy compensation which affects the temperature dependency, the lack of directionality of H-bonds limiting simulations of protein conformational changes or nucleotide hybridization, and the interpretation of the timescale which is nontrivial as a consequence of the nonhomogeneously smoothened potential energy surface on which the CG dynamics take place.[65,66] Another limiting issue is the accuracy of the electrostatic interactions. Although Martini features charged bead types, and may even be used together with common approaches to include the long-range forces such as Particle Mesh Ewald summation, the major problem is due to the lack of nuclear polarizability of Martini water. In standard Martini, water is modeled as an uncharged bead representing four real water molecules, incapable of performing the electrostatic screening of the real solvent. The screening in Martini is represented implicitly, in a distant-dependent manner using a combination of a dielectric constant of 15 and a shifted electrostatic potential.

To improve on this aspect, multipolar and polarizable versions of Martini water[67,68] and polarizable ions[69] have been developed. In addition, a polarized version of the protein force field was parameterized (version 2.2p) to better capture the interactions between charged amino acids.[50] Polarized Martini beads also found their way into other models; in particular, they are proving helpful to stabilize supramolecular polymers.[70,71] Cation-pi interactions were

17590884, 0, Downloaded from https://wires.onlinelibrary.wiley.com/doi/10.1002/wcms.1620 by Cochrane France, Wiley Online Library on [24/11/2022]. See the Terms and Conditions (https://onlinelibrary.wiley.com/terms-and-conditions) on Wiley Online Library for rules of use; OA articles are governed by the applicable Creative Commons License

further added to the mix in version 2.3, released in 2020.[72] Improvements were also achieved in terms of computational speed, through optimization of the use of cutoffs and GPUs.[73] Most recently, a constant pH version of Martini, "Martini-sour", was developed, featuring explicit proton-mimicking beads.[74,75]

2.4 | The road toward Martini 3

Despite the gradual maturation of the Martini force field, and the increasing awareness of the intrinsic limitations to CGing in general,[17,76,77] it became clear that another, more specific problem was haunting the model. Several research groups reported on the apparent overstabilization of biomolecular interactions, noted for soluble[78] and membrane proteins,[79,80] as well as carbohydrates.[41,60,81] This shortcoming became known as the stickiness problem. Ad-hoc remedies included downscaling of solute–solute or upscaling solute–solvent interactions, but the underlying cause of the stickiness problem could be traced back to the imbalance between the small and regular bead types, in combination with the use of weak bond force constants or bonds between beads that were too short in the description of biomolecules.[82]

The stickiness problem, together with the demand for higher chemical resolution has prompted the development of the recently released Martini 3 version,[83] featuring more than 800 bead types and a thoroughly recalibrated interaction matrix. It has now reached a level of what can be called a "generic" force field, applicable to a wide range of problems, not only in biomolecular simulation but also increasingly in materials science,[22] at par with well-known generic all-atom force fields such as CHARMM[84] and Amber.[85] The expanded set of bead types of Martini 3 already has enabled a further extension of the model into the areas of, for example, green solvents (ionic liquids,[86,87] deep eutectic solvents[88]), coacervates,[89] and intrinsically disordered proteins (IDPs).[90]

2.5 | Associated tools

In connection to the actual Martini force field, we, and many others, have developed a wide range of tools to facilitate setting up, running, and analyzing MD simulations with this model (Figure 1). Examples include the widely used tools insane[91] and CHARMM-GUI Martini-maker[92,93] to build multicomponent lipid-based systems, tools to facilitate high-throughput sampling of protein–protein interactions such as DAFT[94] or PANEL,[95] the MERMAID tool[96,97] to help setting up and analyzing membrane proteins, the martinize tool to build Martini topologies from biomolecular structural data,[50] polyply, a python script to build complex starting structures involving arbitrary (bio)polymers,[98] and the Nanodisc Builder, to construct starting structures for protein–lipid nanodiscs.[99]

Another category of auxiliary tools consists of automatic topology builders, ideally converting a simple smiles string into a complete Martini topology file. Some of these focus on generating bonded potentials, such as the pyCGtool[100] and Swarm-CG,[101] whereas others target the challenge of mapping an underlying chemical structure to its CG Martini representation like autoMartini[102] and the graph-based cg_param algorithm.[103] Recently, the multi-objective based Swarm-CG algorithm has also been used as a tool to improve the nonbonded interactions of Martini lipids.[104]

Dedicated analysis tools include Prolint[105] and PyLipID[106] for identifying and analyzing protein–lipid interactions, MemSurfer[107] to define and analyze membrane surfaces, MDVoxelSegmentation[108] for automated lipid leaflet detection, cgHeliParm[109] to analyze CG DNA, a tool based on machine learning to identify membrane domains called NMFk,[110] a tool to directly calculate SAXS spectra from Martini simulations,[111] a tool to analyze the aggregation state of self-assembling systems (MorphoScanner[112]), and a tool to analyze diffusion on curved surfaces (CurD[113]).

Furthermore, many enhanced sampling strategies have been optimized for Martini, including metadynamics,[114,115] temperature replica-exchange,[116] replica-exchange umbrella sampling,[117] ensemble-based CGMD,[118] Monte-Carlo enhanced MD,[119] iMapD,[120] AI-driven transition path sampling,[121] and Markov state models (MSM).[122,123] Also worth mentioning is the recent use of Martini in guiding genetic algorithms for inverse design problems (evo-MD).[124]

2.6 | Multiscale options

The Martini force field has been interfaced with higher or lower resolution models in a variety of multiscale setups (Figure 2). In sequential multiscaling, CG systems are back mapped to all-atom resolution, often used as a validation

17590884, 0, Downloaded from https://wires.onlinelibrary.wiley.com/doi/10.1002/wcms.1620 by Cochrane France, Wiley Online Library on [24/11/2022]. See the Terms and Conditions (https://onlinelibrary.wiley.com/terms-and-conditions) on Wiley Online Library for rules of use; OA articles are governed by the applicable Creative Commons License

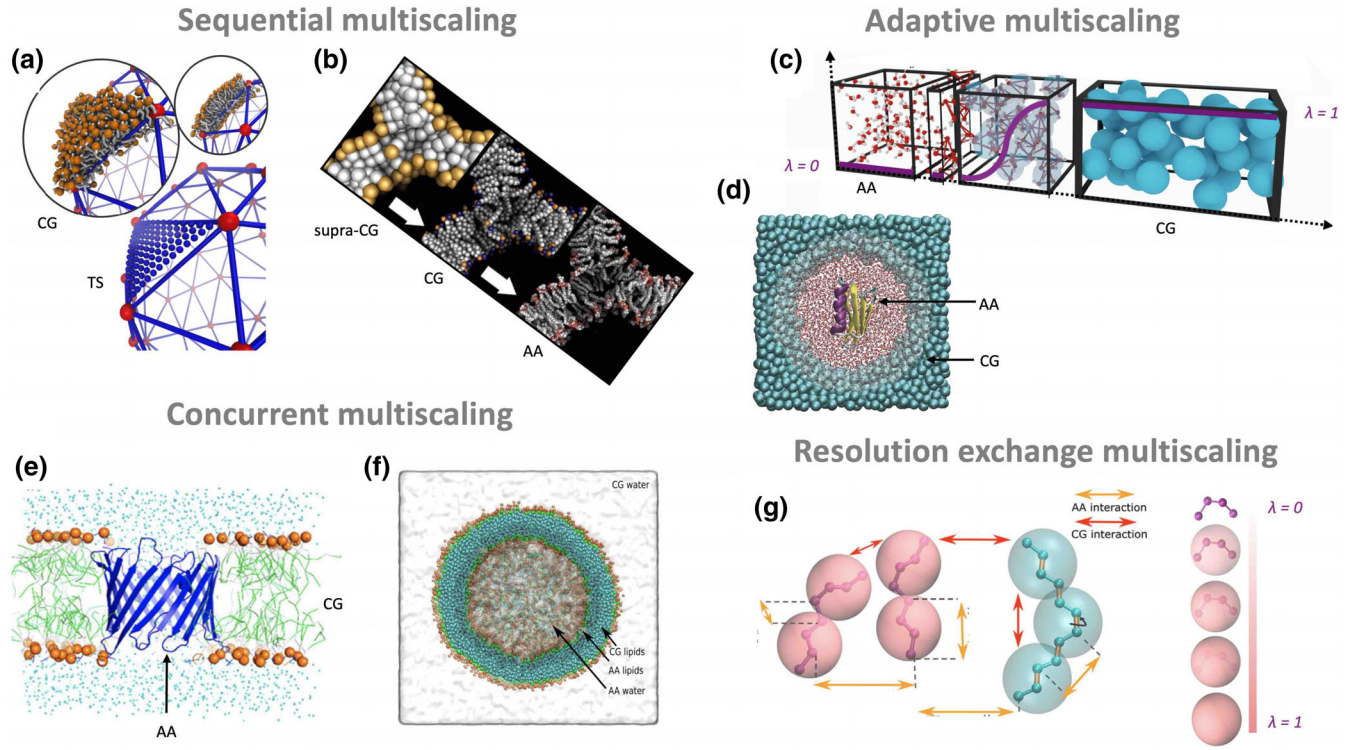

FIGURE 2 Selected Martini multiscale options. (a) Transformation from triangulated surfaces with TS2CG, adapted with permission from Pezeshkian et al.[130] Copyright 2020 Springer Nature. (b) Backmapping from supra CG and to all-atom with insane, adapted with permission from Wassenaar et al.[125] Copyright 2014 ACS. (c) Adaptive resolution setup for water using SWINGER, adapted with permission from Zavadlav et al.[143] Copyright 2019 RSC. (d) Adaptive resolution setup for an all-atom protein in a CG environment, reprinted with permission from Zavadlav et al.[142] Copyright 2014 AIP. (e) Concurrent CG/AA membrane protein systems using the PACE cross-interactions, taken from Qi et al.[138] (f) Concurrent CG/AA lipid vesicle using virtual sites, taken from Liu et al.[133] (g) Resolution exchange protocol for coupling AA and CG resolution, adapted from Liu et al.[145]

test assessing whether or not certain CG configurations remain stable when simulated with a higher resolution force field, or, to obtain more detailed local structural information. Sometimes CG simulations with Martini are only used as an intermediate step during system relaxation, which can be more difficult when directly performed at the all-atom level (e.g., to equilibrate the packing of lipids around a membrane protein). Also, in these cases, a backmapping step is required after the initial equilibration phase. Backmapping can be done in different ways, either using a geometric approach (e.g. with the backward tool[125]), or a fragment-based approach (using CG2AT[126,127]), or more recently with a machine learning-based approach (GLIMPS[128]). At the other end, Martini has been recently connected to mesoscale membrane models with the TS2CG tool, allowing backmapping from triangulated surfaces to the CG level.[129,130]

In concurrent multiscaling approaches, the system is partly described at the all-atom level and partially with Martini. In a typical setup, the region of interest is described in atomistic detail, and the surrounding solvent at the CG level, potentially combining accuracy with speed although often resulting in being neither accurate nor fast. The challenge lies in how the two force fields are combined. This can be achieved with the use of virtual sites,[131–133] or making use of explicit cross-parameterization as is done in the PACE force field[134–138] or in the work of the Jorgensen group, mixing all atom solutes and polarizable Martini water.[139] In principle such a concurrent multiscale setup can be extended to more resolution levels, as was nicely demonstrated in a triple layer QM/MM/Martini simulation.[140] Coupling to a continuum solvent has also been realized.[141]

A third multiscale approach is the use of adaptive resolution schemes, in which the resolution of compounds can change on the fly. Here the main challenge is to define a transition zone that facilitates the change in resolution in a thermodynamically consistent way. Pioneering efforts in this direction, featuring Martini as the CG force field, have been reported for a number of model systems.[142,143] Using such an adaptive resolution scheme, Martini can also be efficiently interfaced with continuum solvent models allowing volume changes on the fly.[144] A connected multiscale approach is that of resolution exchange, a version of Hamiltonian replica exchange coupling parallel simulations

17590884, 0, Downloaded from https://wires.onlinelibrary.wiley.com/doi/10.1002/wcms.1620 by Cochrane France, Wiley Online Library on [24/11/2022]. See the Terms and Conditions (https://onlinelibrary.wiley.com/terms-and-conditions) on Wiley Online Library for rules of use; OA articles are governed by the applicable Creative Commons License

running at different resolutions. Until now, we are aware of only few attempts to use the Martini model in such a setup.[145–147]

2.7 | Open science policy

Following the philosophy of the late Prof. Berendsen to keep things pragmatic and share developments among colleagues,[148] we maintain an active forum and organize regular workshops and tutorials.[149–154] The policy of sharing of data, often preliminary models (beta-versions), has helped in popularizing Martini, and provided valuable feedback from the community to the main developers. The Martini web portal (http://cgmartini.nl/)[149] plays a central role in this respect, with currently >6000 registered users. A Martini twitter account (@CG_Martini) was established in 2020 to further expand the communication options. Currently, we are in the process of establishing a Martini database (MAD, https://mad.ibcp.fr/),[155] which will serve the need for a well-documented repository of both validated and developmental Martini topologies across the molecular sciences.

Due to its popularity, Martini has been implemented not only in its traditional host Gromacs,[156] but also in other software packages including NAMD,[157] LAMMPS,[158] ddcMD,[159] openMM,[160] CEMD,[161,162] Materials Studio,[163] and Genesis.[164] In addition, the Martini force field is integrated into the HADDOCK workflow.[165–167] Note, however, that for the implementations outside Gromacs it is not always clear which version of Martini is available, and the full range of options might not be supported.

3 | MARTINI 3

In this section, we review the novel aspects of Martini 3 compared to the previous versions, including strategic choices made for the parametrization of new beads and improvements of the interaction matrix, improved treatment of proteins, and guidelines for the best practices for Martini 3 simulations.

3.1 | Strategic choices for the bead parametrization

Given the demand for beads that provide broader and more accurate coverage of chemical space[168] and a clear understanding of the stickiness problem,[82] Martini 3[83] adopted a different strategy for the parametrization of its beads compared to previous versions. Overall, the iterative approach did not use a rigorous separation of calibration and validation tests (Figure 3a). In addition, more experimental targets and a large set of simulation systems of different complexity were used for the parametrization of the Lennard–Jones pair interactions. This strategy was fundamentally different from Martini 2, which mainly used liquid–liquid partitioning and simple systems represented by isolated beads for the main calibration step.[35] As Martini is based on pair interactions, additional target systems, and properties helped version 3 to cover more points in the extensive interaction matrix and to prevent possible overestimation of interaction strength involving systems with two or more connected beads.

The first step of this iterative process was to delineate the "Martini universe," which did not only involve defining the number of generic chemical types and sizes of the model, but also a better definition of mapping choices, interaction levels, and bead assignments. For instance, small and tiny beads were not only considered suited to ring-like compounds as in Martini 2, but were redefined here to be also useful for 3-to-1 and 2-to-1 mapping of linear and branched chemical groups.[83] In addition, both self- and cross-interactions of different bead sizes were included as parameters to be calibrated Another novelty was the introduction of the "size-shape concept," which improves the volume and shape of coarse-grained models of molecules compared to their atomistic references (Figure 3b).[83,169] This approach requires the definition of consistent mapping rules for the selection of bead sizes and for the calculation of bond lengths between beads. Together with strategic parametrization choices, the new Martini 3 model presents a fully revised interaction matrix and new intermediate interaction levels, added to smoothen the transition between different chemical types. Additional improvements came from the separation of pair interactions into organic, ions, organic–ion, and water blocks, which were optimized independently. In particular, this approach allowed significant improvements for water, which in Martini 3 has its own bead type (W) and specific interaction levels.[83]

17590884, 0, Downloaded from https://wires.onlinelibrary.wiley.com/doi/10.1002/wcms.1620 by Cochrane France, Wiley Online Library on [24/11/2022]. See the Terms and Conditions (https://onlinelibrary.wiley.com/terms-and-conditions) on Wiley Online Library for rules of use; OA articles are governed by the applicable Creative Commons License

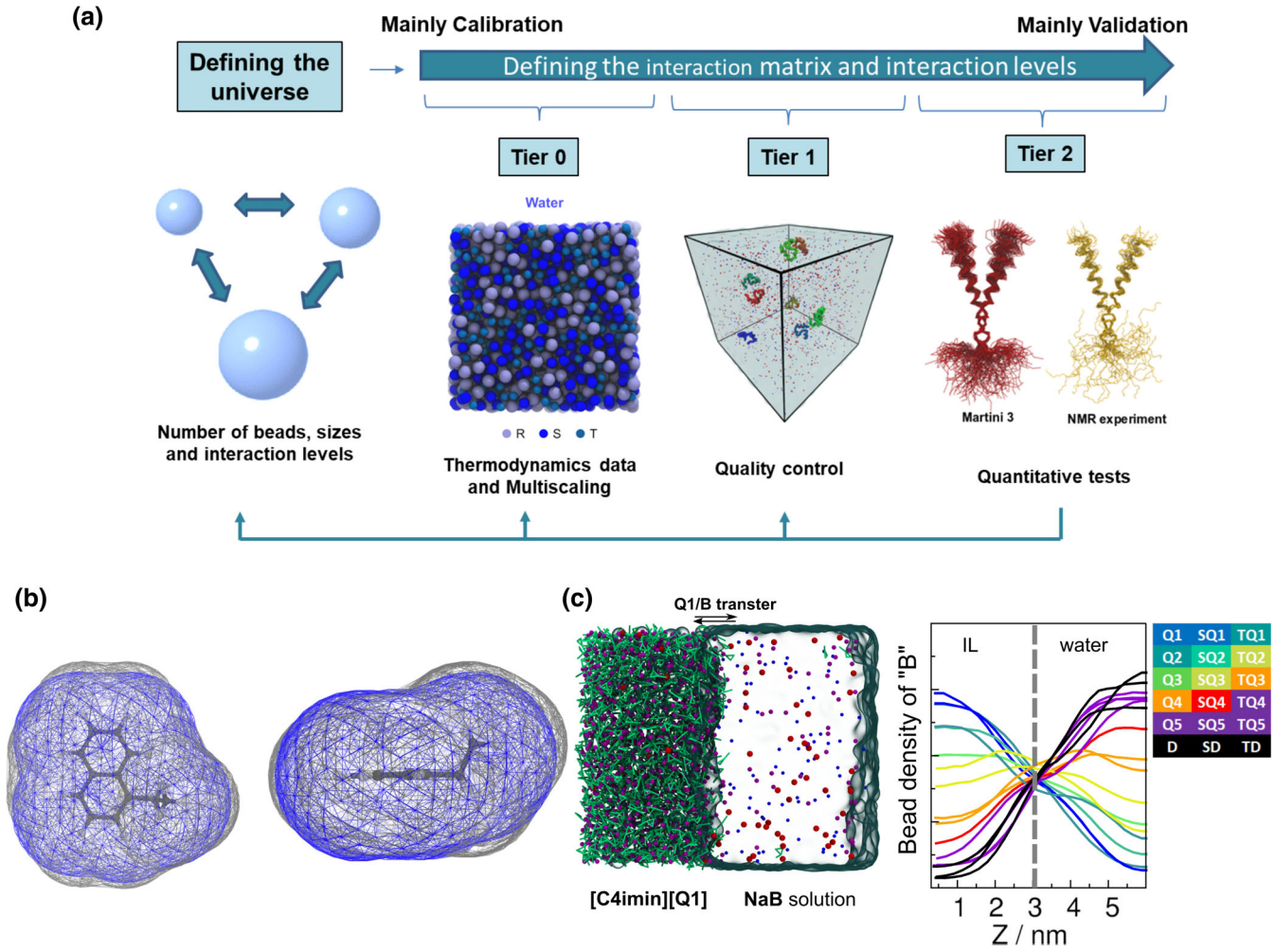

FIGURE 3 Some strategic parametrization choices of Martini 3. (a) The iterative parametrization approach used in Martini 3 for calibration and validation of the bead pair interactions. (b) The "size-shape concept" is illustrated by the comparison of the Connolly surfaces of 1-ethylnaphthalene at the atomistic (gray) and coarse-grained (blue) resolutions. (c) Charged Q beads in Martini 3 follow the classical Hofmeister series, as exemplified by the B^- anion transfer between aqueous solutions and imidazolium-based ionic liquids. (a), (b), and (c) adapted with permission from Souza et al.[83] Copyright 2021, Springer Nature.

With a defined Martini universe, the parametrization strategy was divided into "tiers", which represented systems and target properties with different level of complexity. Tier 0 contained simple molecules (with 1 or more connected beads) and many thermodynamic reference data that were used mainly for calibration of Lennard–Jones parameters. In addition to the liquid–liquid partitioning, miscibility was used as one of the main parametrization targets, allowing to probe at the same time self- and cross-interaction between the two molecular species. In addition, the balance of different bead sizes in this tier was intended to be multiresolution, with ideal mixing behavior[170] of pure solvents composed of molecules mapped at different bead sizes. Excess free energies of mixing and trends in liquid–liquid interfacial tension, densities, and solvation-free energies were also used in this tier. Different classes of molecules used complementary targets for the parametrization. For instance, calibration of charged systems also relied on ion transfer properties between ionic liquids and aqueous salt solution, which can be considered analogs to liquid–liquid partitioning used for neutral molecules. Trends according to Hofmeister series[171,172] were also considered (Figure 3c). Additionally, specific systems such as metal ions, charged amino acids, and simple sugars used osmotic pressures as a reference, which is a target previously used for ad hoc rescaling corrections applied in Martini 2.[60,78,81]

In the intermediate tier 1, tests formulated as "yes-or-no" questions were used to evaluate the quality of the model, with parameters not covered in tier 0 also tested and fine-tuned here. Properties of more complex systems such as soluble proteins, sugars, and bilayers were tested to detect possible emerging artifacts at a larger structural scale than in tier 0. Examples of "yes-or-no" questions were simple self-assembly MD simulations, indicating if certain lipids could or not

17590884, 0, Downloaded from https://wires.onlinelibrary.wiley.com/doi/10.1002/wcms.1620 by Cochrane France, Wiley Online Library on [24/11/2022]. See the Terms and Conditions (https://onlinelibrary.wiley.com/terms-and-conditions) on Wiley Online Library for rules of use; OA articles are governed by the applicable Creative Commons License

form bilayers or if soluble proteins and sugars mainly stay in the monomeric form at low concentrations instead of forming a unique phase-separated aggregate. Additional systems including peripheral membrane proteins, protein nanopores, transmembrane proteins, ionic liquids, and other soft materials were included in these quality control tests as well.[83] In the final tier 2, quantitative tests involving complex systems were performed, including comparisons with experimental or atomistic simulation data. Here most of the systems were considered for validation, and many comparisons involving dimerization free energies were used, including systems such as aedamers (a biomimetic molecular system useful to study folding and self-assembly), nucleobases, and transmembrane helices. At every point that one of these tests failed, initial choices were reconsidered in an iterative process, including the definition of the initial Martini universe of beads.

3.2 | Improved interactions and better coverage of the chemical space

As a result of the parametrization, Martini 3 showed many improvements, in particular for systems which heavily rely on smaller beads, such as aromatic and aliphatic rings or branched fragments.[83,169] Liquid–liquid partitioning involving water/hexadecane, water/chloroform, and water/octanol biphasic systems showed a mean absolute error compared to experimental data of around 2–3 kJ/mol (Figure 4a).[83,169] At the same time, liquid–liquid mixing behavior was captured accurately, from common solvents[83,169] (Figure 4b) to complex mixtures involving small conjugated molecules,[173] coacervates,[89] ionic liquids,[86] and deep eutectic solvents.[88] As a direct consequence of the improved calibration of the

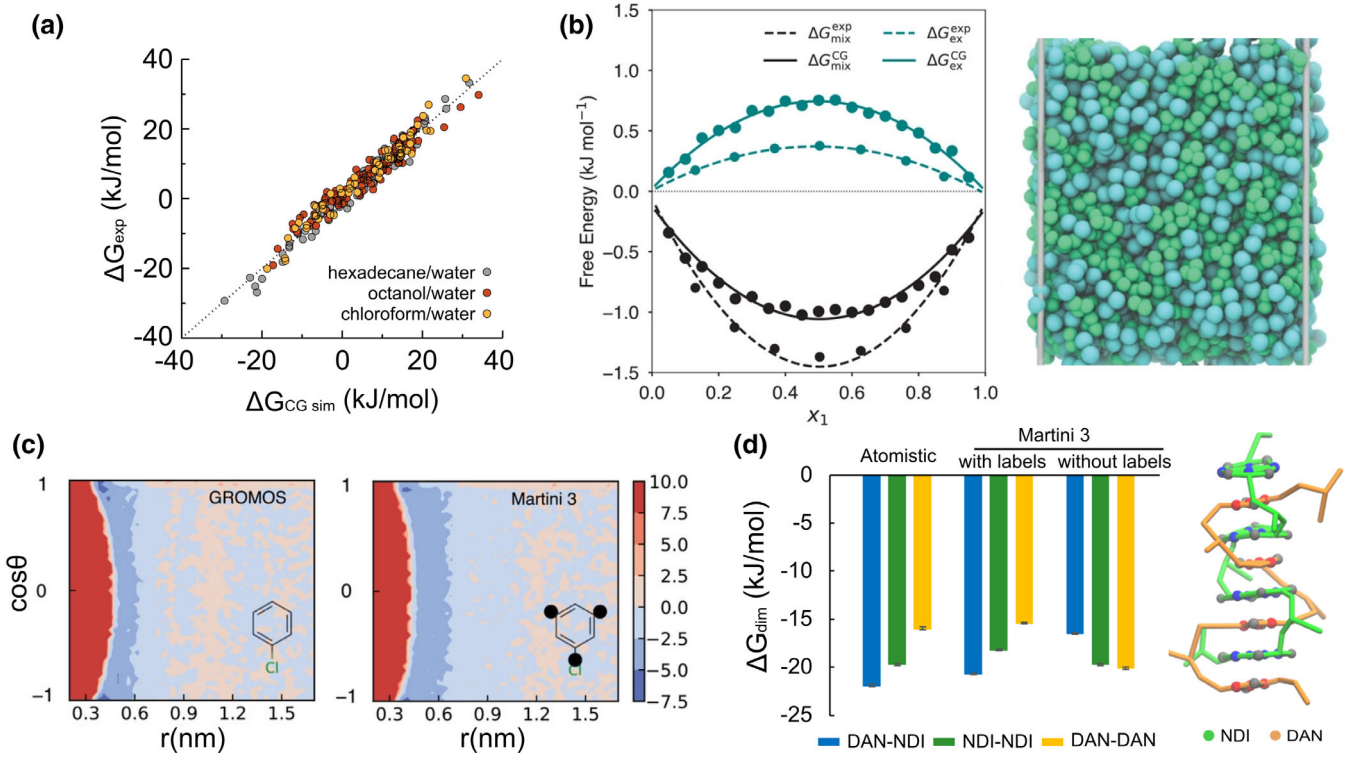

FIGURE 4 Examples of Martini 3 with improved interactions and use of labels. (a) Water–oil transfer free energies (ΔG) were computed for around 260 data points using Martini 3. The plot includes data used for calibration and validation of the Martini 3 beads. (b) Comparison between Martini and experimental free energy of mixing (ΔG_{mix}) and excess free energy of mixing (ΔG_{ex}) for the benzene–cyclohexane mixture as a function of the mixture composition. $\times 1$ is the molar fraction of benzene. The analogous Martini 2 system forms a biphasic system at the same condition. (c) The dimerization free energy surface of chlorobenzene is plotted on the 2D coordinate space formed by the distance between the center of geometries of the two molecules and $\cos\theta$, where θ is the angle between the two vectors perpendicular to the planes of the two molecules. The profiles are obtained with GROMOS (left panel) and Martini 3 (right panel). (d) Self-assembly of aedamers. The left panel shows the dimerization free energies (ΔG_{dim}) of pegylated monomers of DAN and NDI. The right panel shows the self-assembled duplex dimer formed by amide-linked tetramers of NDI (green) and DAN (orange). (a) and (d) Adapted with permission from Souza et al.[83] Copyright 2021, Springer Nature. (b) and (c) Adapted with permission from Alessandri et al.[169]

17590884, 0, Downloaded from https://wires.onlinelibrary.wiley.com/doi/10.1002/wcms.1620 by Cochrane France, Wiley Online Library on [24/11/2022]. See the Terms and Conditions (https://onlinelibrary.wiley.com/terms-and-conditions) on Wiley Online Library for rules of use; OA articles are governed by the applicable Creative Commons License

cross-interactions between the different bead sizes, large dimerization dissociation barrier artifacts between cyclic molecules previously observed in Martini 2 no longer exist.[83,169] Free energy surfaces of dimerization for many aromatic compounds in water were improved, with Martini 3 showing better agreement than the Martini 2 version in terms of depth and position of minima using atomistic force fields as reference (Figure 4c).[169] Similar improvements in nucleobase stacking and packing of poly(3-hexyl-thiophene) in bulk heterojunction solar cells were also observed.[83] However, inaccuracy in packing and binding modes may still be in place, given the directionality limitations of the bead interactions. For instance, similarly to H-bonds, T-shaped stacking interactions are also not captured by standard Martini models, including version 3, due to the lack of specific quadripolar electrostatic interactions.[169]

In combination with the improvements in the interactions of all bead sizes, Martini 3 showed a substantial increase in the number of chemical bead types, which are separated into seven classes: polar (P), intermediately polar (N), apolar (C), halo-compounds (X), monovalent ions (Q), divalent ions (D), and water (W).[83] W and D are classes composed of a special and dedicated bead type, while the other classes show more diversity of options. The main classes of the organic blocks—P, N, and C—are composed of six bead types with different degree of polarity, enabling a more precise definition of different chemical groups compared to the previous version. In particular, the N class was greatly expanded in relation to Martini 2, allowing differentiation of different chemical groups in the most populated region of the chemical space—as observed by Kanekal and Bereau[168]—with compounds that have octanol–water partitioning free energies between -5 and $+5$ kJ/mol. In addition to the expansion of the number of levels representing N beads, Martini 3 introduced a new X class dedicated to model halo-compounds. This approach was necessary because the self-interactions of halo-compounds follow the opposite trends with increasing polarity when compared with typical apolar compounds (represented by the C and part of the N bead types). In analogy with the N class, Q beads were also expanded, allowing the separation of soft hydrophobic-like monovalent ions (e.g., tetrafluoroborate, BF_4^-) from the hard hydrophilic-like ones (e.g., formate, COO^-). Among new applications of the charged beads, the new Martini 3 models of phosphoinositides stand out, as they were able to reproduce experimentally known protein-binding poses as well as phosphoinositide aggregation tendencies in the presence of calcium ions, the latter modeled with D-beads.[174]

In addition to the new bead definitions, Martini 3 enhanced the ability to modify bead properties depending on the chemical details of the underlying moieties. These modifications are controlled via labels, added as subscripts to the bead chemical types. This concept already existed in the previous versions of Martini[29,35] but was only used to account for different hydrogen bonding capabilities of N and Q beads. In Martini 3, the label concept was generalized and can be applied to all beads. Labels slightly change the properties of the beads they are attached to, causing small changes in the interaction matrix in a bead-size dependent way.[83] Three of these labels (hydrogen bonding, electron polarizability, and positive/negative) are chemically specific, which means they are only applied to certain chemical types.[83] Hydrogen bonding labels (applied to P and N classes) are sufficient to reproduce trends in nucleobase pairing selectivity, while electronic polarizability labels (used in C and X classes) allow for specific and strong stacking between electron-donor and electron-acceptor aromatic rings in aedamers (Figure 4d). The other two labels (self-interaction, partial charge) of Martini 3 are more generic, and can be applied on top of all beads of the organic block, including beads that have already been modified with some of the chemically specific labels. Partial charge labels, which are useful for large charged molecules represented by more than one bead, have been used for the modeling of ionic liquids[86,87] and deep eutectic solvents.[88] Together, all combinations of sizes, chemical types, and labels give a total of 843 bead types, which correspond to about 15 times more options than in the previous version of Martini. A recent application of the new bead types by Yu and Wilson[175] to model self-assembling dyes showed their promise: the Martini 3 models outperformed CG models based on a force-matching approach.

3.3 | The differences and improvements of protein models in Martini 3

Currently, proteins are possibly the system with the most obvious improvements in Martini 3. One of the key differences in the Martini 3 protein model compared to the previous version is the total reparametrization of the side-chains. In Martini 2.2, the side chains are considered "overmapped", with on average too few atoms incorporated in a Martini bead. In Martini 3, the new mapping avoids the use of regular size beads for fragments containing less than four non-hydrogen atoms. The packing of aromatic residues also greatly improved with the use of "tiny" beads, the smallest Martini 3 bead size. Although most of the remaining bonded parameters were not changed compared to Martini 2, additional improvements were obtained by side-chain corrections,[176] which are dihedral terms involving side-chain and backbone beads based on experimental reference structures. A final improvement was a new definition of

17590884, 0, Downloaded from https://wires.onlinelibrary.wiley.com/doi/10.1002/wcms.1620 by Cochrane France, Wiley Online Library on [24/11/2022]. See the Terms and Conditions (https://onlinelibrary.wiley.com/terms-and-conditions) on Wiley Online Library for rules of use; OA articles are governed by the applicable Creative Commons License

backbone bead types, which no longer depend on the secondary structure. They are now represented by P2 beads, except for proline (SP1a), alanine (SP2, with an additional bead for the side chain), and glycine (SP1). These are the beads which best represent the liquid–liquid partitioning of the secondary amides in the protein backbone of these residues. As an alternative to ElneDyn,[51] Martini 3 proteins can also be combined with Gō-like models,[177–179] which can greatly improve the representation of protein flexibility. In fact, the recent implementation of GōMartini via virtual particles marked a milestone, showing the use of Martini 3 to study long-range structural communication and allosteric changes caused by single-point mutations.[180]

After the release of the open-beta version, Martini 3 has been evaluated in many protein systems and properties, including peripheral membrane proteins, protein flexibility, protein–small molecule and protein–protein interactions. The group of Vanni demonstrated that the model is mostly able to accurately characterize the membrane-binding behavior of peripheral proteins, identifying key residues found to affect membrane binding.[181,182] As a result of the improvements in packing and interactions in Martini 3, binding of small molecules to protein pockets was successfully reproduced for a variety of systems such as GPCRs, nuclear receptors, and kinases.[183] More of these results are discussed in Section 4.4 of this review. Using parallel tempering metadynamics simulations, the group of Cournia[181] indicated a possible underestimation of the dimerization binding strength for the open-beta release of Martini 3 proteins in solution, while it performs well in describing the association of transmembrane (TM) proteins. Spurious supramolecular protein aggregation, observed in Martini 2.2P, no longer occurs, with near-native dimer complexes identified as minima in the free energy surfaces.[181] As of the time of writing this review, only TM peptides and IDPs have been evaluated with the final release of Martini 3. The dimerization of helical single-pass TM peptides showed high accuracy in predicting binding affinities[83] and dimerization binding modes.[184] The Lindorff–Larsen group tested Martini 3 for IDPs and found that Martini 3 underestimates the global dimensions of IDPs when compared with experimental small-angle x-ray data.[90] IDPs were not considered as part of the calibration and validation tests in Martini 3, explaining this discrepancy. A possible remedy, that would not affect the overall balance of interactions, is to increase the hydration strength of the peptide backbone in disordered regions using virtual sites.

3.4 | Best practices and tips

All the improvements incorporated in Martini 3 are only useful if the force field is properly used by the modeling community. Therefore, in this subsection, we summarize key advice and best practices to parametrize new molecules and run simulations with the new version of Martini. Overall, the molecular dynamics settings for Martini 3 simulations follow the "new" Martini set of parameters proposed by De Jong et al.[73] The default time step is 20 fs. A reaction field should be used as standard option for electrostatic interactions. However, the model was also systematically tested with Particle Mesh Ewald (PME). The use of PME showed some improvements for highly charged systems,[86,88] although with significantly reduced computational performance, in particular, due to the reduced computational scaling over processors. With the ongoing development of a polarizable water model compatible with Martini 3, we expect further benefits in modeling accurate electrostatic interactions. Special attention should also be paid to CG models with highly coupled constraints. As an example, these are present in the current cholesterol topology, which contains two obtuse triangles sharing an edge.[48] This configuration can lead to nonconverged constraints, which cause artificial temperature gradients.[185] For such systems, a more conservative set of LINCS settings is recommended.[185] Lastly, the regular size water bead is the standard option to model liquid water in Martini 3. Although small and tiny water beads were calibrated to have near-to-ideal miscibility between all water bead sizes and also to reproduce the hydration free energies of neutral beads solvated in regular water beads,[83] their use and transferability in different systems should be tested and verified by the user with caution. Small and tiny W-bead sizes are currently recommended only for certain applications, such as the modeling of water in protein pockets or channels where regular water beads would not fit.[183] A small fraction of small or tiny water beads could be added to the solution to fill these pockets. Such an approach can potentially improve the small molecule binding to the pockets of certain proteins.

The parametrization of new Martini models has a well-defined set of rules in version 3, which should be followed to build high-quality models and maintain internal consistency with other Martini 3 molecules. A quick guide for unexperienced users is described as follows.

(1) Mapping of the atomistic model to the CG model: Split the molecule in reasonable chemical groups (the building blocks) in accordance with the standard Martini bead sizes: regular (4-atoms-to-1-bead), small (3-atoms-to-1-bead), and

17590884, 0, Downloaded from https://wires.onlinelibrary.wiley.com/doi/10.1002/wcms.1620 by Cochrane France, Wiley Online Library on [24/11/2022]. See the Terms and Conditions (https://onlinelibrary.wiley.com/terms-and-conditions) on Wiley Online Library for rules of use; OA articles are governed by the applicable Creative Commons License

tiny (2-atoms-to-1-bead). A higher resolution (smaller bead size) allows for a better reproduction of symmetry and chemical details, while larger bead sizes result in simpler models which are more computationally efficient. In terms of volume and shape criteria, tiny beads are the preferred option for aromatic rings, while small beads are preferred for aliphatic rings. If a molecule contains highly branched groups, halo compounds, and/or charged fragments, consult section C1 of the supplementary information of the Martini 3 paper.[83]

(2) Assignment of chemical bead types: According to the chemical group underlying the bead, the user should select a fragment according to the "Martini Bible" (supplementary tables 24 and 25 of the Martini 3 paper[83] or table 1 of the Martini 3 Small Molecule paper[169]). If no matching chemical group is available in these resources, a suitable bead type can be selected using the liquid–liquid partitioning data of the isolated fragments (see supplementary tables 17, 18, and 19 of the Martini 3 paper[83]). Sections A4 and C2 of the supplementary information of Souza et al.[83] provide a detailed description of the use of labels.

(3) Bonded parameters, volume, and shape: Bonded parameters can be obtained from atomistic simulation data. Bond distances should be based on the center of geometry of the atoms that are incorporated in a bead, including the underlying hydrogen atoms. This approach showed a good match with molecular volume, surface accessible areas (SASA), and bulk densities.[83,169] Additional fine-tuning can be performed by scaling selected bond lengths as needed to properly match Connolly surfaces and SASA. We recommend the use of Van der Waals radius from the work of Rowald et al.[186] as a reference for the atomistic calculations. In the case of the Martini models, the radius of the CG beads should be used. Appropriate force constants and additional bonded terms such as angles or dihedrals should be calibrated with respect to structural data obtained from either reference atomistic simulations or a structural databank. Note that the bimodality of the distributions of bonds, angles, and asymmetric dihedrals may not be well-captured by Martini given limitations of potentials implemented in Gromacs (or other MD codes), although cosine-based functions such as the Ryckaert–Bellemans potential could be used in certain cases. Section C3 of the supplementary information of the Martini 3 paper provides more details.[83]

(4) Improving numerical stability and performance: Two main factors affect the numerical stability of Martini simulations: (i) the number of bond constraints and the use of virtual particles to manage this number; and (ii) the definition of proper dihedrals and collinear 3-body angles. Virtual sites can be conveniently used to model extended stiff molecular structures, which reduces the number of constraints that these systems would need. This approach not only increases the numerical stability, reducing the risk of nonconverged constraints,[185] but it also improves the computational performance.[169] Traditional proper dihedrals used in atomistic MD simulations may also be a source of instability in CG simulations. This is usually the situation if the three-body angles i–j–k and j–k–l in a dihedral i–j–k–l are near to 0° or 180°, as described in the work of Bulacu et al.[187] One possible solution involves the use of restricted bending potentials (function type 10 in Gromacs[188]). Alternatively, virtual "dummy" sites can be used to redefine the dihedral in a way that collinear three-body angles are avoided.[187] The Martini 3 Small Molecule paper[169] provides additional advanced design strategies involving virtual sites. Additional discussion involving numerical stability issues is also available in section C4 of the supplementary information of the Martini 3 paper.[83]

(5) Generating protein models in Martini 3: The accuracy of Martini 3 proteins depends on the reference atomistic structure chosen by the user to generate the model. This choice has an impact on the assumption of the secondary structure of the protein, which directly determines the backbone bonded parameters, as in the previous Martini 2 version.[49,50] Additionally, the reference structure is also used to define the dihedral side-chain corrections[176] and provides a bias toward certain tertiary structures, which is mainly controlled by the elastic network[51] or the Gō model.[177] Therefore, the users should be careful with choosing the most appropriate reference structure; detailed knowledge of your protein structure and dynamics is recommended. The possibility of issues in the reference, such as structural crystallographic artifacts or missing regions that need to be computationally modeled, should always be double-checked. As in atomistic simulations, protonation states, the presence of cofactors, or posttranslation modifications cannot be ignored, and maybe need to be manually added. Given a high-quality atomistic reference model, the user still should consider fine-tuning the elastic network and/or Gō model, to improve the representation of protein dynamics. For elastic networks combined with Martini 3, initial choices for force constant should be 700 kJ/mol nm^2, with a cutoff between 0.8 and 0.9 nm. The choice for a higher force constant than Martini 2 is related to the differences of the nonbonded interactions of the models and also to avoid possible pitfalls with low force constants.[82] For Gō models, the initial choice of the depth of the potential is 10–12 kJ/mol. Both elastic and Gō models can also have their contact map manually refined in MAD[155] to improve certain aspects of the flexibility. In the current implementation, Martini 3 protein models should not be used in applications that involve large conformations changes as occurring during protein folding.

17590884, 0, Downloaded from https://wires.onlinelibrary.wiley.com/doi/10.1002/wcms.1620 by Cochrane France, Wiley Online Library on [24/11/2022]. See the Terms and Conditions (https://onlinelibrary.wiley.com/terms-and-conditions) on Wiley Online Library for rules of use; OA articles are governed by the applicable Creative Commons License

4 | EXAMPLE APPLICATIONS

In this section, we will highlight the main application areas of Martini, divided into the categories of biological systems (Section 4.1), the bio–nano interface (Section 4.2), and materials science (Section 4.3). We also include dedicated sections illustrating three of the most important reasons to use a CG model such as Martini, namely in high-throughput workflows (Section 4.4), in systems of increasing complexity (Section 4.5), and to bridge detailed models toward the whole cell level (Section 4.6). In each section, we provide key examples of recent work. By no means, we aim to be comprehensive, which would be nearly impossible given the large number of Martini-based publications (Figure 1b). In Table 1, we provide the current "records" in terms of system size, complexity, and time-scale that have been achieved with Martini to date.

4.1 | Biological systems

Martini has historically primarily been used for biological systems, driven by its initial development as a lipid model followed by protein parameters. The lower level of detail and its correspondingly lower computational cost has enabled a range of applications that are still difficult to reach atomistically. It is remarkable how many important biochemical and biophysical problems can be addressed when simulations can routinely reach time scales of tens to hundreds of microseconds and length scales of tens to hundreds of nanometers. Below we highlight a number of biological applications to illustrate the breadth of biophysical and biochemical problems that can be addressed using Martini.

Many early applications of Martini were on the properties of lipid systems. As the time-scale of mixing even in simple binary mixtures is microseconds and goes up dramatically in the presence of domains, atomistic simulations until recently were limited in modeling many aspects of lipid biophysics. With Martini, processes such as domain formation, membrane fusion, lipid phase transitions, and monolayer breakdown came into reach. Comprehensive reviews of membrane simulations, including many of these pioneering Martini-based papers, were published in 2019.[20,193] A more recent development is the modeling of more realistic and complex membranes. A landmark study by Ingolfsson et al. in 2014 described an asymmetric membrane with over 60 lipid types on a time scale of tens of microseconds,[194] still one of the most detailed models of a generic plasma membrane. Subsequent models have targeted specific cells, including specific neuronal,[195] skin,[196] and epithelial cells,[197] as well as bacterial membranes.[198,199] With the growth of lipidomics data,[200] such simulations continue to be of major interest in the studies of membrane structure and increasingly biological function when combined with proteins. Martini allows also to model the properties of lipid mixtures across an entire phase diagram.[201,202] This is both of basic interest and a possible route to improving lipid parameters, although it continues to be a challenge to efficiently calculate phase diagrams for models as detailed as Martini, let alone more detailed atomistic models. A recent atomistic study of just a few phase points highlights the sampling challenges.[203] Note that, as an inherent drawback of CGing, the entropy/enthalpy balance is distorted, implying that one has to be careful in interpreting temperature-dependent phenomena.[66,83]

TABLE 1 Overview of Martini records

Type	Record	Comment	References
Largest number of particles	132 × 10^6 CG beads	Lipid membrane in excess water (420 × 420 × 100 nm box dimensions)	Vogele et al.[189]
Largest system dimension	792 nm	Membranes of an entire mitochondrion (containing 5 × 10^6 lipids)	Pezeshkian et al.[130]
Longest single simulation time	320 μs	Characterization of transmembrane helix association	Pawar et al.[190]
Largest total simulation time	0.2 s	Membrane patches in MuMMI workflow (120,000 simulations of 1–4 μs each)	Ingolfsson et al.[191]
Largest complexity	67 components	Protein embedded in plasma membrane model (1 protein type, 63 lipid types, 2 ion types, water)	Corradi et al.[192]

Note: The interpretation of the timescale in Martini is not well-defined. Due to the missing friction from the atomistic degrees of freedom, the potential energy landscape is smoothened, resulting in an effective speedup. The amount of speedup is, however, system dependent and has been estimated as ranging from a factor of 2–10.[66] So, a 1 microsecond Martini simulation would correspond to a 2–10 microsecond simulation with an all-atom model.

17590884, 0, Downloaded from https://wires.onlinelibrary.wiley.com/doi/10.1002/wcms.1620 by Cochrane France, Wiley Online Library on [24/11/2022]. See the Terms and Conditions (https://onlinelibrary.wiley.com/terms-and-conditions) on Wiley Online Library for rules of use; OA articles are governed by the applicable Creative Commons License

A second major area of applications in biological systems consists of membrane proteins, in particular addressing lipid–protein interactions at different scales. The time scales involved in sampling many types of lipid–protein interactions are tens to hundreds of microseconds,[192,204] readily achievable for Martini simulations. The Martini 2.2 lipidome and lipid–protein interactions have been shown by a large body of work to be quite accurate, as reviewed comprehensively by Corradi et al.[21] These applications also typically do not require an accurate description of internal protein dynamics, and thus make use of elastic networks to keep the protein close to the reference state (usually a crystal structure). In many cases, simulations have identified specific binding sites for key lipids. An early example is the binding of the cardiolipin to respiratory proteins,[205,206] where Martini simulations reproduced known binding sites and predicted additional ones that have been verified experimentally. Other examples include the binding of PIP lipids and cholesterol to Kir potassium channels,[207–209] which are regulated by these lipids, the binding of ceramides to VDAC,[210] and cholesterol binding to GPCRs[211–215] and various transporters.[216] Martini simulations also lend themselves to identifying specific lipids based on low-resolution cryo-EM or crystallography densities of membrane protein structures.[217,218] As the number of cryo-EM structures continues to explode, this is likely to become increasingly useful to identify specific roles for lipids in membrane protein structure and function.

In addition to specific binding sites, simulations have been used to characterize the local lipid environment around membrane proteins, in a long tradition of research on membrane adaptations to proteins; a tradition going back to theoretical models that introduced the mattress model of hydrophobic matching[219] and some of the earliest atomistic membrane protein simulations.[220] Corradi et al. introduced the concept of lipid fingerprints, the unique local environment near a membrane protein induced by lipid–protein and lipid–lipid interactions in a membrane of a complex composition.[192] This has subsequently been investigated for a range of other membrane proteins, including GPCRs,[221] aquaporins,[222] plant light-harvesting complexes,[223,224] mechanosensitive channels,[225] neurotransmitter transporters,[226] and may play an important role in determining membrane organization. The local membrane environment, as exemplified by a growing number of Martini-based simulations, plays a key role in the organization of membrane protein complexes,[137,227–231] binding of peripheral membrane proteins,[232,233] and the equilibrium distribution of membrane protein conformational states.[191,234–237]

In some cases, Martini simulations can also directly provide a link to the mechanism and function of membrane proteins. Recent examples include the lipid scrambling by TMEM16K[238] and the modulation of the hERG potassium channel by ceramides (Figure 5a, left panel), where a combination of Martini, atomistic simulations, and electrophysiology enabled a detailed functional model.[239] Another example is the mechanism of partitioning between raft and nonraft-like domains in membranes depending on the preferential interaction with specific lipids (PIP2[240] or polyunsaturated chains[241]) or on palmitoylation.[240,242] Also, pore formation and translocation of peptides across membranes have been explored in the case of peptides or proteins with stable secondary structures, such as small, highly helical antimicrobial, and cell-penetrating peptides[243,244] or even larger protein toxins.[245] Note that processes such as translocation of polar compounds that require transient pore formation suffers from a significant overestimation of the pore-free energy in the Martini model.[246]

The scale of Martini furthermore enables large-scale simulations of the role of proteins and lipids in membrane remodeling (Figure 5a, right panel). For instance, to identify possible roles for SNARE-family proteins[247–250] in fusion of synaptic vesicles (notably, proteins increase lipid tail protrusion and promote stalk formation), also relevant for viral infection by enveloped viruses like Influenza B.[251,252] Another example is lipid droplet formation, a rapidly growing area in the literature.[253] Early work in this area was published by Khandelia, who showed that triolein phase separates and forms oil lenses in phospholipid bilayer membranes.[254] More recently, the group of Monticelli showed that membrane asymmetry imposes the direction of lipid droplet budding,[255] and suggested that the preference of monotopic membrane proteins for the lipid droplet surface (measured experimentally) may be due to their stronger interaction with triglycerides.[256] Also, Prasanna et al. showed that seipin, an oligomeric ER protein, can trap triglycerides in the ER bilayer via its luminal hydrophobic helices, lowering the nucleation barrier for the initial lens formation (Figure 5b)[257]—a prediction confirmed by simulations with the SPICA coarse-grained force field.[258] In addition, Martini simulations made significant contributions to exploring the roles of proteins and lipids in curvature sensing,[259,260] curvature induction,[261] and membrane deformation.[262,263] For example, the group of Hummer simulated membrane remodeling by FAM134B reticulon homology domain, important in regulating the size, and shape of the endoplasmic reticulum, and by nhTMEM16,[264] a scramblase that dissipates the compositional asymmetry between membrane leaflets, therefore, inducing the conversion of vesicle buds into flat membranes.[265] For more work in this area, see Pezeshkian and Marrink.[266]

A growing number of papers use Martini for other protein-based applications besides the membrane proteins mentioned above. In principle, the sampling power of Martini enables a large number of problems to be addressed, but in practice limitations of Martini 2.2 made the interpretation of some simulations challenging. One example is the

17590884, 0, Downloaded from https://wires.onlinelibrary.wiley.com/doi/10.1002/wcms.1620 by Cochrane France, Wiley Online Library on [24/11/2022]. See the Terms and Conditions (https://onlinelibrary.wiley.com/terms-and-conditions) on Wiley Online Library for rules of use; OA articles are governed by the applicable Creative Commons License

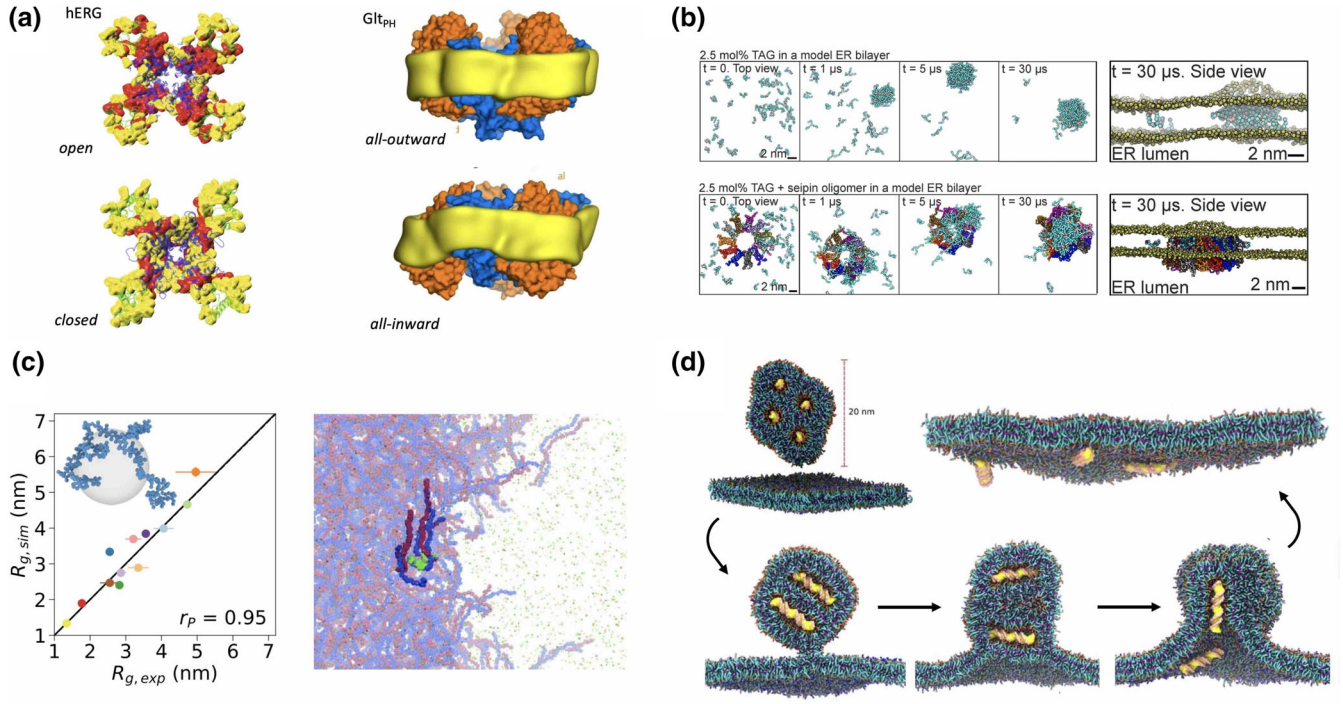

FIGURE 5 Applications of Martini in biology and biophysics. (a) *Left*: Interaction sites between ceramides and the potassium channel hERG identified by Martini simulations depending on the state of the potassium channel. Red and yellow colors indicate stronger and weaker interactions mapped on the structure. Elements of the structure are shown in cartoon representation, purple for the pore domain and green for the voltage-sensor domains. Reproduced with permission from Miranda et al.[239] *Right*: State-dependent remodeling of the local membrane environment by the transporter GltPh. Top panel shows all-outward state, bottom panel all-inward state. The yellow ribbons indicate lipid chain densities. Reproduced with permission from Zhou et al.[262] (b) Recruitment of triacylglycerides (TAGs) by seipin at the initial stages of lipid droplet formation. Taken from Prasanna et al.[257] (c) *Left*: Radius of gyration of an intrinsically disordered protein chain simulated with a Martini 3 beta version. With a proposed correction factor the compactness can match the experimental size quite closely. Reproduced from Thomasen et al.[90] *Right*: Partitioning of single-stranded RNA (green) in a polyLys30/polyGlu30 (blue/red) coacervate phase. Reproduced from Tsanai et al.[89] (d) Key intermediate stages during the lipoplex mediated transfection of dsDNA (yellow/pink) across an endosomal membrane (lipids depicted with gray heads and cyan tails). Taken from Bruininks et al.[271]

simulation of protein solutions, one of the systems Martini 3 parameterization has targeted. In this case, a protein solution now gives the right salt-dependent behavior without ad-hoc adjustments to protein–protein interactions.[267,268] A more elaborate parameterization of protein–protein interactions enables more reliable simulations of complex formation and the free energy of protein–protein interactions.[181] Martini 2 had a limited ability to model small molecules, but Martini 3 has sufficient detail to be used for screening simulations for small molecules binding to proteins.[183,269] Simulations of intrinsically disordered proteins have been challenging for atomistic simulations, in part because force fields had not been fine-tuned to give the correct free energies of solvation for disordered chains[270] and in part because sampling disordered proteins are limited and free energy methods are not readily applicable. A recent paper shows that Martini 3 is a viable method to study IDPs (Figure 5c, left panel), although there is room for improvements that should fit well within the available Martini 3 framework.[90] This opens opportunities for a number of different problems in fluid–fluid phase separation in biological systems. A recent example is the work of Tsanai et al. on the formation of a coacervate phase by polylysine and polyglutamate in solvent and the partitioning of solutes between solvent and coacervate (Figure 5c, right panel).[89] A final application we would like to mention is the use of Martini in integrated modeling approaches. In this case, the physics inherent in the Martini model is one ingredient in more complex calculations that may include a variety of experimental data at different levels of resolution. A very successful example is HADDOCK, developed by the Bonvin group and co-workers, which can incorporate Martini simulations as element in modeling workflows for both protein[166] and protein–DNA complexes.[165]

In this section, we focused on lipids and protein applications, which make up the bulk of the Martini studies in the literature. There have also been interesting recent applications using the nucleic acid parameters, for example, for modeling aspects of drug delivery[196,271] (Figure 5d), nucleosome formation,[272] DNA-scaffolded nanodiscs,[273,274] and

17590884, 0, Downloaded from https://wires.onlinelibrary.wiley.com/doi/10.1002/wcms.1620 by Cochrane France, Wiley Online Library on [24/11/2022]. See the Terms and Conditions (https://onlinelibrary.wiley.com/terms-and-conditions) on Wiley Online Library for rules of use; OA articles are governed by the applicable Creative Commons License

DNA-based nanopores,[275,276] and carbohydrates, in modeling cellulose[277] and glycosylated proteins,[60,278] and development of important biopolymers including peptidoglycans[279] for more realistic simulations of Gram-negative bacterial membranes. We expect such applications to become more prevalent as Martini 3 continues to be developed.

4.2 | The nano–bio interface

Soon after the Martini model was extended to proteins, Martini models for nonbiological materials were developed by different groups, with a particular focus on nano-sized particles. One of the main goals of such models was to characterize the interaction between nonbiological and biological materials, notably model membranes.

Back in 2008, Wong-Ekkabut et al. published the first Martini model of fullerene[64] and characterized the permeation of the nanoparticle through model membranes, as well as its effect on structural, dynamic, and elastic properties of the membrane. Similar models were used around the same time by the group of Sansom to study the interaction of truncated, extremely short carbon nanotubes (CNTs) with lipid membranes, with the aim of exploring the potential use of nano-injectors for the introduction of drugs into cells,[280] and with short peptides, potentially useful for nanotube solubilization.[281] However, it should be noticed that CNTs could not be parameterized based on the experimental partitioning, as normally done within the Martini framework, due to lack of data and major simplifications in the chemistry of the models. The fullerene model, instead, was developed using experimental data on solubility and solid-state properties.[282] The optimized special bead for fullerene was used in subsequent simulations of carbon nanotubes permeation through lipid membranes.[283]

The same optimized fullerene model was also used to answer questions on why lipid membranes are more effective than alkanes at dissolving fullerene aggregates,[284] to explore the interaction of fullerene with monolayer membranes,[285,286] (Figure 6a) and to characterize the size dependence of nanoparticle aggregation in lipid membranes.[287] Models of CNTs were also developed more recently by the group of Hummer, who considered the effect of functional groups at CNT rims, and focused on the interaction of CNTs with lipid membranes in the context of solvent filtration devices.[288] The same group also carried out simulations that enabled an interpretation of cryo-TEM images of CNTs in living cells, suggesting CNT-mediated vesicle fusion (Figure 6c).[289]

Another important nano–bio interface is the one between graphene (and its derivatives) and model membranes. Pioneering work by the group of Kral showed that individual, small graphene sheets can, in principle, be incorporated into the central region of lipid bilayer membranes.[290] Simulations also provided an insight into a possible mechanism of formation of such sandwiched graphene–bilayer system, starting from graphene–POPC micelles.[290] A more recent related study by the group of Reigada suggested that, as previously observed for CNTs, graphene sheets may also promote vesicle fusion, which hints at a possible mechanism of biological activity.[291] Martini models have also been used to simulate the interaction of graphene and graphene oxide with supported lipid bilayers.[292] As expected, the hydrophobic (graphene) or hydrophilic (graphene oxide) nature of the solid support has a major effect on the organization of bilayer membranes, and CG simulations contributed to the interpretation of experimental results.

Besides carbon nanoparticles, during the past decade much work has been devoted to the interaction of metal nanoparticles (NPs) with biological systems, and particularly gold (Au) NPs.[293] Au NPs have numerous applications in biomedicine, as recently highlighted by the development of Au NPs for the detection of SARS-CoV2 infection in antigen tests.[294] Pioneering work on Martini models of Au NPs has been carried out by Lin and Alexander-Katz.[295,296] Lin developed and validated a Martini model of Au NPs coated with alkyl thiol ligands that were hydrophobic, or functionalized with cationic (amino) or anionic (carboxylate) groups.[295] The model was used to study chiefly the interaction of the NPs with model lipid membranes as a function of the chemical nature of the coating ligands.[295] Similar and related questions, regarding the interaction of Au NPs with membranes, were also addressed by a number of other groups (Figure 6b).[296–302] Recent studies tackled more complex questions regarding the NP–membrane interaction. For instance, Rossi et al. used Martini models for Au NPs coated with hydrophobic and anionic ligands to study the effect of NPs on membrane phase separation,[303] the effect of cholesterol on NP passive uptake,[304] and the induction of both positive and negative curvature in liposomes.[305] The effect of phase separation on Au NP–membrane interactions was studied by Van Lehn and coworkers[306] as well as Liang and coworkers.[307] Alexander-Katz considered the synergistic effects of size, surface charge, and ligand chemistry on nanoparticle translocation across membranes,[308] and the effect of applied voltage on the membrane adsorption of cationic nanoparticles was evaluated by Chiarpotti et al.[309] Overall, in these simulation studies, the advantage of the Martini model compared to continuum and all-atom models was clear: continuum models are efficient but lack the level of detail necessary to answer questions related to the effect of specific

17590884, 0, Downloaded from https://wires.onlinelibrary.wiley.com/doi/10.1002/wcms.1620 by Cochrane France, Wiley Online Library on [24/11/2022]. See the Terms and Conditions (https://onlinelibrary.wiley.com/terms-and-conditions) on Wiley Online Library for rules of use; OA articles are governed by the applicable Creative Commons License

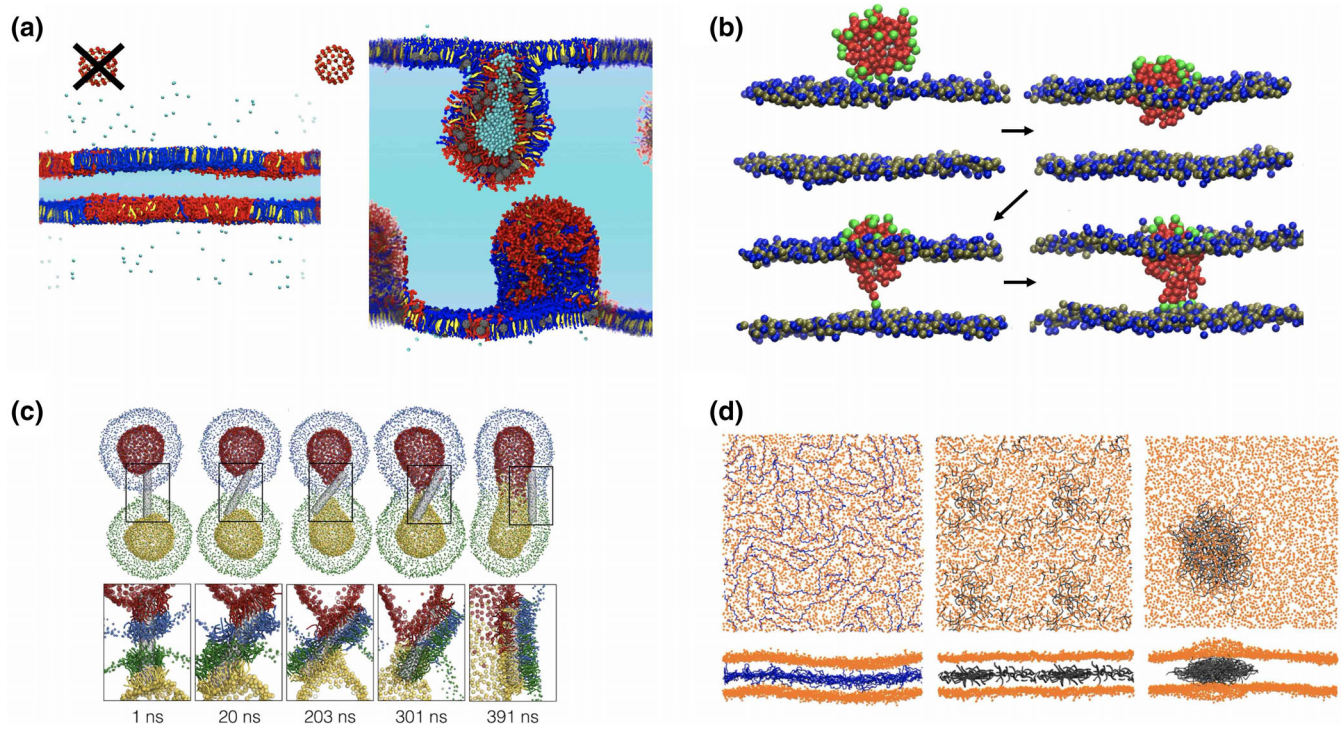

FIGURE 6 Applications in the nano–bio interface (a) fullerene induces collapse of a lipid monolayer consisting of DPPC (green), DOPC (orange), and cholesterol (white) compressed at a surface tension of 10 mN/m. Adapted from Barnoud et al.[285] (b) Mechanism of penetration of Au NPs into POPC lipid bilayer membranes. Initial adsorption is followed by the formation of a hydrophobic contact, followed by ligands crossing the hydrophobic region of the membrane one by one. Adapted with permission from reference Simonelli et al.[335] ACS 2015 copyright. (c) CNT-mediated fusion of vesicles. *Top*: Snapshots of a simulation trajectory showing CNT-mediated vesicle fusion in setup. Lipid phosphate groups are colored to distinguish the two vesicles, their outer leaflets (blue/green in top/bottom vesicle), and their inner leaflets (red/yellow in top/bottom vesicle; drawn larger for clarity). *Bottom*: Zoom-up of the boxes (clipped plane with CNT) showing the coating of the CNT (gray) by lipid tails (colored by their respective leaflets). Adapted with permission from Bhaskara et al.[289] ACS 2017 copyright. (d) Representative distributions of polymers inside POPC membranes (lipid:polymer mass ratio of 6.6%), top view and side view. *Left*: polypropylene (PP107, in blue); *middle*: Short-chain polyethylene (PE10, in gray). *Right*: Longer-chain polyethylene (PE80, in gray). Adapted from Bochicchio et al.[328]

spatial arrangement or the specific chemical nature of the ligands on a nanoparticle, while all-atom simulations provide the most accurate representation for the system, but often proved incapable in reaching the required timescales.

Considering metal nanoparticles, the interaction with peptides/proteins and small biological macromolecules also raised significant interest. Rossi and coworkers studied the interaction of Au NPs with human serum albumin,[310] the most abundant protein in human blood plasma and in the protein corona formed around Au NPs in physiological environments. The same group also developed a model for Au NPs with more weakly bound ligands, notably citrate.[311] Citrate capping is particularly relevant since it is often used to increase the colloidal stability of gold NPs and as an intermediate toward the synthesis of Au NPs with other functional groups. The colloidal stability of citrate-capped Au NPs was also studied by De Vivo and coworkers using experimental and theoretical methods, including Martini CG simulations.[312] The same group also characterized the behavior of more complex metal NPs, bound to multiple copies of a polycationic cell-penetrating peptide, in contact with a model membrane.[313] Peptide-coated NPs strongly interacted with membranes without affecting their mechanical stability; however, the fixed secondary structure of the peptides in Martini is a significant limitation in predictions of their interaction with lipid membranes.

A number of polymers were also studied, in the framework of the Martini model, to probe the interface between biological and nonbiological systems. Here again, the motivation for the studies has been twofold: On the one hand, polymeric systems are increasingly used in biomedical applications, such as drug delivery or biosensors; on the other hand, the massive use of polymer plastics in consumer products (and their disposal, not always controlled) raises concerns about the possible noxious effects on organisms.[314–317] Pioneering work on Martini models of dendrimers interacting with lipid membranes was carried out by Lee and Larson.[318,319] The

17590884, 0, Downloaded from https://wires.onlinelibrary.wiley.com/doi/10.1002/wcms.1620 by Cochrane France, Wiley Online Library on [24/11/2022]. See the Terms and Conditions (https://onlinelibrary.wiley.com/terms-and-conditions) on Wiley Online Library for rules of use; OA articles are governed by the applicable Creative Commons License

same authors also pioneered the use of the PME algorithm for long-range electrostatics in Martini simulations, which turned out to be important to reproduce the behavior of polyelectrolytes, in particular the formation of pores in lipid membrane by interaction with charged dendrimers.[318,319] Recent examples related to biomedical applications include the works on poloxamers (i.e., Pluronics) and their interaction with lipid membranes[320–322] and studies on the complexation of RNA with polymers.[323,324]

Another class of copolymers that attracted significant attention for their interaction with biological membranes is styrene–maleic acid (SMA) copolymers. SMA molecules mixed with lipids form disk-shaped nanoparticles known as SMA lipid particles (SMALPs), and are used to extract membrane proteins from lipid membranes without the use of detergents or membrane scaffold proteins. Martini models for SMA copolymers were developed by several groups and used to characterize the mechanism of the formation of nanodiscs.[325,326] Finally, polymer–membrane interactions were investigated by Rossi and co-workers focusing on industrial plastic polymers. It was found that nano-sized polymeric particles can be dissolved easily in phospholipid membranes and alter most of their properties (Figure 6d),[327,328] as later also observed by all-atom simulations.[329] In addition, Martini PEG polymers have been used in a biological context as crowding agent,[330] to induce membrane fusion,[331] and as hybrid lipid/polymer biomimetics.[332]

Overall, simulations of nano-sized materials at the interface with biological systems highlight some of the major assets of the Martini model: its versatility, simplicity, and the benefits of an open science policy. Development of Martini models for various materials has often been carried out by groups not related to the groups of initial Martini developers; this has been made possible by the intuitive nature of the model and the availability on the web of all resources and information necessary to carry out the development. The building block approach, in which beads are parameterized individually, makes the model extremely versatile, as it allows to easily combine of existing (and new) particle types to cover unexplored regions of the chemical space, while retaining the ability to mix them with particles originally developed to reproduce the behavior of biological systems. Such a combination of biological and nonbiological building blocks has also facilitated a growing number of Martini models for "hybrid" molecules, such as PEGylated lipids and proteins,[150] peptide amphiphiles,[333] or drug–polymer conjugates,[334] to name but a few.

4.3 | Materials science

Soft functional materials are implicated in many innovative applications and their tailored design is expected to lean increasingly on advanced computational modeling.[336] As discussed, the Martini model has matured into a generic force field; the assumptions underlying the model do not preclude its application in (soft) materials science. Indeed, in the last decade, Martini has been increasingly used to model materials such as (block-co)polymers,[44,337] self-assembled supramolecular systems,[70,71,338] organic semiconductors,[339,340] polymer–nanoparticle composites,[341,342] surfaces,[343–345] ion-conducting materials,[346,347] and green solvents.[86–88] Here, we highlight a few recent and diverse examples spanning the breadth of studies performed with Martini in materials science. For a comprehensive overview of such materials science studies, we refer to our recent perspective.[22]

Self-assembled supramolecular materials, featuring a wide range of nanotechnological applications,[348] have been extensively simulated with Martini to elucidate experimental findings or to predict assembly outcomes solely based on the structure of the molecular building blocks.[338,349–353] Pioneering studies have used short peptides as building blocks to explore biocompatible supramolecular nanostructures.[350–352] More recently, supramolecular materials composed of self-assembling synthetic molecules have been increasingly investigated, in particular, by the group of Pavan.[71,349,354,355] A recent highlight is the work of Sarkar and co-workers, who investigated two-component supramolecular polymerization by both experiments and Martini-based MD.[349] Even with two monomeric components, supramolecular copolymerization can lead to several structural outcomes, including supramolecular homopolymers, random copolymers, alternate copolymers, and block copolymers. Comparable interaction energies between the monomer components resulted in supramolecular random copolymers (Figure 7a). In contrast, supramolecular homopolymers could be achieved by leveraging high kinetic stability of the supramolecular structures or low monomer exchange dynamics. Martini simulations, enhanced with well-tempered metadynamics, delivered mechanistic insights into the strength of the interactions between the different monomer components and the monomer exchange dynamics in the supramolecular structures, and provided to be vital for rationalizing the experimental outcomes.

One of the latest materials science branches where Martini has been used is the field of green solvents, with several recent studies modeling ionic liquids[86,87,356,357] and deep eutectic solvents.[88] Green solvents promise to replace more traditional solvents by providing more environmentally friendly solutions. One of the most intriguing areas of

17590884, 0, Downloaded from https://wires.onlinelibrary.wiley.com/doi/10.1002/wcms.1620 by Cochrane France, Wiley Online Library on [24/11/2022]. See the Terms and Conditions (https://onlinelibrary.wiley.com/terms-and-conditions) on Wiley Online Library for rules of use; OA articles are governed by the applicable Creative Commons License

application is separation science, given green solvents' tunable, specific, and performant extraction properties. As is common for organic-based materials, their chemical tunability allows for great customization. However, this flexibility also leads to an extremely large number of potential material candidates, giving rise to a chemical space impossible to explore experimentally. Hence, efficient computational modeling of green solvents is vital to enable the targeted design of green solvents. In a recent work, Vainikka et al. developed Martini 3 models for deep eutectic solvents (DESs).[88] The authors selected some well-known and actively studied DES systems and investigated the ability of the models to capture the properties of these green solvents. In particular, they found the models able to capture known liquid–liquid extraction processes—such as, for example, the extraction of 2-methylthiophene and benzothiophene from octane by the DES tetrabutylammonium chloride–acetic acid (Figure 7b)—as well as the morphological changes of the shape of surfactant aggregates as a function of DES concentration. The study opens possibilities for in silico design of DESs aided by Martini simulations.

A growing library of Martini polymer models is available,[22] including simple linear polymers,[44,337] branched and hyperbranched polymers,[358,359] conjugated polymers,[339,340,360] block copolymers,[361–363] and polyelectrolytes.[364] Several of these models are included in the library of Polyply.[98] Since the pioneering development of Martini models for polyethylene oxide (PEO)[63] and polystyrene (PS),[337] more recent works in this area have explored different aspects and applications of polymers, such as thoroughly revising the transferability of developed polymer models,[44] combining polymers with nanoparticles,[341,342] or simulating complex multi-component systems (e.g., Figure 7c).[98,365] As an example of complex multi-component systems, Li et al. recently developed a hybrid synthetic structure that mimics mechanical actuation, with Martini simulations providing insights into the microscopic processes taking place during actuation.[365] The hybrid material consists of peptide amphiphile supramolecular fibers covalently linked to polymers

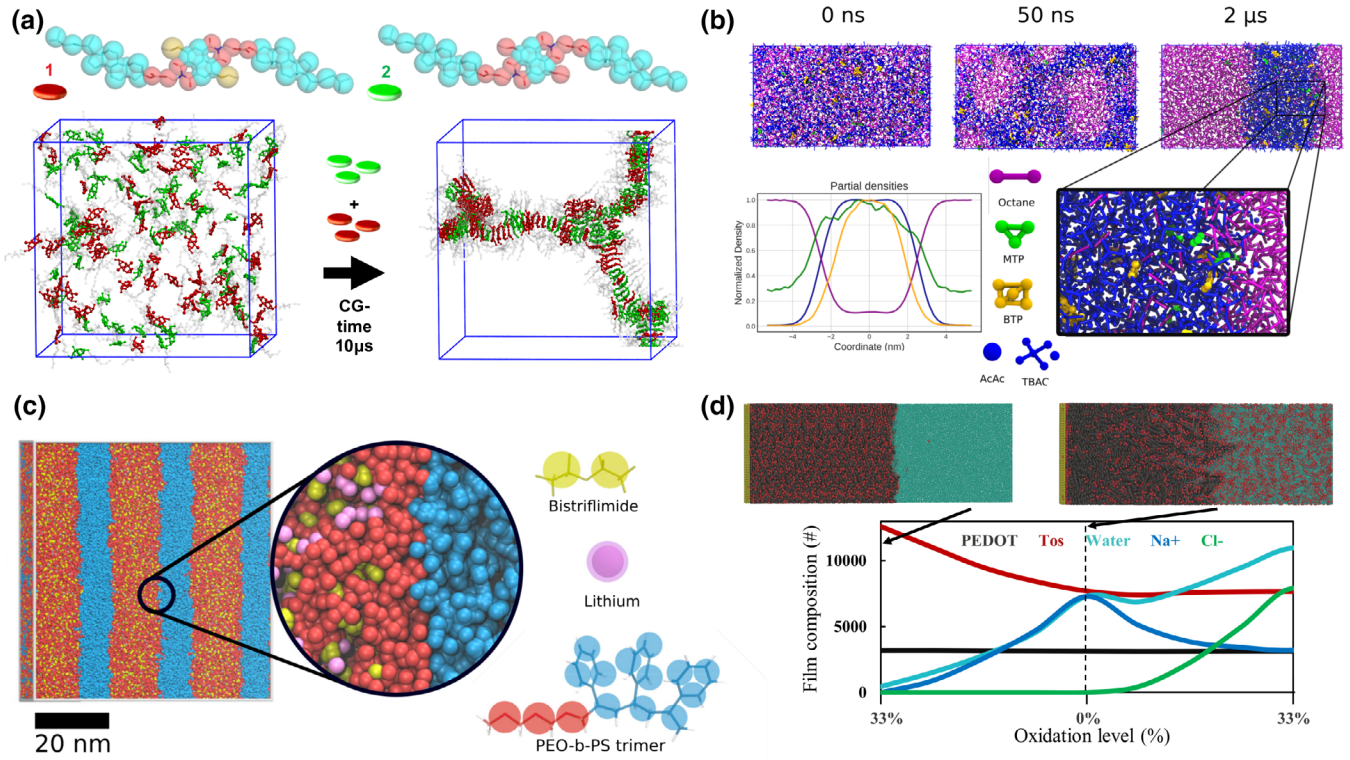

FIGURE 7 Applications of Martini in Materials Science. (a) Supramolecular (random) block copolymer self-assembly. (b) Extraction of 2-methylthiophene (MTP, green) and benzothiophene (BTP, yellow) from octane (purple) by the deep eutectic solvent tetrabutylammonium chloride (TBAC, blue)–acetic acid (AcAc, blue). The plot shows the partial density for each component, with the same color scheme: MTP is seen favoring the deep eutectic solvent phase but still partially residing at the interface and in the octane phase; BTP is instead almost completely extracted. (c) Phase-separated block-copolymer of PS (rendered in blue) and PEO (in red) doped with lithium (in purple) bistriflimide (in yellow) as a prototypical soft material for energy storage applications. (d) Simulated cyclic voltammetry experiments showing water intake and ion exchange in conducting polymer films. (a) Adapted with permission from Sarkar et al.[349] Copyright 2020, American Chemical Society. (b) Adapted from Vainikka et al.,[88] under CC-BY. (c) Adapted from Grünewald et al.,[98] under CC-BY. (d) Adapted with permission Delavari et al.[371] Copyright 2021, American Chemical Society.

17590884, 0, Downloaded from https://wires.onlinelibrary.wiley.com/doi/10.1002/wcms.1620 by Cochrane France, Wiley Online Library on [24/11/2022]. See the Terms and Conditions (https://onlinelibrary.wiley.com/terms-and-conditions) on Wiley Online Library for rules of use; OA articles are governed by the applicable Creative Commons License

which are crosslinked across fibers to form a network. The polymers contain a spiropyran-based switch that can be activated with light: depending on light exposure, either a charged hydrophilic form or a noncharged hydrophobic form of the switch can be realized. Switching to the hydrophobic forms leads to water expulsion and an associated shrinkage of the material. By constructing a minimal Martini model of the hybrid material using two crosslinked fibers, Li et al. found that Martini could reproduce the amount of shrinkage in a quantitative way, while providing a microscopic view of the actuation process.[365]

The development of robust relationships connecting molecular structure to material nanomorphology remains a key challenge in organic electronics.[366,367] To this end, Martini-level simulations have started to play an important role in elucidating local molecular packing and morphology features as a function of processing conditions and molecular structure.[173,342,367–369] Computational modeling of systems for organic electronics necessitates being able to simulate mixtures of polymers, nanoparticles, and small molecules, and the widening library of corresponding Martini models has enabled such studies.[173,339,340,369,370] Moreover, synthetic molecules can be mixed with biomolecules, as in the work of Mehandzhiyski and Zozoulenko where the conjugated polymer PEDOT:PSS—polymer poly(3,4-ethylenedioxythiophene) blended with poly(styrenesulfonate) (PEDOT:PSS)—is mixed with cellulose nanofibers to investigate PEDOT:PSS/cellulose composites, a material with prospective applications as conductive paper.[368] The group of Zozoulenko has made extensive use of Martini to model conducting polymer-based systems.[340,369] Besides the PEDOT:PSS/cellulose example, a recent highlight includes the development of a protocol to simulate cyclic voltammetry experiments.[371] The protocol consists of a stepwise change of the oxidation state of PEDOT—compensated by the introduction of appropriate counterions—to which the system is allowed to respond. As such, the protocol allows to study the water intake, swelling, and exchange of ions in the conducting polymer morphologies during cyclic voltammetry. When applied to PEDOT:tosylate morphologies, the authors observed significant changes in the morphology during the redox process, with the loss of mass during reduction being in agreement with spectroscopic findings and revealing how tosylate ions are replaced by chlorine ions as the counterions for PEDOT (Figure 7d). Finally, an added benefit of Martini that is particularly important in the field of organic electronics is the possibility of directly backmapping[125] structures to atomistic resolution given the high degree of molecular specificity of the Martini model. This possibility allows to carry out quantum chemical calculations on structures derived from large-scale self-assembly processes, hence enabling advanced multiscale studies aimed at connecting structural and electronic properties.[342,372]

4.4 | High-throughput workflows

The ability to perform high-throughput (HT) simulations is key to the rational design process of new materials, improved enzymes, or novel drugs.[373] In addition, HT simulations are important to generate fundamental understanding of a system's behavior by systematically probing many different state conditions. Furthermore, HT workflows can be used to create databases that are subsequently mined by bio- or chem-informatics tools. The inherent speed of simulations with CG resolution, in combination with the ease of generating CG topologies and starting structures, has prompted the use of Martini in a variety of HT pipelines, some of which are illustrated in Figure 8 and further discussed as follows.

An early example of such a HT pipeline is from the folding@home project of the Pande group, utilizing the power of a large number of home computers to simulate lipid membrane fusion.[122] The generated ensemble, based on 10,000 short MD trajectories, was combined with MSM to provide the underlying energy landscape of the fusion process. A more recent example in this area is from Hub and coworkers.[377] In their study, they addressed the propensity of membranes to fuse from a computational lipidomics perspective. In particular, the CG resolution enabled computation of ~200 free energies of stalk formation in membranes with different lipid headgroups, tail lengths, tail unsaturations, and sterol content. The results from this dataset were subsequently used to explain the finding that the inner leaflet of a typical plasma membrane is far more fusogenic than the outer leaflet.

The group of Stansfeld has used HT Martini-based simulations to maintain a database of membrane proteins and associated webserver (http://memprotmd.bioch.ox.ac.uk/).[374,378] To fill the database, membrane protein structures are automatically identified in the PDB on a weekly basis and converted to Martini representation (Figure 8b). This is followed by a 100 ns MD simulation in the presence of lipids and water to allow a lipid bilayer to self-assemble around the protein. The simulation is continued for another 900 ns simulation to study the dynamics of the assembled membrane, and subsequently converted to atomistic resolution and analyzed. Currently, the database contains almost 6000 simulations of intrinsic membrane proteins. The database can be explored in many ways, for example, to see how a

17590884, 0, Downloaded from https://wires.onlinelibrary.wiley.com/doi/10.1002/wcms.1620 by Cochrane France, Wiley Online Library on [24/11/2022]. See the Terms and Conditions (https://onlinelibrary.wiley.com/terms-and-conditions) on Wiley Online Library for rules of use; OA articles are governed by the applicable Creative Commons License

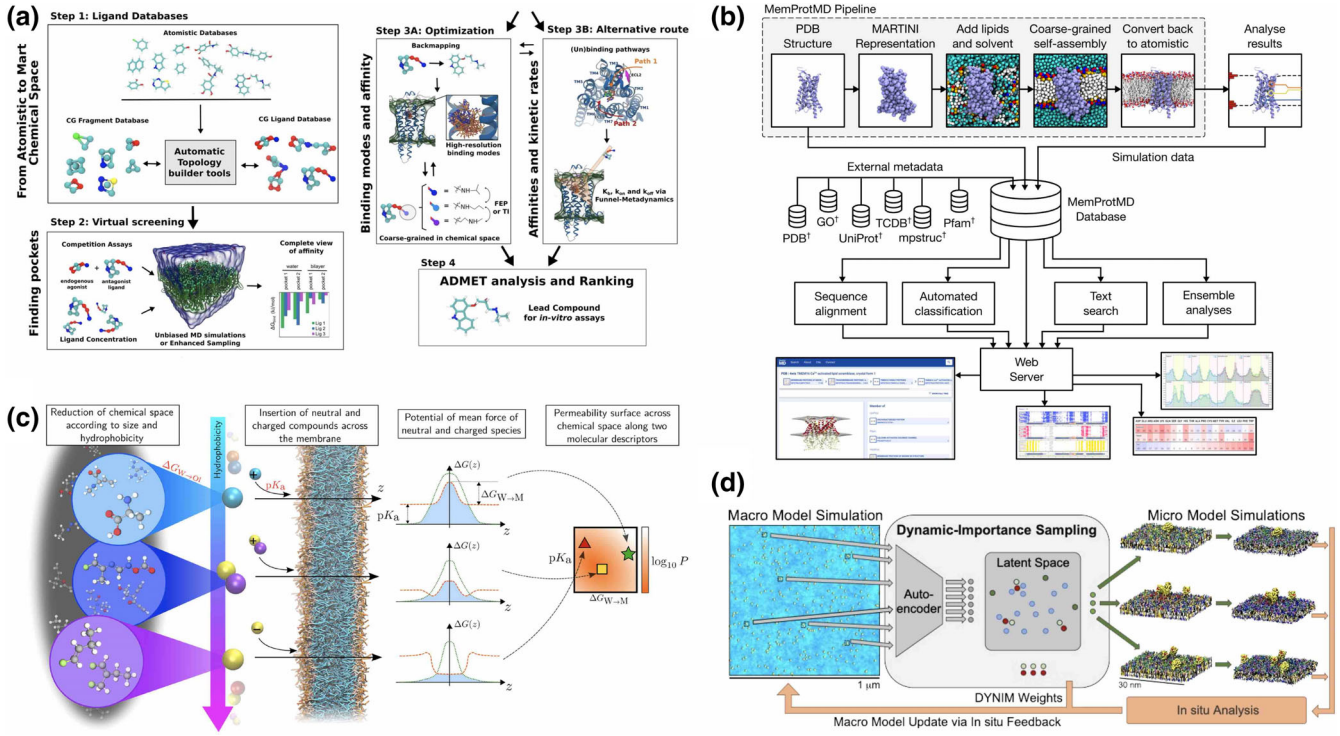

FIGURE 8 Examples of HT workflows based on Martini. (a) Pipeline for rational drug design, taken from Souza et al.[269] (b) Protocol underlying the membrane protein database, taken from Newport et al.[374] (c) Chem-informatics workflow for predicting membrane permeability, reprinted with permission from Menichetti et al.[375] Copyright 2019 ACS. (d) Multiscale workflow "MuMMI" to couple mesoscale and CG simulations, adapted from Bhatia et al.[376]

specific protein is embedded in the membrane, or run statistics on a subset of proteins to explore protein–lipid contacts, for instance. In a recent application, cardiolipin binding sites of a large set of 42 different *Escherichia coli* inner membrane proteins were analyzed and compared.[379] More than 700 specific binding sites were detected, leading to the identification of the molecular basis of a prototypical cardiolipin binding site. A related database that has just been released, SuPepMem,[380] aims to collect simulations of host defense peptides (HDPs) interacting with lipid membranes, at different resolutions including Martini. A first set of 403 systems resulting from the combination of 52 HDPs and six different membranes models, simulated using the Martini 2.2 force field for 5 μs each, is currently available. Further examples of HT work in this area are studies of the Tieleman group comparing lipid fingerprints of 10 generic plasma membrane proteins[192] as well as of 20 different GPCRs,[221] and work from the Stansfeld group reporting affinities for cholesterol binding to a range of membrane proteins based on the computation of binding saturation curves, designed to mimic experimental protocols.[381]

Another example of a HT pipeline is the MuMMI workflow (Figure 8d). This pipeline features HT Martini simulations on RAS–RAF protein complexes interacting with a multi-component plasma membrane model, that are coupled to a mesoscale simulation running in parallel.[191,376] In total, 120,000 Martini simulations were performed on patches consisting of about 3000 lipids and containing one or more proteins, with starting configurations extracted from the mesoscale simulation based on a machine learning algorithm. Each patch was simulated for between 1 and 4 ms, with an aggregated simulation time of almost 0.2 s, a record in terms of aggregated simulation time (Table 1). An extended three-scale version of MuMMI has also been developed, coupling between a continuum model, CG Martini, and AA CHARMM to resolve RAS–RAF protein complex membrane dynamics (featuring over 34,000 CG simulations of nearly 0.1 s aggregated simulation time).[382] These huge efforts required dedicated time on next-generation exascale supercomputers, and while some of the final results are still pending, the establishment of the pipeline by itself is already a major feat. A smaller-scale example of HT simulations involving membrane protein aggregation is provided by the group of Sansom, who performed more than 60 independent simulations of GPCR clustering, combined with MSM to reveal cluster populations and dynamics of oligomerization.[228]

The release of Martini 3 has opened also the way to HT screening of protein–drug interactions. For a number of different proteins, including membrane-embedded ones, Souza et al. demonstrated that brute force simulations with

17590884, 0, Downloaded from https://wires.onlinelibrary.wiley.com/doi/10.1002/wcms.1620 by Cochrane France, Wiley Online Library on [24/11/2022]. See the Terms and Conditions (https://onlinelibrary.wiley.com/terms-and-conditions) on Wiley Online Library for rules of use; OA articles are governed by the applicable Creative Commons License

Martini can correctly identify known binding pockets.[183] Moreover, the amount of sampling is so large that accurate statistics on binding free energies and entry and exit pathways are obtained at the same time. A potential pipeline for HT ligand screening is illustrated in Figure 8a,[269] combining the benefits of fast methods such as docking and including protein and solvent dynamics. In a related study, Melo et al. used a high-throughput protocol to explore the effect of bilayer environment on the gating kinetics of the membrane channel MscL. Based on over 500 independent CG MD simulations totaling more than 10 ms of effective sampling time, the study revealed that short-chain alcohols have an impeding effect on the opening threshold of MscL, which was corroborated by an experimental efflux assay.[383]

The potential for HT drug lead optimization with Martini has also been explored by the group of Bereau. They make clever use of the fact that CG beads in Martini can actually map to multiple chemical fragments.[168] In a landmark paper,[375] they performed HT simulations to derive a membrane–drug permeability surface in terms of two simple molecular descriptors, namely the bulk partitioning free energy and p*K*a (Figure 8c). The surface is constructed by exhaustively simulating all CG Martini compounds that are representative of small organic molecules. Connecting back to the atomic resolution, their predictions extrapolate to more than 500,000 compounds, covering a large part of the chemical space and providing a clear connection between specific chemical groups and the resulting permeability coefficient. In a follow-up study, the generated data set was interrogated with an artificial intelligence technique to identify the driving forces governing passive drug transport across membranes.[384] A recent study by Melcr et al. also uses HT lipidomics-based computational screening to unravel the role of membrane properties on permeability.[385]

HT screening with the Martini force field is also increasingly used in the field of materials science. A prime example is the simulation by Frederix et al. of all possible 400 dipeptides and 8000 tripeptides in search for new peptide-based hydrogels.[338,350] A classification based on peptide hydrophobicity versus aggregation propensity—as estimated from the simulations—resulted in a selection of promising candidates for hydrogel formation. Some of these peptides were subsequently synthesized, and indeed led to the discovery of novel hydrogels. A very recent example of HT Martini-based simulations, also aimed at finding new hydrogels, is from the work of Cardellini et al.[386] In their study, a protein–polymer compositional phase diagram was constructed based on a large set of simulations, to establish guidelines for protein–polymer coassembly. Another recent example is from the Tuttle group, screening more than 80,000 tri/tetrapeptides on their ability to adsorb at an interface, aiming to identify peptides suitable to act as emulsifiers.[387] An HT example from a different part of materials science is the work of Alessandri et al. on bulk heterojunction morphologies of polymer/fullerene blends that form the basis of organic photovoltaic devices.[339,342] The experimental setup of solution processing to form the bulk heterojunction was mimicked by stepwise evaporation of the solvent from the system during the simulation. A systematic exploration of polymer weight and drying time on the formed morphologies, as well as the impact of polymer side chains, provided important insight into this process, with the prospect of designing more efficient light-harvesting materials in the future. More HT examples of Martini in soft matter systems can be found in Alessandri et al.[22]

4.5 | Increasing complexity

The availability of many Martini molecule types and the longer length and time scales afforded by CG have been key enablers of multi-component system simulations. (Number of component copies or total system size can also be evoked, on their own, as criteria for complexity; those examples are addressed over the next sections.) In multi-component systems, a larger size is often a direct consequence because (1) the simulation box must hold all the different components, and (2) for mixtures of different proportions of components, enough molecules must be simulated so that species with the lowest concentration is still present in representative numbers. Together with size requirements, equilibration times of multi-component systems can also be longer than those of similarly sized systems with fewer components. This reflects the need to properly sample the several relevant component–component configurations, at the different length scales of the system.[388,389]

Figure 9e shows the time evolution of Martini simulation records, regarding the number of nonsolvent components, since the Martini 2.0 release. All records have been of systems involving lipids—the initial focus of Martini—but not always of bilayer systems. The group of Vattulainen[390,391] has simulated realistic lipoprotein[392]particles using up to eight nonsolvent components (six lipid types and two proteins), in an application example where, incidentally, total system size does not grow with complexity. Monolayer systems such as those of lung[393] and tear fluid surfactant films[394] have also been successfully simulated with up to five protein and lipid components. Figure 9a also highlights the paradigm shift brought by Ingólfsson et al.'s simulation of a 63-component plasma membrane of realistic lipid composition.[194] That effort showcased Martini's maturity and suitability to this type of systems and kick-started an entire sub-field in simulations of

17590884, 0, Downloaded from https://wires.onlinelibrary.wiley.com/doi/10.1002/wcms.1620 by Cochrane France, Wiley Online Library on [24/11/2022]. See the Terms and Conditions (https://onlinelibrary.wiley.com/terms-and-conditions) on Wiley Online Library for rules of use; OA articles are governed by the applicable Creative Commons License

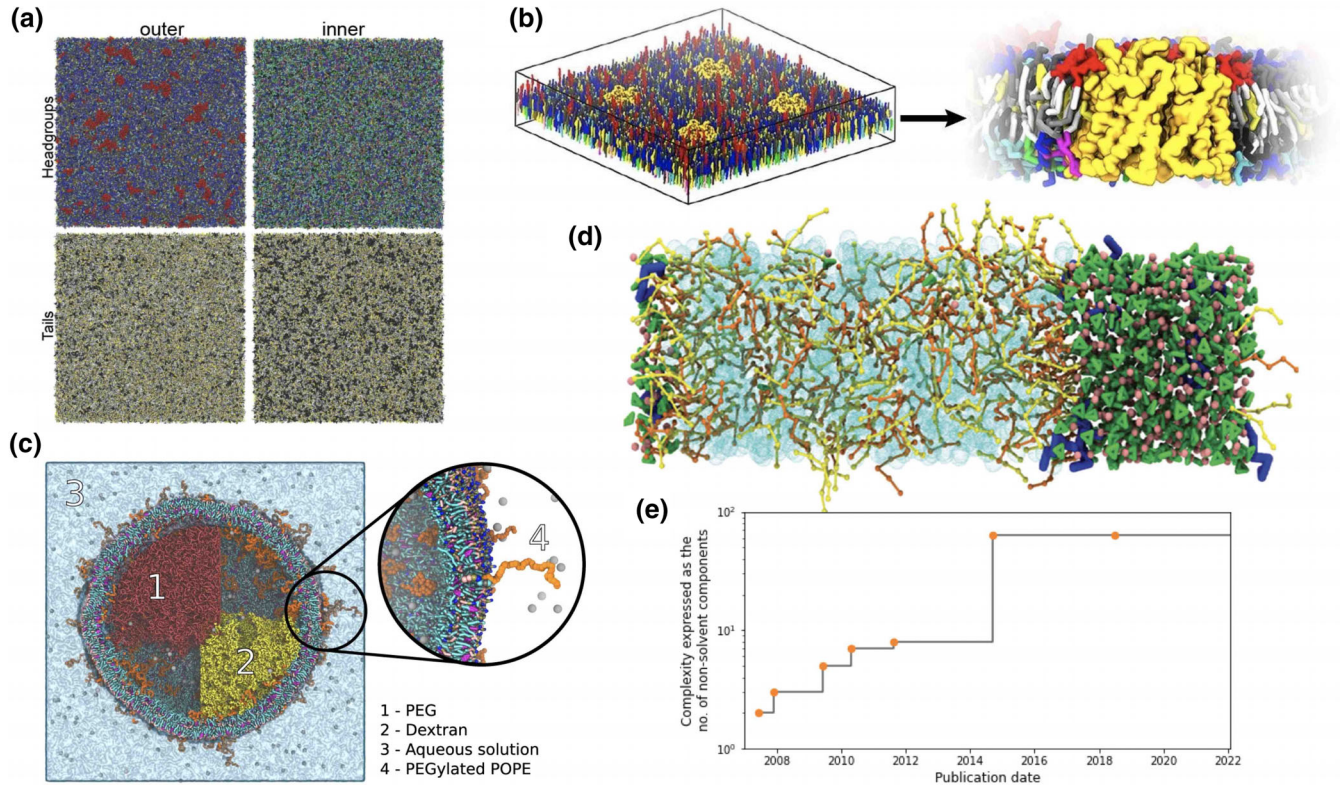

FIGURE 9 Examples of multi-component Martini systems. (a) Final snapshots of the 63-lipid asymmetric membrane simulated by Ingólfsson et al.,[194] highlighting the several headgroup and tail components. (b) Corradi et al.'s simulations[192] of proteins embedded in membranes of similar composition to those in panel a, from system preparation with the insane tool[91] to the evolution of heterogeneity local to proteins; at 64 components, these are the record holders for Martini simulation complexity. (c) Polyethylene oxide-dextran coacervate mixtures, encapsulated in a liposome containing PEG-derivatized lipids, as an example use of the polyply tool[98] that illustrates the coexistence of different types of molecules and phase separations. (d) Setup for the imidazolium ionic-liquid selective extraction of docosahexaenoic acid from a fish oil mixture (oleic and palmitic acids) as one of the most complex nonmembrane examples. Taken from Vazquez-Salazar et al.[86] (e) Time evolution of the complexity of Martini simulations, expressed as the number of nonaqueous-solvent components versus publication date, since the release of Martini 2. All records have been held by lipid simulations but not all correspond to membrane simulations (the record-breaking simulations in 2010 and 2011 are of lipoprotein systems). The 2014 and 2018 records correspond to panels a and b, respectively, and the ground-breaking nature of Ingólfsson et al.'s work is evident from the 2014 jump in system complexity. The full list of record holders is, in chronological order.[35,192,194,390,391,402,403]

realistic lipid bilayers[192,195,395,396] (of which the current complexity record, held by Corradi et al. on lipid interactions of membrane proteins,[192] is an example; Table 1, Figure 9b). These simulations also underscore the simulation size and time requirements that high complexity can entail: Ingólfsson et al. had to simulate a membrane patch of over 70×70 nm^2 so that, at 0.03% mole fraction, the least represented lipid could still be present in multiple copies.[194] In this system, the evolution of heterogeneity in lateral lipid organization approached 10^2 μs timescale.[194,195]

Since Risselada and Marrink's initial work[36] on lipid phase coexistence, Martini has been extensively used to study interactions with phase-separated membranes.[397,398] In these examples, complexity also arises from the number of phases that coexist, since systems are of obviously higher complexity than the same lipids in a homogeneous mixture. For these cases, the effective number of components is then perhaps best interpreted scaled by the number of phases, since simulation size and time requirements will typically be those of more complex systems. Highly complex systems can also lead to, or suffer from, subtle artifacts that may be less readily detectable than in simpler set-ups. This was recently demonstrated in the context of phase separation by Thallmair et al.,[185] whereby nonconverged constraints of the Martini cholesterol model can result in temperature gradients between different membrane domains if simulation settings are not chosen carefully.

Martini has also been used to simulate systems where complexity arises less from the total number of lipids, and more from the combination of different-natured components, most notably those mixing lipids with proteins and/or

17590884, 0, Downloaded from https://wires.onlinelibrary.wiley.com/doi/10.1002/wcms.1620 by Cochrane France, Wiley Online Library on [24/11/2022]. See the Terms and Conditions (https://onlinelibrary.wiley.com/terms-and-conditions) on Wiley Online Library for rules of use; OA articles are governed by the applicable Creative Commons License

nucleic acids. For instance, Van Eerden et al.'s simulations of the photosystem II complex in a realistic thylakoid membrane involved modeling of 19 different protein subunits, six cofactors, five ions, and five lipid types.[399,400] Nonlipid systems have also been studied at some degree of complexity, though nowhere near that of lipids. A biological example is the Martini ribosome,[58] developed with six components (two subunits, each with protein and RNA content, plus mRNA, and tRNA), but that could conceptually be extended to include, among others, nascent chains and chaperones as was done in a mixed resolution study using the PACE force field.[401]

Nonbiological applications that stand out, complexity-wise, are the ones involving phase separation and/or morphology. Here, complexity again emerges from heterogeneity rather than from shear component number. One of the earliest examples is Alessandri et al.'s three-component simulation of solvent processing of organic solar cell bulk heterojunctions.[339] More recently, enabled by the development of Martini 3, Vazquez-Salazar et al. simulated the phase behavior and oil extraction capabilities of imidazolium-based ionic liquids[86]—these extraction simulations, at six components, also contend for the most complex nonlipid Martini system to date (Figure 9d). Also leveraging Martini 3, Tsanai et al. have simulated complex coacervate aqueous–aqueous phase coexistence using a polylysine/polyglutamate mixture, in which additional components (proteins, RNA) exhibited phase selectivity.[89]

The successful examples in this section show that complexity can be confidently tackled with Martini and are a testament to the framework's transferability qualities—by which molecular models behave representatively in a range of environments, all coexisting in the same simulation box. With novel tools such as polyply,[98] it becomes increasingly easy to construct starting structures of multi-component systems in a variety of spatial geometries, as further exemplified by a PEGylated lipid vesicle containing a phase-separated polymer mixture (Figure 9c). Given this sound CG basis, we expect also nonlipid simulations to explode in complexity, paralleling the one that occurred for lipid membranes.

4.6 | Connecting to the whole cell scale

One of the key features of CG models is the connection between the atomistic detailed simulations and the mesoscale which is traditionally the realm of continuum models. Martini has proven efficient in building this bridge, allowing it to reach spatiotemporal scales of hundreds of nm and hundreds of microseconds (Table 1) while keeping a near-atomic resolution. With increasing computer power, we currently see that Martini-based simulations can truly reach the mesoscale even with modest computational resources, in contrast to all-atom simulations which require massive use of state-of-the-art facilities.[404–406] It is not far-fetched to expect that whole cell simulations are within reach, a prospect enabled by the progress made in the experimental characterization of cell organization fuelling integrative research efforts in this direction.[407,408]

A first example of a "Martini mesoscale simulation" is given by the work of Vögele et al.,[189] who performed simulations of increasingly large lipid bilayers to evaluate the effect of periodic boundary conditions on lipid diffusion in order to test the underlying assumptions of a hydrodynamic theory. They nicely showed how predictions form the theory match those from Martini simulations, converging to the continuum limit for systems of $420 \times 420 \times 100$ nm box dimensions, with 132 million CG particles, the largest Martini system simulated to date (Table 1). Simulations of cellular membranes also steadily increase in size. A first step-up in lateral dimensions was achieved by Arnarez et al., reporting on a mitochondrial membrane patch containing 45 respiratory chain proteins, about 18,500 lipids, and approaching the 0.1 μm length scale.[409] An even larger system was simulated by the Sansom group.[410] They performed a 2.5-μs simulation of a bacterial membrane patch with lateral dimensions close to 0.5×0.5 μm, containing 1152 BtuB + 1152 OmpF proteins for a total of more than 22 million particles. The length scale of the simulated system corresponded to that probed experimentally, but the limited time scale proved still insufficient for a meaningful one-to-one comparison.

An important prospect of Martini is to enable molecularly detailed simulations of entire cells. Although we are not there yet, progress toward this challenging goal is being made by many groups. For instance, simulations of entire viruses have already been reported,[411–414] and protocols for setting up such simulations are becoming available.[413,415,416] An advantage of using a CG model is that many conditions can be probed, in particular with placing reasonable amounts of lipids in both leaflets and an appropriate amount of interior solvent, including ions. Initial choices often lead to instabilities which only become apparent after many microseconds of simulation. Most recently, the COVID-19 viral envelope has been simulated with Martini[417–419] (Figure 10a). In the work of the Tieleman group,[417] both SARS-CoV and SARS-CoV-2 envelopes were simulated and their dynamics and supramolecular organization explored. Structural proteins were found to form multiple string-like islands in the membrane, and clusters appeared between the

17590884, 0, Downloaded from https://wires.onlinelibrary.wiley.com/doi/10.1002/wcms.1620 by Cochrane France, Wiley Online Library on [24/11/2022]. See the Terms and Conditions (https://onlinelibrary.wiley.com/terms-and-conditions) on Wiley Online Library for rules of use; OA articles are governed by the applicable Creative Commons License

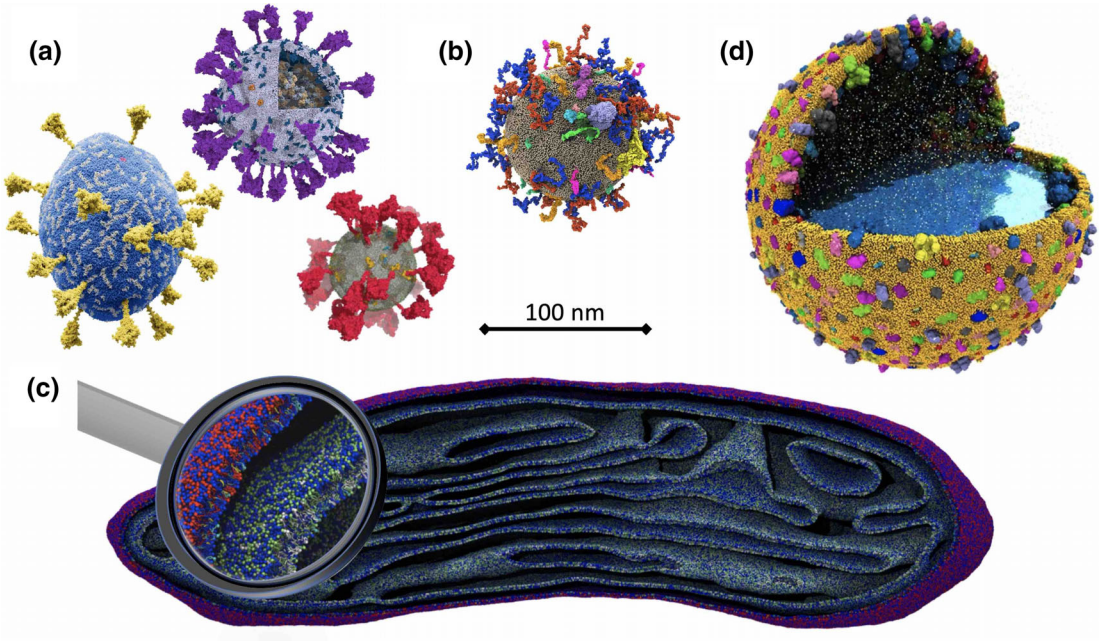

FIGURE 10 Applications toward the whole cell level. (a) SARS-CoV-2 viral envelopes, taken from References 417–419. Copyright 2022 ACS.[417] (b) Autophagosome model, taken from Sawa-Makarska et al.[421] (c) Membranes of an entire mitochondrion, adapted with permission from Pezeshkian et al.[130] Copyright 2022 AAAS. (d) Protocell envelope, reproduced with permission from Vermaas et al.[423] Copyright 2022 ACS.

heads of spike proteins with noticeable differences between the SARS-CoV and SARS-CoV-2 envelopes. The models of Pezeshkian et al.[418] represent a larger and more accurate SARS-COV-2 envelope, featuring more than 1000 proteins (25 S, 2 E, 1003 M), more than 60,000 lipids (of six different types), and up to 35 million solvent particles. Based on simulations of 1–4 μs, interesting patterns emerged of the abundant M-dimers, in good agreement with electron microscopy data. In the work of Wang et al.,[419] a part of the RNA bound to the envelope was also included in their virion model, and the full structure was backmapped to all-atom resolution. Another noteworthy large-scale effort to probe viral envelope dynamics is the simulation of a HIV-I liposome, measuring 150 nm in diameter and containing about 300,000 lipids and 200 million solvent particles, performed by Bryer et al.[420]

Beyond viruses, organelles are the next obvious target for detailed simulations. A first example is the autophagosome constructed by Hummer and coworkers[421] (Figure 10b). The autophagosome model features a 60-nm diameter Martini lipid vesicle filled with proteins at stoichiometries as derived from experiments. Although the proteins are represented at different (available) resolutions, and the model is just a static picture, it reveals the crowded nature of such a relatively simple organelle. Another example is the model of a full endosome measuring about 50 nm in diameter with a total of almost 3 million beads from the study of Bruininks et al.[271] Although the endosomal membrane model is lipid only, it allowed the simulation of the translocation of lipoplexed genetic material across the endosomal membrane in a 5 μs simulation. In a comparable study, Khalid and coworkers simulated the interaction of lipid liposomes representing both smooth and rough outer membrane vesicles—particles that are in reality secreted by various bacteria—with realistic models of the host plasma membrane.[422]

A primary example of the capability of Martini to simulate entire organelles is the mitochondrion model from Pezeshkian et al.[130] (Figure 10c). The model is lipid only, featuring about 5 million lipids (more than 80 million particles) of different types with distinct compositions for the two leaflets of both inner and outer membranes mimicking real mitochondrial membranes. The model was simulated for a short period (2 ns) with the Dry Martini force field. Although a relatively small mitochondrion, with system dimensions of 341 × 488 × 792 nm,^{3} it is currently the largest Martini-based system in terms of spatial dimension (Table 1). The system was constructed from electron microscopy density maps using the TS2CG software.[130]

On the way to full cell models, Tajkhorshid and co-workers recently simulated a cell-scale membrane envelope with Martini[423] (Figure 10d). The model consists of a 200 nm diameter vesicle, containing 14 different proteins at a protein–lipid ratio approaching that of real cell membranes, totaling about 100 million CG particles. Multiple conditions were

17590884, 0, Downloaded from https://wires.onlinelibrary.wiley.com/doi/10.1002/wcms.1620 by Cochrane France, Wiley Online Library on [24/11/2022]. See the Terms and Conditions (https://onlinelibrary.wiley.com/terms-and-conditions) on Wiley Online Library for rules of use; OA articles are governed by the applicable Creative Commons License

probed in terms of lipid and solvent content, eventually resulting in a final protocell model that proved stable during a 500 ns simulation.

5 | OUTLOOK

In this final section, we discuss some of the ongoing and planned developments, by us and with the help of the larger Martini community, to further improve on the Martini model. With the release of Martini 3 and the availability of many new and more accurate bead types, there is a lot of room to improve the currently available molecular models. This is not a trivial task, given the multi-objective nature of the underlying parameterization strategy. Optimizing parameters to reproduce a single target property is easily feasible, but when aiming to capture many different types of properties simultaneously, the task becomes challenging. To address this challenge, refinement of the different categories of molecules is currently organized into dedicated taskforces.

To improve lipids, the better balance between standard and smaller bead types in Martini 3 enables a finer mapping of the lipid tails, allowing one to distinguish between, for example, C16 and C18 tails, something that was not possible in Martini 2. In addition, the lipid headgroups are being revised, not only considering the new bead types that are available, but also including more sophisticated bonded potentials to better capture the headgroup flexibility in comparison to all-atom simulations. A glimpse of how this can improve lipid behavior is provided by the recently released PIP models.[174] We expect that the forthcoming generation of lipid models will improve the behavior of both pure lipid systems, such as correctly reproducing phase diagrams including liquid-order domain formation, and specific protein–lipid binding interactions.

A main limitation for proteins in Martini is the lack of an accurate description of conformational flexibility, which means most simulations use fixed secondary and tertiary structures with some flexibility for loops or specific domains, requiring specific assumptions by the investigator. Although there are several examples of proteins with relative domain motions,[383,424] including individual helices,[399,425] and proteins can sometimes be simulated in different, but fixed, conformational states,[239,262] we expect a major improvement to be made with the further fine-tuning of Gō-type potentials.[177] Such potentials can be efficiently incorporated into Martini models using virtual sites. A similar approach is also being tried to fine-tune protein–solvent interactions, which appears to be required to accurately reproduce the conformational ensembles of disordered proteins.[90] Together with the obvious improvement in Martini 3 in its ability to model elements of a system at higher resolution, we foresee more applications directly aimed at the mechanism of proteins including functional aspects of protein–ligand interactions and transport mechanisms of membrane proteins. Fine-tuning of interactions to more accurately model protein–protein interactions is a less fundamental problem and has been incorporated to a significant degree in Martini 3.[83] The new version already shows a major improvement in its ability to model dimerization of transmembrane helices and the resulting structures are very close to experimental structures in a number of test cases,[83,184] promising further improvements in the treatment of membrane proteins.

For carbohydrates, the restricted choice of particle types and sizes in Martini 2 has limited its possibility to capture the chemical complexity and subtlety of carbohydrates, but with the new Martini 3 bead sizes the available universe of possible structures is much larger. Clever choices of virtual sites also allow for a better mimicking of the conformation flexibilities. Similar considerations apply to the modeling of other types of polymers. Based on the new Martini 3 bead types, we are currently constructing a library of validated topologies for a wide range of common polymers. In addition, the release of the polyply tool[98] enables users to generate topologies and starting structures for both linear and branched copolymers of arbitrary composition. The improvement of nucleic acids involves multiple challenges, including capturing backbone conformations, subtleties in base–base interactions, and accurate treatment of electrostatics,[57] all of which are likely to be improved significantly in Martini 3 with both a broader choice of bead sizes, the option to fine-tune specific interactions, and improved modeling of ions. The ultimate aim is to allow hybridization with the next generation Martini nucleotides, perhaps with the help of Go-potentials in analogy to the proteins.

In addition to the progress made in the dedicated taskforces, we are working on porting the polarizable water model to Martini 3, to account for a more accurate description of long-range electrostatic effects and systems with dielectric gradients. Also, the titratable water model is being integrated into Martini 3, and further expanded to enable constant pH simulations involving proteins. A new implementation of lambda-dynamics into Gromacs offers another route to constant pH simulations with Martini.[426] As a prospect further down the line, we are investigating the possibility to model chemical reactions on the fly with the Martini model, which would open up a large number of new applications. A proof of principle along these lines has recently been demonstrated in the case of silica polymerization reactions.[427]

17590884, 0, Downloaded from https://wires.onlinelibrary.wiley.com/doi/10.1002/wcms.1620 by Cochrane France, Wiley Online Library on [24/11/2022]. See the Terms and Conditions (https://onlinelibrary.wiley.com/terms-and-conditions) on Wiley Online Library for rules of use; OA articles are governed by the applicable Creative Commons License

An important additional development is the construction of MAD, the Martini database,[155] allowing deposit and retrieval of all Martini models developed so far, with detailed version tracking, through a simple graphical interface. The MAD sever will also integrate and provide a graphical interface for the most commonly used Martini tools, such as martinize, insane, and polyply, therefore promoting adoption of the force field by new users. Finally, new and accurate automatic topology builders, properly including all the steps of Martini 3 parametrization protocol, should be of the paramount importance for high-throughput applications and for overall progress of the model.

Finally, we would like to stress the importance of the continuous development and support of other CG models. As mentioned in the Introduction, different philosophies to CGing exist, each with their own merits and shortcomings. For certain application areas, specific CG force fields optimized for the task at hand can be a better choice—examples include protein folding studies with the UNRES force field,[19] prediction of nucleotide structure and hybridization with oxDNA,[18] studying molecular fluids with SAFT-γ,[428] or simulation of polymer dynamics either with generic models[429,430] or with bottom-up constructed (structure-based) CG models.[431–433] Further advancement of machine learning[434,435] will certainly contribute to this development, either by producing target force fields on demand, or in the process of integrating data from various resources to optimize existing ones, including Martini.[104] Encouraging is also to see the efforts of other CG force field developers to extend their models toward broader application ranges, providing more future opportunities to cross-validate predictions from Martini.

6 | CONCLUSION

Looking back at two decades of development, the Martini model has taken a firm place among the established force fields for molecular simulations. This is evidenced by the large number of groups that have embraced the model, in fields ranging all the way from cell biophysics to materials chemistry. Due to its inherent speedup compared to all-atom models, and its ease of use, the model has been integrated into many workflows, to aid in the interpretation of experimental data, to unravel molecular driving forces, and in the rational design of novel materials.

With the Martini 3 version recently established, and ongoing efforts to update the basic lipid, protein, saccharide, and nucleotide parameters taking full advantage of the new parameters, we can expect a further increase in accuracy and widening of the application horizons for the coming decade. At the same time, we expect a growing awareness of the limitations of coarse-graining in general (and Martini in particular), implying the ongoing need to validate predictions by experiments, and to benefit from multiscale approaches including higher resolution models. In combination with the ever-expanding number of auxiliary tools, we foresee breakthroughs in the coming years toward whole cell modeling, drug screening, and design of supramolecular materials.

AUTHOR CONTRIBUTIONS

Siewert J. Marrink: Conceptualization (lead); writing – original draft (lead); writing – review and editing (equal). **Luca Monticelli:** Conceptualization (supporting); writing – original draft (supporting); writing – review and editing (equal). **Manuel N. Melo:** Conceptualization (supporting); writing – original draft (supporting); writing – review and editing (equal). **Riccardo Alessandri:** Conceptualization (supporting); writing – original draft (supporting); writing – review and editing (equal). **D. Peter Tieleman:** Conceptualization (equal); writing – original draft (equal); writing – review and editing (equal). **Paulo C. T. Souza:** Conceptualization (equal); writing – original draft (equal); writing – review and editing (equal).

ACKNOWLEDGMENTS

Siewert J. Marrink acknowledges Gerhard Hummer for providing the image of the autophagosome, Chen Song for providing the image of the SARS-CoV2 viral envelope, Helgi Ingolfsson for providing the image of the multiscale MuMMi workflow, and both Helgi and Bart Bruininks for proofreading the manuscript. Riccardo Alessandri acknowledges Charly Empereur-Mot, Petteri Vainikka, and Najmeh Delavari for providing images for Figure 7.

FUNDING INFORMATION

Work in DPTs group is supported by the Natural Sciences and Engineering Research Council (Canada). Further support came from the Canada Research Chairs program. Riccardo Alessandri is supported by the Dutch Research Council (NWO Rubicon 019.202EN.028). Luca Monticelli is supported by the French National Institute of Health and Medical Research (INSERM). Paulo C. T. Souza is supported by French National Center for Scientific Research (CNRS).

17590884, 0, Downloaded from https://wires.onlinelibrary.wiley.com/doi/10.1002/wcms.1620 by Cochrane France, Wiley Online Library on [24/11/2022]. See the Terms and Conditions (https://onlinelibrary.wiley.com/terms-and-conditions) on Wiley Online Library for rules of use; OA articles are governed by the applicable Creative Commons License

Further funding of Paulo C. T. Souza and Luca Monticelli came from a research collaboration with PharmCADD. Siewert J. Marrink is supported by an Advanced Grant (COMP-O-CELL) from the European Research Council.

CONFLICT OF INTEREST

The authors have declared no conflicts of interest for this article.

DATA AVAILABILITY STATEMENT

Data sharing is not applicable to this article as no new data were created or analyzed in this study.

ORCID

Siewert J. Marrink https://orcid.org/0000-0001-8423-5277
Luca Monticelli https://orcid.org/0000-0002-6352-4595
Manuel N. Melo https://orcid.org/0000-0001-6567-0513
Riccardo Alessandri https://orcid.org/0000-0003-1948-5311
D. Peter Tieleman https://orcid.org/0000-0001-5507-0688
Paulo C. T. Souza https://orcid.org/0000-0003-0660-1301

RELATED WIREs ARTICLES

The power of coarse graining in biomolecular simulations

FURTHER READING

https://bioexcel.eu/webinar-perspective-on-the-martini-force-field-2018-04-18/.

REFERENCES

1. Levitt M, Warshel A. Computer simulation of protein folding. Nature. 1975;253:694–8.
2. Baumgärtner A, Binder K. Dynamics of entangled polymer melts: a computer simulation. J Chem Phys. 1998;75:2994–3005.
3. Hollingsworth SA, Dror RO. Molecular dynamics simulation for all. Neuron. 2018;99:1129–43.
4. Hsieh M-K, Yu Y, Klauda JB. All-atom modeling of complex cellular membranes. Langmuir. 2021;38:3–17.
5. Gupta C, Sarkar D, Tieleman DP, Singharoy A. The ugly, bad, and good stories of large-scale biomolecular simulations. Curr Opin Struct Biol. 2022;73:102338.
6. Saunders MG, Voth GA. Coarse-graining methods for computational biology. Annu Rev Biophys. 2013;42:73–93.
7. Ingólfsson HI, Lopez CA, Uusitalo JJ, de Jong DH, Gopal SM, Periole X, et al. The power of coarse graining in biomolecular simulations. WIREs Comput Mol Sci. 2014;4:225–48.
8. Kmiecik S, Gront D, Kolinski M, Wieteska L, Dawid AE, Kolinski A. Coarse-grained protein models and their applications. Chem Rev. 2016;116:7898–936.
9. Joshi SY, Deshmukh SA. A review of advancements in coarse-grained molecular dynamics simulations. Mol Simul. 2020;47:786–803.
10. Giulini M, Rigoli M, Mattiotti G, Menichetti R, Tarenzi T, Fiorentini R, et al. From system modeling to system analysis: the impact of resolution level and resolution distribution in the computer-aided investigation of biomolecules. Front Mol Biosci. 2021;8:460.
11. Singh N, Li W. Recent advances in coarse-grained models for biomolecules and their applications. Int J Mol Sci. 2019;20:3774.
12. Seo S, Shinoda W. SPICA force field for lipid membranes: domain formation induced by cholesterol. J Chem Theory Comput. 2019;15:762–74.
13. Kawamoto S, Liu H, Seo S, Miyazaki Y, Dixit M, DeVane R, et al. The SPICA force field for proteins and peptides. bio J. Chem. Theory Comput. 2022;18(5):3204–3217.
14. Machado MR, Barrera EE, Klein F, Sónora M, Silva S, Pantano S. The SIRAH 2.0 force field: Altius, Fortius. Citius J Chem Theory Comput. 2019;15:2719–33.
15. Barrera EE, Machado MR, Pantano S. Fat SIRAH: coarse-grained phospholipids to explore membrane-protein dynamics. J Chem Theory Comput. 2019;15:5674–88.
16. Lu L, Dama JF, Voth GA. Fitting coarse-grained distribution functions through an iterative force-matching method. J Chem Phys. 2013;139:121906.
17. Foley TT, Kidder KM, Scott Shell M, Noid WG. Exploring the landscape of model representations. Proc Natl Acad Sci USA. 2020;117:24061–8.
18. Sengar A, Ouldridge TE, Henrich O, Rovigatti L, Šulc P. A primer on the oxDNA model of DNA: when to use it, how to simulate it and how to interpret the results. Front Mol Biosci. 2021;8:551.
19. Sieradzan AK, Czaplewski C, Krupa P, Mozolewska MA, Karczyńska AS, Lipska AG, et al. Modeling the structure, dynamics, and transformations of proteins with the UNRES force field—methods in molecular biology. In: Muñoz V, editor. Protein Folding. New York, NY: Humana Press; 2022. p. 399–416.

17590884, 0, Downloaded from https://wires.onlinelibrary.wiley.com/doi/10.1002/wcms.1620 by Cochrane France, Wiley Online Library on [24/11/2022]. See the Terms and Conditions (https://onlinelibrary.wiley.com/terms-and-conditions) on Wiley Online Library for rules of use; OA articles are governed by the applicable Creative Commons License

20. Marrink SJ, Corradi V, Souza PCT, Ingólfsson HI, Tieleman DP, Sansom MSP. Computational modeling of realistic cell membranes. Chem Rev. 2019;119:6184–226.
21. Corradi V, Sejdiu BI, Mesa-Galloso H, Abdizadeh H, Noskov SY, Marrink SJ, et al. Emerging diversity in lipid-protein interactions. Chem Rev. 2019;119:5775–848.
22. Alessandri R, Grünewald F, Marrink SJ. The martini model in materials science. Adv Mater. 2021;33:2008635.
23. Panzuela S, Delgado-Buscalioni R. Solvent hydrodynamics enhances the collective diffusion of membrane lipids. Phys Rev Lett. 2018; 121:048101.
24. Tascini AS, Wang S, Seddon JM, Bresme F, Chen R. Fats' love–hate relationships: a molecular dynamics simulation and hands-on experiment outreach activity to introduce the amphiphilic nature and biological functions of lipids to young students and the general public. J Chem Educ. 2020;97:1360–7.
25. Coronavirus sculpture by Angela Palmer. [cited January 20, 2022). Available from https://www.angelaspalmer.com/coronavirus.
26. Martini Publications. See the link for the profile in this page. [cited February 6, 2022]. Available from http://cgmartini.nl/index.php/publications.
27. Marrink SJ, Mark AE. Molecular dynamics simulation of the formation, structure, and dynamics of small phospholipid vesicles. J Am Chem Soc. 2003;125:15233–42.
28. Marrink SJ, Mark AE. The mechanism of vesicle fusion as revealed by molecular dynamics simulations. J Am Chem Soc. 2003;125: 11144–5.
29. Marrink SJ, De Vries AH, Mark AE. Coarse grained model for Semiquantitative lipid simulations. J Phys Chem B. 2004;108:750–60.
30. Smit B, Hilbers PAJ, Esselink K, Rupert LAM, Van Os NM, Schlijper AG. Computer simulations of a water/oil interface in the presence of micelles. Nature. 1990;348:624–5.
31. Smit B, Esselink K, Hilbers PAJ, van Os NM, Rupert LAM, Szleifer I. Computer simulations of surfactant self-assembly. Langmuir. 1993;9:9–11.
32. Goetz R, Lipowsky R. Computer simulations of bilayer membranes: self-assembly and interfacial tension. J Chem Phys. 1998;108: 7397–409.
33. Shillcock JC, Lipowsky R. Equilibrium structure and lateral stress distribution of amphiphilic bilayers from dissipative particle dynamics simulations. J Chem Phys. 2002;117:5048–61.
34. Shelley JC, Shelley MY, Reeder RC, Bandyopadhyay S, Klein ML. A coarse grain model for phospholipid simulations. J Phys Chem B. 2001;105:4464–70.
35. Marrink SJ, Risselada HJ, Yefimov S, Tieleman DP, De Vries AH. The MARTINI force field: coarse grained model for biomolecular simulations. J Phys Chem B. 2007;111:7812–24.
36. Risselada HJ, Marrink SJ. The molecular face of lipid rafts in model membranes. Proc Natl Acad Sci. 2008;105:17367–72.
37. Arnarez C, Uusitalo JJ, Masman MF, Ingólfsson HI, De Jong DH, Melo MN, et al. Dry martini, a coarse-grained force field for lipid membrane simulations with implicit solvent. J Chem Theory Comput. 2015;11:260–75.
38. Zgorski A, Lyman E. Toward hydrodynamics with solvent free lipid models: STRD martini. Biophys J. 2016;111:2689–97.
39. Brandner AF, Timr S, Melchionna S, Derreumaux P, Baaden M, Sterpone F. Modelling lipid systems in fluid with lattice Boltzmann molecular dynamics simulations and hydrodynamics. Sci Rep. 2019;9:1–14.
40. López CA, Sovova Z, Van Eerden FJ, De Vries AH, Marrink SJ. Martini force field parameters for glycolipids. J Chem Theory Comput. 2013;9:1694–708.
41. Gu RX, Ingólfsson HI, De Vries AH, Marrink SJ, Tieleman DP. Ganglioside-lipid and ganglioside-protein interactions revealed by coarse-grained and atomistic molecular dynamics simulations. J Phys Chem B. 2017;121:3262–75.
42. Dahlberg M. Polymorphic phase behavior of Cardiolipin derivatives studied by coarse-grained molecular dynamics. J Phys Chem B. 2007;111:7194–200.
43. Lee H, Pastor RW. Coarse-grained model for PEGylated lipids: effect of PEGylation on the size and shape of self-assembled structures. J Phys Chem B. 2011;115:7830–7.
44. Grunewald F, Rossi G, de Vries AH, Marrink SJ, Monticelli L. Transferable MARTINI model of poly(ethylene oxide). J Phys Chem B. 2018;122:7436–49.
45. Ma H, Cummins DD, Edelstein NB, Gomez J, Khan A, Llewellyn MD, et al. Modeling diversity in structures of bacterial outer membrane lipids. J Chem Theory Comput. 2017;13:811–24.
46. Hsu PC, Jefferies D, Khalid S. Molecular dynamics simulations predict the pathways via which pristine fullerenes penetrate bacterial membranes. J Phys Chem B. 2016;120:11170–9.
47. Van Oosten B, Harroun TA. A MARTINI extension for *Pseudomonas aeruginosa* PAO1 lipopolysaccharide. J Mol Graph Model. 2016;63: 125–33.
48. Melo MN, Ingólfsson HI, Marrink SJ. Parameters for martini sterols and hopanoids based on a virtual-site description. J Chem Phys. 2015;143:243152.
49. Monticelli L, Kandasamy SK, Periole X, Larson RG, Tieleman DP, Marrink SJ. The MARTINI coarse-grained force field: extension to proteins. J Chem Theory Comput. 2008;4:819–34.
50. De Jong DH, Singh G, Bennett WFD, Arnarez C, Wassenaar TA, Schäfer LV, et al. Improved parameters for the martini coarse-grained protein force field. J Chem Theory Comput. 2013;9:687–97.
51. Periole X, Cavalli M, Marrink S-JJ, Ceruso MA. Combining an elastic network with a coarse-grained molecular force field: structure, dynamics, and intermolecular recognition. J Chem Theory Comput. 2009;5:2531–43.

17590884, 0, Downloaded from https://wires.onlinelibrary.wiley.com/doi/10.1002/wcms.1620 by Cochrane France, Wiley Online Library on [24/11/2022]. See the Terms and Conditions (https://onlinelibrary.wiley.com/terms-and-conditions) on Wiley Online Library for rules of use; OA articles are governed by the applicable Creative Commons License

52. Periole X, Huber T, Marrink SJ, Sakmar TP. G protein-coupled receptors self-assemble in dynamics simulations of model bilayers. J Am Chem Soc. 2007;129:10126–32.
53. Yefimov S, Van Der Giessen E, Onck PR, Marrink SJ. Mechanosensitive membrane channels in action. Biophys J. 2008;94: 2994–3002.
54. Bond PJ, Sansom MSP. Insertion and assembly of membrane proteins via simulation. J Am Chem Soc. 2006;128:2697–704.
55. Shih AY, Arkhipov A, Freddolino PL, Schulten K. Coarse grained protein−lipid model with application to lipoprotein particles†. J Phys Chem B. 2006;110:3674–84.
56. López CA, Rzepiela AJ, de Vries AH, Dijkhuizen L, Hünenberger PH, Marrink SJ. Martini coarse-grained force field: extension to carbohydrates. J Chem Theory Comput. 2009;5:3195–210.
57. Uusitalo JJ, Ingólfsson HI, Akhshi P, Tieleman DP, Marrink SJ. Martini coarse-grained force field: extension to DNA. J Chem Theory Comput. 2015;11:3932–45.
58. Uusitalo JJ, Ingólfsson HI, Marrink SJ, Faustino I. Martini coarse-grained force field: extension to RNA. Biophys J. 2017;113:246–56.
59. Atsmon-Raz Y, Tieleman DP. Parameterization of Palmitoylated cysteine, Farnesylated cysteine, Geranylgeranylated cysteine, and Myristoylated glycine for the martini force field. J Phys Chem B. 2017;121:11132–43.
60. Shivgan AT, Marzinek JK, Huber RG, Krah A, Henchman RH, Matsudaira P, et al. Extending the martini coarse-grained force field to N-Glycans. J Chem Inf Model. 2020;60:3864–83.
61. De Jong DH, Liguori N, Van Den Berg T, Arnarez C, Periole X, Marrink SJ. Atomistic and coarse grain topologies for the cofactors associated with the photosystem II Core complex. J Phys Chem B. 2015;119:7791–803.
62. Sousa FM, Lima LMP, Arnarez C, Pereira MM, Melo MN. Coarse-grained parameterization of nucleotide cofactors and metabolites: protonation constants, partition coefficients, and model topologies. J Chem Inf Model. 2021;61:335–46.
63. Lee H, De Vries AH, Marrink SJ, Pastor RW. A coarse-grained model for polyethylene oxide and polyethylene glycol: conformation and hydrodynamics. J Phys Chem B. 2009;113:13186–94.
64. Wong-Ekkabut J, Baoukina S, Triampo W, Tang IM, Tieleman DP, Monticelli L. Computer simulation study of fullerene translocation through lipid membranes. Nat Nanotechnol. 2008;3:363–8.
65. Jarin Z, Newhouse J, Voth GA. Coarse-grained force fields from the perspective of statistical mechanics: better understanding of the origins of a MARTINI hangover. J Chem Theory Comput. 2021;17:1170–80.
66. Marrink SJ, Tieleman DP. Perspective on the martini model. Chem Soc Rev. 2013;42:6801–22.
67. Yesylevskyy SO, Schäfer LV, Sengupta D, Marrink SJ. Polarizable water model for the coarse-grained MARTINI force field. PLoS Comput Biol. 2010;6:e1000810.
68. Michalowsky J, Schäfer LV, Holm C, Smiatek J. A refined polarizable water model for the coarse-grained MARTINI force field with long-range electrostatic interactions. J Chem Phys. 2017;146:054501.
69. Michalowsky J, Zeman J, Holm C, Smiatek J. A polarizable MARTINI model for monovalent ions in aqueous solution. J Chem Phys. 2018;149:163319.
70. Piskorz TK, De Vries AH, Van Esch JH. How the choice of force-field affects the stability and self-assembly process of supramolecular CTA fibers. J Chem Theory Comput. 2021;18:431–40.
71. Bochicchio D, Pavan GM. From cooperative self-assembly to water-soluble supramolecular polymers using coarse-grained simulations. ACS Nano. 2017;11:1000–11.
72. Khan HM, Souza PCT, Thallmair S, Barnoud J, De Vries AH, Marrink SJ, et al. Capturing choline-aromatics cation-πInteractions in the MARTINI force field. J Chem Theory Comput. 2020;16:2550–60.
73. De Jong DH, Baoukina S, Ingólfsson HI, Marrink SJ. Martini straight: boosting performance using a shorter cutoff and GPUs. Comput Phys Commun. 2016;199:1–7.
74. Grünewald F, Souza PCT, Abdizadeh H, Barnoud J, De Vries AH, Marrink SJ. Titratable Martini model for constant pH simulations. J Chem Phys. 2020;153:024118.
75. Hossain S, Parrow A, Kabedev A, Kneiszl RC, Leng Y, Larsson P. Explicit-pH coarse-grained molecular dynamics simulations enable insights into restructuring of intestinal colloidal aggregates with permeation enhancers. Processes. 2022;10:29.
76. Jin J, Pak AJ, Voth GA. Understanding missing entropy in coarse-grained systems: addressing issues of representability and transferability. J Phys Chem Lett. 2019;10:4549–57.
77. Wagner JW, Dama JF, Durumeric AEP, Voth GA. On the representability problem and the physical meaning of coarse-grained models. J Chem Phys. 2016;145:044108.
78. Stark AC, Andrews CT, Elcock AH. Toward optimized potential functions for protein-protein interactions in aqueous solutions: osmotic second virial coefficient calculations using the MARTINI coarse-grained force field. J Chem Theory Comput. 2013;9:4176–85.
79. Javanainen M, Martinez-Seara H, Vattulainen I. Excessive aggregation of membrane proteins in the martini model. PLoS One. 2017;12: e0187936.
80. Majumder A, Straub JE. Addressing the excessive aggregation of membrane proteins in the MARTINI model. J Chem Theory Comput. 2021;17:2513–21.
81. Schmalhorst PS, Deluweit F, Scherrers R, Heisenberg CP, Sikora M. Overcoming the limitations of the MARTINI force field in simulations of polysaccharides. J Chem Theory Comput. 2017;13:5039–53.
82. Alessandri R, Souza PCT, Thallmair S, Melo MN, De Vries AH, Marrink SJ. Pitfalls of the martini model. J Chem Theory Comput. 2019; 15:5448–60.

17590884, 0, Downloaded from https://wires.onlinelibrary.wiley.com/doi/10.1002/wcms.1620 by Cochrane France, Wiley Online Library on [24/11/2022]. See the Terms and Conditions (https://onlinelibrary.wiley.com/terms-and-conditions) on Wiley Online Library for rules of use; OA articles are governed by the applicable Creative Commons License

83. Souza PCT, Alessandri R, Barnoud J, Thallmair S, Faustino I, Grünewald F, et al. Martini 3: a general purpose force field for coarse-grained molecular dynamics. Nat Methods. 2021;18:382–8.
84. Vanommeslaeghe K, Hatcher E, Acharya C, Kundu S, Zhong S, Shim J, et al. CHARMM general force field: a force field for drug-like molecules compatible with the CHARMM all-atom additive biological force fields. J Comput Chem. 2010;31:671–90.
85. Wang J, Wolf RM, Caldwell JW, Kollman PA, Case DA. Development and testing of a general amber force field. J Comput Chem. 2004; 25:1157–74.
86. Vazquez-Salazar LI, Selle M, De Vries AH, Marrink SJ, Souza PCT. Martini coarse-grained models of imidazolium-based ionic liquids: from nanostructural organization to liquid–liquid extraction. Green Chem. 2020;22:7376–86.
87. Barbosa GD, Turner CH. Martini coarse-grained model for poly(alkylimidazolium) Ionenes and applications in aromatic compound extraction. Macromolecules. 2021;55:26–34.
88. Vainikka P, Thallmair S, Souza PCT, Marrink SJ. Martini 3 coarse-grained model for type III deep eutectic solvents: thermodynamic, structural, and extraction properties. ACS Sustain Chem Eng. 2021;9:17338–50.
89. Tsanai M, Frederix PWJM, Schroer CFE, Souza PCT, Marrink SJ. Coacervate formation studied by explicit solvent coarse-grain molecular dynamics with the martini model. Chem Sci. 2021;12:8521–30.
90. Thomasen FE, Pesce F, Roesgaard MA, Tesei G, Lindorff-Larsen K. Improving Martini 3 for disordered and multidomain proteins. J Chem Theory Comput. 2022;18:2033–41.
91. Wassenaar TA, Ingólfsson HI, Böckmann RA, Tieleman DP, Marrink SJ. Computational Lipidomics with insane: a versatile tool for generating custom membranes for molecular simulations. J Chem Theory Comput. 2015;11:2144–55.
92. Qi Y, Ingólfsson HI, Cheng X, Lee J, Marrink SJ, Im W. CHARMM-GUI martini maker for coarse-grained simulations with the martini force field. J Chem Theory Comput. 2015;11:4486–94.
93. Hsu PC, Bruininks BMH, Jefferies D, Souza PCT, Lee J, Patel DS, et al. CHARMM-GUI martini maker for modeling and simulation of complex bacterial membranes with lipopolysaccharides. J Comput Chem. 2017;38:2354–63.
94. Wassenaar TA, Pluhackova K, Moussatova A, Sengupta D, Marrink SJ, Tieleman DP, et al. High-throughput simulations of dimer and trimer assembly of membrane proteins. The DAFT approach. J Chem Theory Comput. 2015;11:2278–91.
95. Rajagopal N, Nangia S. Obtaining protein association energy landscape for integral membrane proteins. J Chem Theory Comput. 2019; 15:6444–55.
96. Damre M, Marchetto A, Giorgetti A. MERMAID: dedicated web server to prepare and run coarse-grained membrane protein dynamics. Nucleic Acids Res. 2019;47:W456–61.
97. Marchetto A, Si Chaib Z, Rossi CA, Ribeiro R, Pantano S, Rossetti G, et al. CGMD platform: integrated web servers for the preparation, running, and analysis of coarse-grained molecular dynamics simulations. Molecules. 2020;25:5934.
98. Grünewald F, Alessandri R, Kroon PC, Monticelli L, Souza PCT, Siewert, et al. Polyply: a python suite for facilitating simulations of macromolecules and nanomaterials. Nat Commun. 2022;13:68.
99. Kjølbye LR, De Maria L, Wassenaar TA, Abdizadeh H, Marrink SJ, Ferkinghoff-Borg J, et al. General protocol for constructing molecular models of nanodiscs. J Chem Inf Model. 2021;61:2869–83.
100. Graham JA, Essex JW, Khalid S. PyCGTOOL: automated generation of coarse-grained molecular dynamics models from atomistic trajectories. J Chem Inf Model. 2017;57:650–6.
101. Empereur-Mot C, Pesce L, Doni G, Bochicchio D, Capelli R, Perego C, et al. Swarm-CG: automatic parametrization of bonded terms in MARTINI-based coarse-grained models of simple to complex molecules via fuzzy self-tuning particle swarm optimization. ACS Omega. 2020;5:32823–43.
102. Bereau T, Kremer K. Automated parametrization of the coarse-grained martini force field for small organic molecules. J Chem Theory Comput. 2015;11:2783–91.
103. Potter TD, Barrett EL, Miller MA. Automated coarse-grained mapping algorithm for the martini force field and benchmarks for membrane-water partitioning. J Chem Theory Comput. 2021;17:5791–1.
104. Empereur-mot C, Capelli R, Perrone M, Caruso C, Doni G, Pavan GM. Automatic multi-objective optimization of coarse-grained lipid force fields using SwarmCG. J Chem Phys. 2022;156:024801.
105. Sejdiu BI, Tieleman DP. ProLint: a web-based framework for the automated data analysis and visualization of lipid–protein interactions. Nucleic Acids Res. 2021;49:W544–50.
106. Song W, Corey RA, Ansell TB, Cassidy CK, Horrell MR, Duncan AL, et al. PyLipID: a python package for analysis of protein–lipid interactions from molecular dynamics simulations. J Chem Theory Comput. 2022;18:1188–201.
107. Bhatia H, Ingólfsson HI, Carpenter TS, Lightstone FC, Bremer PT. MemSurfer: a tool for robust computation and characterization of curved membranes. J Chem Theory Comput. 2019;15:6411–21.
108. Bruininks BMH, Thie AS, Souza PCT, Wassenaar TA, Faraji S, Marrink SJ. Sequential voxel-based leaflet segmentation of complex lipid morphologies. J Chem Theory Comput. 2021;17:7885–5.
109. Faustino I, Marrink SJ. cgHeliParm: analysis of dsDNA helical parameters for coarse-grained MARTINI molecular dynamics simulations. Bioinformatics. 2017;33:3813–5.
110. López CA, Vesselinov VV, Gnanakaran S, Alexandrov BS. Unsupervised machine learning for analysis of phase separation in ternary lipid mixture. J Chem Theory Comput. 2019;15:6343–57.
111. Paissoni C, Jussupow A, Camilloni C. Martini bead form factors for nucleic acids and their application in the refinement of protein–nucleic acid complexes against SAXS data. J Appl Cryst. 2019;52:394–402.

17590884, 0, Downloaded from https://wires.onlinelibrary.wiley.com/doi/10.1002/wcms.1620 by Cochrane France, Wiley Online Library on [24/11/2022]. See the Terms and Conditions (https://onlinelibrary.wiley.com/terms-and-conditions) on Wiley Online Library for rules of use; OA articles are governed by the applicable Creative Commons License

112. Saracino GAA, Fontana F, Jekhmane S, Medeiros Silva J, Weingarth M, Gelain F, et al. Elucidating self-assembling peptide aggregation via Morphoscanner: a new tool for protein-peptide structural characterization. Adv Sci. 2018;5:1800471.
113. Fábián B, Javanainen M. CurD: a tool for diffusion analyses on curved membranes. ChemRxiv. 2021. doi:10.26434/chemrxiv-2021-6wksn
114. Lelimousin M, Limongelli V, Sansom MSP. Conformational changes in the epidermal growth factor receptor: role of the transmembrane domain investigated by coarse-grained MetaDynamics free energy calculations. J Am Chem Soc. 2016;138:10611–22.
115. Corey RA, Vickery ON, Sansom MSP, Stansfeld PJ. Insights into membrane protein-lipid interactions from free energy calculations. J Chem Theory Comput. 2019;15:5727–36.
116. Nagai T, Okamoto Y. Replica-exchange molecular dynamics simulation of a lipid bilayer system with a coarse-grained model. Mol Simul. 2012;38:437–41.
117. Domański J, Hedger G, Best RB, Stansfeld PJ, Sansom MSP. Convergence and sampling in determining free energy landscapes for membrane protein association. J Phys Chem B. 2017;121:3364–75.
118. Altwaijry NA, Baron M, Wright DW, Coveney PV, Townsend-Nicholson A. An ensemble-based protocol for the computational prediction of helix–helix interactions in G protein-coupled receptors using coarse-grained molecular dynamics. J Chem Theory Comput. 2017;13:2254–70.
119. Cherniavskyi YK, Fathizadeh A, Elber R, Tieleman DP. Computer simulations of a heterogeneous membrane with enhanced sampling techniques. J Chem Phys. 2020;153:144110.
120. Chiavazzo E, Covino R, Coifman RR, Gear CW, Georgiou AS, Hummer G, et al. Intrinsic map dynamics exploration for uncharted effective free-energy landscapes. Proc Natl Acad Sci USA. 2017;114:E5494–503.
121. Jung H, Covino R, Arjun A, Bolhuis PG, Hummer G. Autonomous artificial intelligence discovers mechanisms of molecular self-organization in virtual experiments. arXiv. 2021. doi:10.48550/arXiv.2105.06673
122. Kasson PM, Kelley NW, Singhal N, Vrljic M, Brunger AT, Pande VS. Ensemble molecular dynamics yields submillisecond kinetics and intermediates of membrane fusion. Proc Natl Acad Sci USA. 2006;103:11916–21.
123. Amos SBTA, Schwarz TC, Shi J, Cossins BP, Baker TS, Taylor RJ, et al. Membrane interactions of α-Synuclein revealed by multiscale molecular dynamics simulations, Markov state models, and NMR. J Phys Chem B. 2021;125:2929–41.
124. Methorst J, van Hilten N, Risselada HJ. Inverse design of cholesterol attracting transmembrane helices reveals a paradoxical role of hydrophobic length. bioRxiv. 2021. doi:10.1101/2021.07.01.450699
125. Wassenaar TA, Pluhackova K, Böckmann RA, Marrink SJ, Tieleman DP. Going backward: a flexible geometric approach to reverse transformation from coarse grained to atomistic models. J Chem Theory Comput. 2014;10:676–90.
126. Stansfeld PJ, Sansom MSP. From coarse grained to atomistic: a serial multiscale approach to membrane protein simulations. J Chem Theory Comput. 2011;7:1157–66.
127. Vickery ON, Stansfeld PJ. CG2AT2: an enhanced fragment-based approach for serial multi-scale molecular dynamics simulations. J Chem Theory Comput. 2021;17:6472–82.
128. Louison KA, Dryden IL, Laughton CA. GLIMPS: a machine learning approach to resolution transformation for multiscale modeling. J Chem Theory Comput. 2021;17:7930–7.
129. Pezeshkian W, König M, Marrink SJ, Ipsen JH. A multi-scale approach to membrane remodeling processes. Front Mol Biosci. 2019;6:59.
130. Pezeshkian W, König M, Wassenaar TA, Marrink SJ. Backmapping triangulated surfaces to coarse-grained membrane models. Nat Commun. 2020;11:2296.
131. Rzepiela AJ, Louhivuori M, Peter C, Marrink SJ. Hybrid simulations: combining atomistic and coarse-grained force fields using virtual sites. Phys Chem Chem Phys. 2011;13:10437–48.
132. Wassenaar TA, Ingoífsson HI, Prieß M, Marrink SJ, Schäfer LV. Mixing MARTINI: electrostatic coupling in hybrid atomistic−coarse-grained biomolecular simulations. J Phys Chem B. 2013;117(13):3516–30.
133. Liu Y, De Vries AH, Barnoud J, Pezeshkian W, Melcr J, Marrink SJ. Dual resolution membrane simulations using virtual sites. J Phys Chem B. 2020;124:3944–53.
134. Han W, Wan CK, Jiang F, Wu YD. PACE force field for protein simulations. 1. Full parameterization of version 1 and verification. J Chem Theory Comput. 2010;6:3373–89.
135. Wan CK, Han W, Wu YD. Parameterization of PACE force field for membrane environment and simulation of helical peptides and helix-helix association. J Chem Theory Comput. 2012;8:300–13.
136. Han W, Schulten K. Further optimization of a hybrid united-atom and coarse-grained force field for folding simulations: improved backbone hydration and interactions between charged side chains. J Chem Theory Comput. 2012;8:4413–24.
137. Fuladi S, McGuinness S, Shen L, Weber CR, Khalili-Araghi F. Molecular mechanism of claudin-15 strand flexibility. bioRxiv. 2021. doi:10.1101/2021.12.07.471660
138. Qi Y, Cheng X, Han W, Jo S, Schulten K, Im W. CHARMM-GUI PACE CG builder for solution, micelle, and bilayer coarse-grained simulations. J Chem Inf Model. 2014;54:1003–9.
139. Yan XC, Tirado-Rives J, Jorgensen WL. Hydration properties and solvent effects for all-atom solutes in polarizable coarse-grained water. J Phys Chem B. 2016;120:8102–14.
140. Sokkar P, Boulanger E, Thiel W, Sanchez-Garcia E. Hybrid quantum mechanics/molecular mechanics/coarse grained modeling: a triple-resolution approach for biomolecular systems. J Chem Theory Comput. 2015;11:1809–18.

17590884, 0, Downloaded from https://wires.onlinelibrary.wiley.com/doi/10.1002/wcms.1620 by Cochrane France, Wiley Online Library on [24/11/2022]. See the Terms and Conditions (https://onlinelibrary.wiley.com/terms-and-conditions) on Wiley Online Library for rules of use; OA articles are governed by the applicable Creative Commons License

141. Risselada HJ, Mark AE, Marrink SJ. Application of mean field boundary potentials in simulations of lipid vesicles. J Phys Chem B. 2008;112:7438–47.
142. Zavadlav J, Melo MN, Marrink SJ, Praprotnik M. Adaptive resolution simulation of an atomistic protein in MARTINI water. J Chem Phys. 2014;140:054114.
143. Zavadlav J, Marrink SJ, Praprotnik M. SWINGER: a clustering algorithm for concurrent coupling of atomistic and supramolecular liquids. Interface Focus. 2019;9:20180075.
144. Wagoner JA, Pande VS. Communication: adaptive boundaries in multiscale simulations. J Chem Phys. 2018;148:141104.
145. Liu Y, Pezeshkian W, Barnoud J, De Vries AH, Marrink SJ. Coupling coarse-grained to fine-grained models via Hamiltonian replica exchange. J Chem Theory Comput. 2020;16:5313–22.
146. Yasar F, Ray AJ, Hansmann UHE. Resolution exchange with tunneling for enhanced sampling of protein landscapes. arXiv. 2021. doi: 10.48550/arXiv.2110.12546
147. Christen M, Van Gunsteren WF. Multigraining: an algorithm for simultaneous fine-grained and coarse-grained simulation of molecular systems. J Chem Phys. 2006;124:154106.
148. van Gunsteren WF. The roots of bio-molecular simulation: the eight-week CECAM workshop 'models for protein dynamics' of 1976. Helv Chim Acta. 2019;102:e1800239.
149. Martini Coarse-Grained Force Field Web-portal. [cited January 20, 2022]. Available from: http://cgmartini.nl/.
150. Grünewald F, Kroon PC, Souza PCT, Marrink SJ. Protocol for simulations of PEGylated proteins with martini 3. In: Chen YW, Yiu C-PB, editors. Structural genomics—general applications. New York, NY: Humana Press; 2021. p. 315–35.
151. Jefferies D, Khalid S. Atomistic and coarse-grained simulations of membrane proteins: a practical guide. Methods. 2021;185:15–27.
152. Bruininks BMH, Souza PCT, Marrink SJ. A practical view of the martini force field. In: Bonomi M, Camilloni C, editors. Biomolecular simulations—methods and protocols. Humana Press: New York, NY; 2019. p. 105–27.
153. Periole X, Marrink SJ. The martini coarse-grained force field. In: Monticelli L, Salonen E, editors. Biomolecular simulations - methods in molecular biology (methods and protocols). Totowa, NJ: Humana Press; 2013. p. 533–65.
154. Barnoud J, Monticelli L. Coarse-grained force fields for molecular simulations. In: Kukol A, editor. Molecular modeling of proteins—methods in molecular biology (methods and protocols). New York, NY: Humana Press; 2015. p. 125–49.
155. MAD - MArtini Database. [cited January 20, 2022]. Available from: https://mad.ibcp.fr/explore.
156. Abraham MJ, Murtola T, Schulz R, Páll S, Smith JC, Hess B, et al. GROMACS: high performance molecular simulations through multi-level parallelism from laptops to supercomputers. SoftwareX. 2015;1–2:19–25.
157. Phillips JC, Hardy DJ, Maia JDC, Stone JE, Ribeiro JV, Bernardi RC, et al. Scalable molecular dynamics on CPU and GPU architectures with NAMD. J Chem Phys. 2020;153:044130.
158. Jewett AI, Stelter D, Lambert J, Saladi SM, Roscioni OM, Ricci M, et al. Moltemplate: a tool for coarse-grained modeling of complex biological matter and soft condensed matter physics. J Mol Biol. 2021;433:166841.
159. Zhang X, Sundram S, Oppelstrup T, Kokkila-Schumacher SIL, Carpenter TS, Ingólfsson HI, et al. ddcMD: a fully GPU-accelerated molecular dynamics program for the martini force field. J Chem Phys. 2020;153:045103.
160. Eastman P, Swails J, Chodera JD, McGibbon RT, Zhao Y, Beauchamp KA, et al. OpenMM 7: rapid development of high performance algorithms for molecular dynamics. PLoS Comput Biol. 2017;13:e1005659.
161. ACEMD Manual. [cited January 20, 2022]. Available from https://software.acellera.com/docs/stable/acemd/usermanual.html.
162. Harvey MJ, Giupponi G, De Fabritiis G. ACEMD: accelerating biomolecular dynamics in the microsecond time scale. J Chem Theory Comput. 2009;5:1632–9.
163. Sharma S, Kumar P, Chandra R. Applications of BIOVIA materials studio, LAMMPS, and GROMACS in various fields of science and engineering. In: Sharma S, editor. Molecular dynamics simulation of nanocomposites using BIOVIA materials studio, Lammps and Gromacs. Amsterdam: Elsevier; 2019. p. 329–41.
164. Kobayashi C, Jung J, Matsunaga Y, Mori T, Ando T, Tamura K, et al. GENESIS 1.1: a hybrid-parallel molecular dynamics simulator with enhanced sampling algorithms on multiple computational platforms. J Comput Chem. 2017;38:2193–206.
165. Honorato RV, Roel-Touris J, Bonvin AMJJ. MARTINI-based protein-DNA coarse-grained HADDOCKing. Front Mol Biosci. 2019;6:102.
166. Roel-Touris J, Don CG, Honorato RR, Rodrigues JPGLM, Bonvin AMJJ. Less is more: coarse-grained integrative modeling of large biomolecular assemblies with HADDOCK. J Chem Theory Comput. 2019;15:6358–67.
167. Roel-Touris J, Jiménez-García B, Bonvin AMJJ. Integrative modeling of membrane-associated protein assemblies. Nat Commun. 2020;11:6210.
168. Kanekal KH, Bereau T. Resolution limit of data-driven coarse-grained models spanning chemical space. J Chem Phys. 2019;151:164106.
169. Alessandri R, Barnoud J, Gertsen AS, Patmanidis I, De Vries AH, Souza PCT, et al. Martini 3 coarse-grained force field: small molecules. Adv Theory Simulations. 2022;5:2100391.
170. Ploetz EA, Bentenitis N, Smith PE. Kirkwood-buff integrals for ideal solutions. J Chem Phys. 2010;132:164501.
171. Okur HI, Hladílková J, Rembert KB, Cho Y, Heyda J, Dzubiella J, et al. Beyond the Hofmeister series: ion-specific effects on proteins and their biological functions. J Phys Chem B. 2017;121:1997–2014.
172. Dupont D, Depuydt D, Binnemans K. Overview of the effect of salts on biphasic ionic liquid/water solvent extraction systems: anion exchange, mutual solubility, and thermomorphic properties. J Phys Chem B. 2015;119:6747–57.

17590884, 0, Downloaded from https://wires.onlinelibrary.wiley.com/doi/10.1002/wcms.1620 by Cochrane France, Wiley Online Library on [24/11/2022]. See the Terms and Conditions (https://onlinelibrary.wiley.com/terms-and-conditions) on Wiley Online Library for rules of use; OA articles are governed by the applicable Creative Commons License

173. Liu J, Qiu L, Alessandri R, Qiu X, Portale G, Dong JJ, et al. Enhancing molecular n-type doping of donor–acceptor copolymers by tailoring side chains. Adv Mater. 2018;30:1704630.
174. Borges-Araújo L, Souza PCT, Fernandes F, Melo MN. Improved parameterization of Phosphatidylinositide lipid Headgroups for the martini 3 coarse-grain force field. J Chem Theory Comput. 2022;18:357–73.
175. Yu G, Wilson MR. Molecular simulation studies of self-assembly for a chromonic perylene dye: all-atom studies and new approaches to coarse-graining. J Mol Liq. 2022;345:118210.
176. Herzog FA, Braun L, Schoen I, Vogel V. Improved side chain dynamics in MARTINI simulations of protein-lipid interfaces. J Chem Theory Comput. 2016;12:2446–58.
177. Poma AB, Cieplak M, Theodorakis PE. Combining the MARTINI and structure-based coarse-grained approaches for the molecular dynamics studies of conformational transitions in proteins. J Chem Theory Comput. 2017;13:1366–74.
178. Liu Z, Moreira RA, Dujmović A, Liu H, Yang B, Poma AB, et al. Mapping Mechanostable pulling geometries of a therapeutic Anticalin/CTLA-4 protein complex. Nano Lett. 2022;22:179–87.
179. Mahmood MI, Poma AB, Okazak KI. Optimizing Gō-MARTINI coarse-grained model for F-BAR protein on lipid membrane. Front Mol Biosci. 2021;8:32.
180. Souza PCT, Thallmair S, Marrink SJ, Mera-Adasme R. An allosteric pathway in copper, zinc superoxide dismutase unravels the molecular mechanism of the G93A amyotrophic lateral sclerosis-linked mutation. J Phys Chem Lett. 2019;10:7740–4.
181. Lamprakis C, Andreadelis I, Manchester J, Velez-Vega C, Duca JS, Cournia Z. Evaluating the efficiency of the martini force field to study protein dimerization in aqueous and membrane environments. J Chem Theory Comput. 2021;17:3088–102.
182. Srinivasan S, Zoni V, Vanni S. Estimating the accuracy of the MARTINI model towards the investigation of peripheral protein–membrane interactions. Faraday Discuss. 2021;232:131–48.
183. Souza PCT, Thallmair S, Conflitti P, Ramírez-Palacios C, Alessandri R, Raniolo S, et al. Protein–ligand binding with the coarse-grained martini model. Nat Commun. 2020;11:3714.
184. Sahoo AR, Souza PCT, Meng Z, Buck M. Predicting transmembrane (TM) domain dimer structures using martini. bioRxiv. 2021;3. doi: 10.1101/2021.09.10.459840
185. Thallmair S, Javanainen M, Fábián B, Martinez-Seara H, Marrink SJ. Nonconverged constraints cause artificial temperature gradients in lipid bilayer simulations. J Phys Chem B. 2021;125:9537–46.
186. Rowland RS, Taylor R. Intermolecular nonbonded contact distances in organic crystal structures: comparison with distances expected from van der Waals radii. J Phys Chem. 1996;100:7384–91.
187. Bulacu M, Goga N, Zhao W, Rossi G, Monticelli L, Periole X, et al. Improved angle potentials for coarse-grained molecular dynamics simulations. J Chem Theory Comput. 2013;9:3282–92.
188. Abraham MJ, Murtola T, Schulz R, Pálla S, Smith JC, Hess B, et al. GROMACS: high performance molecular simulations through multi-level parallelism from laptops to supercomputers. SoftwareX. 2015;1–2:19–25.
189. Vögele M, Köfinger J, Hummer G. Hydrodynamics of diffusion in lipid membrane simulations. Phys Rev Lett. 2018;120:268104.
190. Pawar AB, Deshpande SA, Gopal SM, Wassenaar TA, Athale CA, Sengupta D. Thermodynamic and kinetic characterization of transmembrane helix association. Phys Chem Chem Phys. 2014;17:1390–8.
191. Ingólfsson HI, Neale C, Carpenter TS, Shrestha R, López CA, Tran TH, et al. Machine learning–driven multiscale modeling reveals lipid-dependent dynamics of RAS signaling proteins. Proc Natl Acad Sci USA. 2022;119:e2113297119.
192. Corradi V, Mendez-Villuendas E, Ingólfsson HI, Gu R-XX, Siuda I, Melo MN, et al. Lipid-protein interactions are unique fingerprints for membrane proteins. ACS Cent Sci. 2018;4:709–17.
193. Enkavi G, Javanainen M, Kulig W, Róg T, Vattulainen I. Multiscale simulations of biological membranes: the challenge to understand biological phenomena in a living substance. Chem Rev. 2019;119:5607–774.
194. Ingolfsson HI, Melo MN, van Eerden FJ, Arnarez C, Lopez CA, Wassenaar TA, et al. Lipid Organization of the Plasma Membrane. J Am Chem Soc. 2014;136:14554–9.
195. Ingólfsson HI, Carpenter TS, Bhatia H, Bremer PT, Marrink SJ, Lightstone FC. Computational Lipidomics of the neuronal plasma membrane. Biophys J. 2017;113:2271–80.
196. Machado N, Bruininks BMH, Singh P, Dos Santos L, Dal Pizzol C, Dieamant GDC, et al. Complex nanoemulsion for vitamin delivery: droplet organization and interaction with skin membranes. Nanoscale. 2022;14:506–14.
197. Wilson KA, Fairweather SJ, Macdermott-Opeskin HI, Wang L, Morris RA, O'mara ML. The role of plasmalogens, Forssman lipids, and sphingolipid hydroxylation in modulating the biophysical properties of the epithelial plasma membrane. J Chem Phys. 2021;154:095101.
198. Ma H, Irudayanathan FJ, Jiang W, Nangia S. Simulating gram-negative bacterial outer membrane: a coarse grain model. J Phys Chem B. 2015;119:14668–82.
199. Jefferies D, Shearer J, Khalid S. Role of O-antigen in response to mechanical stress of the E. coli outer membrane: insights from coarse-grained MD simulations. J Phys Chem B. 2019;123:3567–75.
200. Sezgin E, Levental I, Mayor S, Eggeling C. The mystery of membrane organization: composition, regulation and roles of lipid rafts. Nat Rev Mol Cell Biol. 2017;18:361–74.
201. Wang Y, Gkeka P, Fuchs JE, Liedl KR, Cournia Z. DPPC-cholesterol phase diagram using coarse-grained molecular dynamics simulations. Biochim Biophys Acta Biomembranes. 2016;1858:2846–57.

17590884, 0, Downloaded from https://wires.onlinelibrary.wiley.com/doi/10.1002/wcms.1620 by Cochrane France, Wiley Online Library on [24/11/2022]. See the Terms and Conditions (https://onlinelibrary.wiley.com/terms-and-conditions) on Wiley Online Library for rules of use; OA articles are governed by the applicable Creative Commons License

202. Carpenter TS, López CA, Neale C, Montour C, Ingólfsson HI, Di Natale F, et al. Capturing phase behavior of ternary lipid mixtures with a refined martini coarse-grained force field. J Chem Theory Comput. 2018;14:6050–62.
203. Gu RX, Baoukina S, Peter TD. Phase separation in atomistic simulations of model membranes. J Am Chem Soc. 2020;142:2844–56.
204. Muller MP, Jiang T, Sun C, Lihan M, Pant S, Mahinthichaichan P, et al. Characterization of lipid–protein interactions and lipid-mediated modulation of membrane protein function through molecular simulation. Chem Rev. 2019;119:6086–161.
205. Arnarez C, Marrink SJ, Periole X. Identification of cardiolipin binding sites on cytochrome c oxidase at the entrance of proton channels. Sci Rep. 2013;3:1263.
206. Arnarez C, Mazat J-P, Elezgaray J, Marrink S-J, Periole X. Evidence for Cardiolipin binding sites on the membrane-exposed surface of the cytochrome bc 1. J Am Chem Soc. 2013;135:3112–20.
207. Stansfeld PJ, Hopkinson R, Ashcroft FM, Sansom MSP. PIP2-binding site in Kir channels: definition by multiscale biomolecular simulations. Biochemistry. 2009;48:10926–33.
208. Duncan AL, Corey RA, Sansom MSP. Defining how multiple lipid species interact with inward rectifier potassium (Kir2) channels. Proc Natl Acad Sci USA. 2020;117:7803–13.
209. Corradi V, Bukiya AN, Miranda WE, Cui M, Plant LD, Logothetis DE, et al. A molecular switch controls the impact of cholesterol on a Kir channel. Proc Natl Acad Sci USA. 2022;119:e2109431119.
210. Dadsena S, Bockelmann S, Mina JGM, Hassan DG, Korneev S, Razzera G, et al. Ceramides bind VDAC2 to trigger mitochondrial apoptosis. Nat Commun. 2019;10:1832.
211. Prasanna X, Sengupta D, Chattopadhyay A. Cholesterol-dependent conformational plasticity in GPCR dimers. Sci Rep. 2016;6:31858.
212. Genheden S, Essex JW, Lee AG. G protein coupled receptor interactions with cholesterol deep in the membrane. Biochim Biophys Acta Biomembranes. 2017;1859:268–81.
213. Prasanna X, Mohole M, Chattopadhyay A, Sengupta D. Role of cholesterol-mediated effects in GPCR heterodimers. Chem Phys Lipids. 2020;227:104852.
214. Sengupta D, Prasanna X, Mohole M, Chattopadhyay A. Exploring GPCR–lipid interactions by molecular dynamics simulations: excitements, challenges, and the way forward. J Phys Chem B. 2018;122:5727–37.
215. Hedger G, Koldsø H, Chavent M, Siebold C, Rohatgi R, Sansom MSP. Cholesterol interaction sites on the transmembrane domain of the hedgehog signal transducer and class F G protein-coupled receptor smoothened. Structure. 2019;27:549–59.
216. Zeppelin T, Ladefoged LK, Sinning S, Periole X, Schiøtt B. A direct interaction of cholesterol with the dopamine transporter prevents its out-to-inward transition. PLoS Comput Biol. 2018;14:e1005907.
217. Bountra K, Hagelueken G, Choudhury HG, Corradi V, El Omari K, Wagner A, et al. Structural basis for antibacterial peptide self-immunity by the bacterial ABC transporter McjD. EMBO J. 2017;36:3062–79.
218. Jussupow A, Di Luca A, Kaila VRI. How cardiolipin modulates the dynamics of respiratory complex I. Sci Adv. 2019;5:eaav1850.
219. Mouritsen OG, Bloom M. Mattress model of lipid-protein interactions in membranes. Biophys J. 1984;46:141–53.
220. Tieleman DP, Forrest LR, Sansom MSP, Berendsen HJC. Lipid properties and the orientation of aromatic residues in OmpF, influenza M2, and Alamethicin systems: molecular dynamics simulations. Biochemistry. 1998;37:17554–61.
221. Sejdiu BI, Tieleman DP. Lipid-protein interactions are a unique property and defining feature of G protein-coupled receptors. Biophys J. 2020;118:1887–900.
222. Schmidt V, Sidore M, Bechara C, Duneau J-P, Sturgis JN. The lipid environment of Escherichia coli aquaporin Z. Biochim Biophys Acta Biomembranes. 2019;1861:431–40.
223. Thallmair S, Vainikka PA, Marrink SJ. Lipid fingerprints and cofactor dynamics of light-harvesting complex II in different membranes. Biophys J. 2019;116:1446–55.
224. Van Eerden FJ, Melo MN, Frederix PWJM, Marrink SJ. Prediction of thylakoid lipid binding sites on photosystem II. Biophys J. 2017;113:2669–81.
225. Buyan A, Cox CD, Barnoud J, Li J, Chan HSM, Martinac B, et al. Piezo1 forms specific, functionally important interactions with phosphoinositides and cholesterol. Biophys J. 2020;119:1683–97.
226. Wilson KA, Wang L, Lin YC, O'Mara ML. Investigating the lipid fingerprint of SLC6 neurotransmitter transporters: a comparison of dDAT, hDAT, hSERT, and GlyT2. BBA Adv. 2021;1:100010.
227. Davies KM, Anselmi C, Wittig I, Faraldo-Gomez JD, Kuhlbrandt W. Structure of the yeast F1Fo-ATP synthase dimer and its role in shaping the mitochondrial cristae. Proc Natl Acad Sci USA. 2012;109:13602–7.
228. Song W, Duncan AL, Sansom MSP. Modulation of adenosine A2a receptor oligomerization by receptor activation and PIP2 interactions. Structure. 2021;29:1312–25.
229. Heit S, Geurts MMG, Murphy BJ, Corey RA, Mills DJ, Kühlbrandt W, et al. Structure of the hexameric fungal plasma membrane proton pump in its autoinhibited state. Sci Adv. 2021;7:5255.
230. Banterle N, Nievergelt AP, de Buhr S, Hatzopoulos GN, Brillard C, Andany S, et al. Kinetic and structural roles for the surface in guiding SAS-6 self-assembly to direct centriole architecture. Nat Commun. 2021;12(1):6180.
231. Gupta K, Donlan JAC, Hopper JTS, Uzdavinys P, Landreh M, Struwe WB, et al. The role of interfacial lipids in stabilizing membrane protein oligomers. Nature. 2017;541:421–4.
232. Yamamoto E, Domański J, Naughton Fiona B, Best Robert B, Kalli Antreas C, Stansfeld Phillip J, et al. Multiple lipid binding sites determine the affinity of PH domains for phosphoinositide-containing membranes. Sci Adv. 2020;6:eaay5736.

17590884, 0, Downloaded from https://wires.onlinelibrary.wiley.com/doi/10.1002/wcms.1620 by Cochrane France, Wiley Online Library on [24/11/2022]. See the Terms and Conditions (https://onlinelibrary.wiley.com/terms-and-conditions) on Wiley Online Library for rules of use; OA articles are governed by the applicable Creative Commons License

233. Schroer CFE, Baldauf L, van Buren L, Wassenaar TA, Melo MN, Koenderink GH, et al. Charge-dependent interactions of monomeric and filamentous Actin with lipid bilayers. Proc Natl Acad Sci USA. 2020;117:5861–72.
234. Yen H-Y, Hoi KK, Liko I, Hedger G, Horrell MR, Song W, et al. PtdIns(4,5)P2 stabilizes active states of GPCRs and enhances selectivity of G-protein coupling. Nature. 2018;559:423–7.
235. Faustino I, Abdizadeh H, Souza PCT, Jeucken A, Stanek WK, Guskov A, et al. Membrane mediated toppling mechanism of the folate energy coupling factor transporter. Nat Commun. 2020;11:1763.
236. Song W, Yen H-Y, Robinson CV, Sansom MSP. State-dependent lipid interactions with the A2a receptor revealed by MD simulations using in Vivo-mimetic membranes. Structure. 2019;27:392–403.
237. Borcik CG, Eason IR, Yekefellah M, Amani R, Han R, Vanderloop BH, et al. A cholesterol dimer stabilizes the inactivated state of an inward-rectifier Potassium Channel. Angew Chem Int Ed. 2022;61:e202112232.
238. Bushell SR, Pike ACW, Falzone ME, Rorsman NJG, Ta CM, Corey RA, et al. The structural basis of lipid scrambling and inactivation in the endoplasmic reticulum scramblase TMEM16K. Nat Commun. 2019;10:3956.
239. Miranda WE, Guo JQ, Mesa-Galloso H, Corradi V, Lees-Miller JP, Tieleman DP, et al. Lipid regulation of hERG1 channel function. Nat Commun. 2021;12:1409.
240. Sun F, Schroer CFE, Palacios CR, Xu L, Luo S-Z, Marrink SJ. Molecular mechanism for bidirectional regulation of CD44 for lipid raft affiliation by palmitoylations and PIP2. PLoS Comput Biol. 2020;16:e1007777.
241. Javanainen M, Enkavi G, Guixà-Gonzaléz R, Kulig W, Martinez-Seara H, Levental I, et al. Reduced level of docosahexaenoic acid shifts GPCR neuroreceptors to less ordered membrane regions. PLoS Comput Biol. 2019;15:e1007033.
242. Rajagopal N, Irudayanathan FJ, Nangia S. Palmitoylation of Claudin-5 proteins influences their lipid domain affinity and tight junction assembly at the blood–brain barrier Interface. J Phys Chem B. 2019;123:983–93.
243. Tuerkova A, Kabelka I, Králová T, Sukeník L, Pokorná Š, Hof M, et al. Effect of helical kink in antimicrobial peptides on membrane pore formation. Elife. 2020;9:e47946.
244. Kabelka I, Vácha R. Advances in molecular understanding of α-helical membrane-active peptides. Acc Chem Res. 2021;54:2196–204.
245. Vögele M, Bhaskara RM, Mulvihill E, van Pee K, Yildiz Ö, Kühlbrandt W, et al. Membrane perforation by the pore-forming toxin pneumolysin. Proc Natl Acad Sci USA. 2019;116:13352–7.
246. Bennett WFD, Tieleman DP. Water defect and pore formation in atomistic and coarse-grained lipid membranes: pushing the limits of coarse graining. J Chem Theory Comput. 2011;7:2981–8.
247. Risselada HJ, Bubnis G, Grubmüller H. Expansion of the fusion stalk and its implication for biological membrane fusion. Proc Natl Acad Sci. 2014;111:11043–8.
248. Smirnova YG, Risselada HJ, Müller M. Thermodynamically reversible paths of the first fusion intermediate reveal an important role for membrane anchors of fusion proteins. Proc Natl Acad Sci USA. 2019;116:2571–6.
249. Risselada HJ, Grubmüller H. How proteins open fusion pores: insights from molecular simulations. Eur Biophys J. 2021;50:279–93.
250. Sharma S, Lindau M. Molecular mechanism of fusion pore formation driven by the neuronal SNARE complex. Proc Natl Acad Sci USA. 2018;115:12751–6.
251. Pabis A, Rawle RJ, Kasson PM. Influenza hemagglutinin drives viral entry via two sequential intramembrane mechanisms. Proc Natl Acad Sci USA. 2020;117:7200–7.
252. Risselada HJ, Marelli G, Fuhrmans M, Smirnova YG, Grubmüller H, Marrink SJ, et al. Line-tension controlled mechanism for influenza fusion. PLoS One. 2012;7:e38302.
253. Zoni V, Nieto V, Endter LJ, Risselada HJ, Monticelli L, Vanni S. To bud or not to bud: a perspective on molecular simulations of lipid droplet budding. Front Mol Biosci. 2019;6:124.
254. Khandelia H, Duelund L, Pakkanen KI, Ipsen JH. Triglyceride blisters in lipid bilayers: implications for lipid droplet biogenesis and the Mobile lipid signal in cancer cell membranes. PLoS One. 2010;5:e12811.
255. Chorlay A, Monticelli L, Veríssimo Ferreira J, Ben M'barek K, Ajjaji D, Wang S, et al. Membrane asymmetry imposes directionality on lipid droplet emergence from the ER. Dev Cell. 2019;50:25–42.
256. Caillon L, Nieto V, Gehan P, Omrane M, Rodriguez N, Monticelli L, et al. Triacylglycerols sequester monotopic membrane proteins to lipid droplets. Nat Commun. 2020;11:3944.
257. Prasanna X, Salo VT, Li S, Ven K, Vihinen H, Jokitalo E, et al. Seipin traps triacylglycerols to facilitate their nanoscale clustering in the endoplasmic reticulum membrane. PLoS Biol. 2021;19:e3000998.
258. Zoni V, Khaddaj R, Lukmantara I, Shinoda W, Yang H, Schneiter R, et al. Seipin accumulates and traps diacylglycerols and triglycerides in its ring-like structure. Proc Natl Acad Sci USA. 2021;118(10):e2017205118.
259. Stroh KS, Risselada HJ. Quantifying membrane curvature sensing of peripheral proteins by simulated buckling and umbrella sampling. J Chem Theory Comput. 2021;17:5276–86.
260. Baoukina S, Ingólfsson HI, Marrink SJ, Tieleman DP. Curvature-induced sorting of lipids in plasma membrane tethers. Adv Theory Simulat. 2018;1:1800034.
261. Krishna A, Sengupta D. Interplay between membrane curvature and cholesterol: role of Palmitoylated Caveolin-1. Biophys J. 2019;116:69–78.
262. Zhou W, Fiorin G, Anselmi C, Karimi-Varzaneh HA, Poblete H, Forrest LR, et al. Large-scale state-dependent membrane remodeling by a transporter protein. Elife. 2019;8:e50576.

17590884, 0, Downloaded from https://wires.onlinelibrary.wiley.com/doi/10.1002/wcms.1620 by Cochrane France, Wiley Online Library on [24/11/2022]. See the Terms and Conditions (https://onlinelibrary.wiley.com/terms-and-conditions) on Wiley Online Library for rules of use; OA articles are governed by the applicable Creative Commons License

263. Liaci AM, Steigenberger B, de Souza PCT, Tamara S, Gröllers-Mulderij M, Ogrissek P, et al. Structure of the human signal peptidase complex reveals the determinants for signal peptide cleavage. Mol Cell. 2021;81:3934–48.
264. Bhaskara RM, Grumati P, Garcia-Pardo J, Kalayil S, Covarrubias-Pinto A, Chen W, et al. Curvature induction and membrane remodeling by FAM134B reticulon homology domain assist selective ER-phagy. Nat Commun. 2019;10:2370.
265. Siggel M, Bhaskara RM, Hummer G. Phospholipid scramblases remodel the shape of asymmetric membranes. J Phys Chem Lett. 2019; 10:6351–4.
266. Pezeshkian W, Marrink SJ. Simulating realistic membrane shapes. Curr Opin Cell Biol. 2021;71:103–11.
267. Pluhackova K, Wilhelm FM, Müller DJ. Lipids and phosphorylation conjointly modulate complex formation of β2-adrenergic receptor and β-arrestin2. Front Cell Dev Biol. 2021;9:3610.
268. Sun F, Schroer CFE, Xu L, Yin H, Marrink SJ, Luo SZ. Molecular dynamics of the association of L-selectin and FERM regulated by PIP2. Biophys J. 2018;114(8):1858–68.
269. Souza PCT, Limongelli V, Wu S, Marrink SJ, Monticelli L. Perspectives on high-throughput ligand/protein docking with martini MD simulations. Front Mol Biosci. 2021;8:199.
270. Huang J, Rauscher S, Nawrocki G, Ran T, Feig M, De Groot BL, et al. CHARMM36m: an improved force field for folded and intrinsically disordered proteins. Nat Methods. 2017;14(1):71–3.
271. Bruininks BMH, Souza PCT, Ingolfsson H, Marrink SJ. A molecular view on the escape of lipoplexed dna from the endosome. Elife. 2020;9:e52012.
272. Bae S, Kim JS. Potential of mean force for DNA wrapping around a cationic nanoparticle. J Chem Theory Comput. 2021;17:7952–61.
273. Iric K, Subramanian M, Oertel J, Agarwal NP, Matthies M, Periole X, et al. DNA-encircled lipid bilayers. Nanoscale. 2018;10:18463–7.
274. Maingi V, Rothemund PWK. Properties of DNA-and protein-Scaffolded lipid Nanodiscs. ACS Nano. 2021;15:751–64.
275. Maingi V, Burns JR, Uusitalo JJ, Howorka S, Marrink SJ, Sansom MSP. Stability and dynamics of membrane-spanning DNA nanopores. Nat Commun. 2017;8:14784.
276. Diederichs T, Ahmad K, Burns JR, Nguyen QH, Siwy ZS, Tornow M, et al. Principles of small-molecule transport through synthetic Nanopores. ACS Nano. 2021;15:16194–206.
277. López CA, Bellesia G, Redondo A, Langan P, Chundawat SPS, Dale BE, et al. MARTINI coarse-grained model for crystalline cellulose microfibers. J Phys Chem B. 2015;119:465–73.
278. Chakraborty S, Wagh K, Gnanakaran S, López CA. Development of martini 2.2 parameters for N-glycans: a case study of the HIV-1 Env glycoprotein dynamics. Glycobiology. 2021;31:787–99.
279. Vaiwala R, Sharma P, Puranik M, Ayappa KG. Developing a coarse-grained model for bacterial cell walls: evaluating mechanical properties and free energy barriers. J Chem Theory Comput. 2020;16:5369–84.
280. Wallace JE, Sansom MSP. Blocking of carbon nanotube based nanoinjectors by lipids: a simulation study. Nano Lett. 2008;8:2751–6.
281. Wallace EJ, D'Rozario RSG, Sanchez BM, Sansom MSP. A multiscale simulation study of carbon nanotube interactions with designed amphiphilic peptide helices. Nanoscale. 2010;2:967–75.
282. Monticelli L. On atomistic and coarse-grained models for C60 fullerene. J Chem Theory Comput. 2012;8:1370–8.
283. Baoukina S, Monticelli L, Tieleman DP. Interaction of pristine and functionalized carbon nanotubes with lipid membranes. J Phys Chem B. 2013;117:12113–23.
284. Barnoud J, Rossi G, Monticelli L. Lipid membranes as solvents for carbon nanoparticles. Phys Rev Lett. 2014;112:68102.
285. Barnoud J, Urbini L, Monticelli L. C60 fullerene promotes lung monolayer collapse. J R Soc Interface. 2015;12:20140931.
286. Nisoh N, Karttunen M, Monticelli L, Wong-Ekkabut J. Lipid monolayer disruption caused by aggregated carbon nanoparticles. RSC Adv. 2015;5:11676–85.
287. Lavagna E, Barnoud J, Rossi G, Monticelli L. Size-dependent aggregation of hydrophobic nanoparticles in lipid membranes. Nanoscale. 2020;12:9452–61.
288. Vögele M, Kofinger J, Hummer G. Molecular dynamics simulations of carbon nanotube porins in lipid bilayers. Faraday Discuss. 2018; 209:341–58.
289. Bhaskara RM, Linker SM, Vögele M, Köfinger J, Hummer G. Carbon nanotubes mediate fusion of lipid vesicles. ACS Nano. 2017;11: 1273–80.
290. Titov AV, Král P, Pearson R. Sandwiched graphene−membrane superstructures. ACS Nano. 2010;4:229–34.
291. Santiago R, Reigada R. Interaction modes between nanosized graphene flakes and liposomes: adsorption, insertion and membrane fusion. Biochim Biophys Acta-Gen Subj. 2019;1863:723–31.
292. Willems N, Urtizberea A, Verre AF, Iliut M, Lelimousin M, Hirtz M, et al. Biomimetic phospholipid membrane organization on graphene and graphene oxide surfaces: a molecular dynamics simulation study. ACS Nano. 2017;11:1613–25.
293. Rossi G, Monticelli L. Gold nanoparticles in model biological membranes: a computational perspective. Biochim Biophys Acta-Biomembranes. 2016;1858:2380–9.
294. Wang J, Drelich AJ, Hopkins CM, Mecozzi S, Li L, Kwon G, et al. Gold nanoparticles in virus detection: recent advances and potential considerations for SARS-CoV-2 testing development. WIREs Nanomed Nanobiotechnol. 2022;14:e1754.
295. Lin J, Zhang H, Chen Z, Zheng Y. Penetration of lipid membranes by gold nanoparticles: insights into cellular uptake, cytotoxicity, and their relationship. ACS Nano. 2010;4:5421–9.
296. Lin J, Alexander-Katz A. Cell membranes open "doors" for cationic nanoparticles/biomolecules: insights into uptake kinetics. ACS Nano. 2013;7:10799–808.

17590884, 0, Downloaded from https://wires.onlinelibrary.wiley.com/doi/10.1002/wcms.1620 by Cochrane France, Wiley Online Library on [24/11/2022]. See the Terms and Conditions (https://onlinelibrary.wiley.com/terms-and-conditions) on Wiley Online Library for rules of use; OA articles are governed by the applicable Creative Commons License

297. Gkeka P, Sarkisov L, Angelikopoulos P. Homogeneous hydrophobic–hydrophilic surface patterns enhance permeation of nanoparticles through lipid membranes. J Phys Chem Lett. 2013;4:1907–12.
298. Gkeka P, Angelikopoulos P, Sarkisov L, Cournia Z. Membrane partitioning of anionic, ligand-coated nanoparticles is accompanied by ligand snorkeling, local disordering, and cholesterol depletion. PLoS Comput Biol. 2014;10:e1003917.
299. Jackson AM, Myerson JW, Stellacci F. Spontaneous assembly of subnanometre-ordered domains in the ligand shell of monolayer-protected nanoparticles. Nat Mater. 2004;3:330–6.
300. Verma A, Uzun O, Hu Y, Hu Y, Han H-S, Watson N, et al. Surface-structure-regulated cell-membrane penetration by monolayer-protected nanoparticles. Nat Mater. 2008;7:588–95.
301. Angelikopoulos P, Sarkisov L, Cournia Z, Gkeka P. Self-assembly of anionic, ligand-coated nanoparticles in lipid membranes. Nanoscale. 2017;9:1040–8.
302. Noh SY, Nash A, Notman R. The aggregation of striped nanoparticles in mixed phospholipid bilayers. Nanoscale. 2020;12:4868–81.
303. Canepa E, Salassi S, de Marco AL, Lambruschini C, Odino D, Bochicchio D, et al. Amphiphilic gold nanoparticles perturb phase separation in multidomain lipid membranes. Nanoscale. 2020;12:19746–59.
304. Canepa E, Bochicchio D, Gasbarri M, Odino D, Canale C, Ferrando R, et al. Cholesterol hinders the passive uptake of amphiphilic nanoparticles into fluid lipid membranes. J Phys Chem Lett. 2021;12:8583–90.
305. Lavagna E, Güven ZP, Bochicchio D, Olgiati F, Stellacci F, Rossi G. Amphiphilic nanoparticles generate curvature in lipid membranes and shape liposome–liposome interfaces. Nanoscale. 2021;13:16879–84.
306. Sheavly JK, Pedersen JA, Van Lehn RC. Curvature-driven adsorption of cationic nanoparticles to phase boundaries in multicomponent lipid bilayers. Nanoscale. 2019;11:2767–78.
307. Chen X, Tieleman DP, Liang Q. Modulating interactions between ligand-coated nanoparticles and phase-separated lipid bilayers by varying the ligand density and the surface charge. Nanoscale. 2018;10:2481–91.
308. Lin J, Miao L, Zhong G, Lin C-H, Dargazangy R, Alexander-Katz A. Understanding the synergistic effect of physicochemical properties of nanoparticles and their cellular entry pathways. Commun Biol. 2020;3:205.
309. Chiarpotti MV, Longo GS, Del PMG. Voltage-induced adsorption of cationic nanoparticles on lipid membranes. J Phys Chem B. 2022; 126:2230–40.
310. Simonelli F, Rossi G, Monticelli L. Role of ligand conformation on nanoparticle–protein interactions. J Phys Chem B. 2019;123:1764–9.
311. Salassi S, Caselli L, Cardellini J, Lavagna E, Montis C, Berti D, et al. A martini coarse grained model of citrate-capped gold nanoparticles interacting with lipid bilayers. J Chem Theory Comput. 2021;17:6597–609.
312. Franco-Ulloa S, Tatulli G, Bore SL, Moglianetti M, Pompa PP, Cascella M, et al. Dispersion state phase diagram of citrate-coated metallic nanoparticles in saline solutions. Nat Commun. 2020;11:5422.
313. Franco-Ulloa S, Guarnieri D, Riccardi L, Pompa PP, De Vivo M. Association mechanism of peptide-coated metal nanoparticles with model membranes: a coarse-grained study. J Chem Theory Comput. 2021;17:4512–23.
314. Rossi G, Monticelli L. Modeling the effect of nano-sized polymer particles on the properties of lipid membranes. J Phys Condens Matter. 2014;26:503101.
315. Rossi G, Monticelli L. Simulating the interaction of lipid membranes with polymer and ligand-coated nanoparticles. Adv Phys-X. 2016; 1:276–96.
316. da Costa JP, Santos PSM, Duarte AC, Rocha-Santos T. (Nano)plastics in the environment—sources, fates and effects. Sci Total Environ. 2016;566–567:15–26.
317. Besseling E, Wang B, Lürling M, Koelmans AA. Nanoplastic affects growth of S. obliquus and reproduction of D. magna. Environ Sci Technol. 2014;48:12336–43.
318. Lee H, Larson RG. Molecular dynamics simulations of PAMAM dendrimer-induced pore formation in DPPC bilayers with a coarse-grained model. J Phys Chem B. 2006;110:18204–11.
319. Lee H, Larson RG. Coarse-grained molecular dynamics studies of the concentration and size dependence of fifth- and seventh-generation PAMAM dendrimers on pore formation in DMPC bilayer. J Phys Chem B. 2008;112:7778–84.
320. Hezaveh S, Samanta S, De Nicola A, Milano G, Roccatano D. Understanding the interaction of block copolymers with DMPC lipid bilayer using coarse-grained molecular dynamics simulations. J Phys Chem B. 2012;116:14333–45.
321. Nawaz S, Carbone P. Coarse-graining poly(ethylene oxide)–poly(propylene oxide)–poly(ethylene oxide) (PEO–PPO–PEO) block copolymers using the MARTINI force field. J Phys Chem B. 2014;118:1648–59.
322. Adhikari U, Goliaei A, Tsereteli L, Berkowitz ML. Properties of Poloxamer molecules and Poloxamer micelles dissolved in water and next to lipid bilayers: results from computer simulations. J Phys Chem B. 2016;120:5823–30.
323. Wang D, Lin J, Jia F, Tan X, Wang Y, Sun X, et al. Bottlebrush-architectured poly(ethylene glycol) as an efficient vector for RNA interference in vivo. Sci Adv. 2019;5:eaav9322.
324. Stojceski F, Grasso G, Pallante L, Danani A. Molecular and coarse-grained modeling to characterize and optimize dendrimer-based Nanocarriers for short interfering RNA delivery. ACS Omega. 2020;5:2978–86.
325. Xue M, Cheng L, Faustino I, Guo W, Marrink SJ. Molecular mechanism of lipid Nanodisk formation by styrene-maleic acid copolymers. Biophys J. 2018;115:494–502.
326. Orekhov PS, Bozdaganyan ME, Voskoboynikova N, Mulkidjanian AY, Steinhoff H-J, Shaitan KV. Styrene/maleic acid copolymers form SMALPs by pulling lipid patches out of the lipid bilayer. Langmuir. 2019;35:3748–58.
327. Rossi G, Barnoud J, Monticelli L. Polystyrene nanoparticles perturb lipid membranes. J Phys Chem Lett. 2014;5:241–6.

17590884, 0, Downloaded from https://wires.onlinelibrary.wiley.com/doi/10.1002/wcms.1620 by Cochrane France, Wiley Online Library on [24/11/2022]. See the Terms and Conditions (https://onlinelibrary.wiley.com/terms-and-conditions) on Wiley Online Library for rules of use; OA articles are governed by the applicable Creative Commons License

328. Bochicchio D, Panizon E, Monticelli L, Rossi G. Interaction of hydrophobic polymers with model lipid bilayers. Sci Rep. 2017;7:6357.
329. Bochicchio D, Cantu L, Cadario MV, Palchetti L, Natali F, Monticelli L, et al. Polystyrene perturbs the structure, dynamics, and mechanical properties of DPPC membranes: an experimental and computational study. J Colloid Interface Sci. 2022;605:110–9.
330. Liu B, Åberg C, van Eerden FJ, Marrink SJ, Poolman B, Boersma AJ. Design and properties of genetically encoded probes for sensing macromolecular crowding. Biophys J. 2017;112:1929–39.
331. Pannuzzo M, De Jong DH, Raudino A, Marrink SJ. Simulation of polyethylene glycol and calcium-mediated membrane fusion. J Chem Phys. 2014;140:124905.
332. Hammons JA, Ingólfsson HI, Lee JRI, Carpenter TS, Sanborn J, Tunuguntla R, et al. Decoupling copolymer, lipid and carbon nanotube interactions in hybrid, biomimetic vesicles. Nanoscale. 2020;12:6545–55.
333. Álvarez Z, Kolberg-Edelbrock AN, Sasselli IR, Ortega JA, Qiu R, Syrgiannis Z, et al. Bioactive scaffolds with enhanced supramolecular motion promote recovery from spinal cord injury. Science (80-). 2021;374:848–56.
334. Gao P, Nicolas J, Ha-Duong T. Supramolecular Organization of Polymer Prodrug Nanoparticles Revealed by coarse-grained simulations. J Am Chem Soc. 2021;143:17412–23.
335. Simonelli F, Bochicchio D, Ferrando R, Rossi G. Monolayer-protected anionic au nanoparticles walk into lipid membranes step by step. J Phys Chem Lett. 2015;6:3175–9.
336. de Pablo JJ, Jackson NE, Webb MA, Chen LQ, Moore JE, Morgan D, et al. New frontiers for the materials genome initiative. NPJ Comput Mater. 2019;5:1–23.
337. Rossi G, Monticelli L, Puisto SR, Vattulainen I, Ala-Nissila T. Coarse-graining polymers with the MARTINI force-field: polystyrene as a benchmark case. Soft Matter. 2011;7:698–708.
338. Frederix PWJM, Scott GG, Abul-Haija YM, Kalafatovic D, Pappas CG, Javid N, et al. Exploring the sequence space for (tri-)peptide self-assembly to design and discover new hydrogels. Nat Chem. 2014;7:30–7.
339. Alessandri R, Uusitalo JJ, De Vries AH, Havenith RWA, Marrink SJ. Bulk heterojunction morphologies with atomistic resolution from coarse-grain solvent evaporation simulations. J Am Chem Soc. 2017;139:3697–705.
340. Modarresi M, Franco-Gonzalez JF, Zozoulenko I. Computational microscopy study of the granular structure and pH dependence of PEDOT:PSS. Phys Chem Chem Phys. 2019;21:6699–711.
341. Dahal U, Dormidontova EE. Chain conformation and hydration of polyethylene oxide grafted to gold nanoparticles: curvature and chain length effect. Macromolecules. 2020;53:8160–70.
342. Alessandri R, Sami S, Barnoud J, de Vries AH, Marrink SJ, Havenith A, et al. Resolving donor–acceptor interfaces and charge carrier energy levels of organic semiconductors with polar side chains. Adv Funct Mater. 2020;30:2004799.
343. Wu D, Yang X. Coarse-grained molecular simulation of self-assembly for nonionic surfactants on graphene nanostructures. J Phys Chem B. 2012;116:12048–56.
344. Gobbo C, Beurroies I, De Ridder D, Eelkema R, Marrink SJ, De Feyter S, et al. MARTINI model for Physisorption of organic molecules on graphite. J Phys Chem C. 2013;117:15623–31.
345. Piskorz TK, Gobbo C, Marrink SJ, De Feyter S, De Vries AH, Van Esch JH. Nucleation mechanisms of self-assembled Physisorbed monolayers on graphite. J Phys Chem C. 2019;123:17510–20.
346. Yang Y, Fu N, Dong Q, Li M, Li J, Li C, et al. Self-aggregation to construct hydroxide highways in anion exchange membranes. Adv Mater Interfaces. 2020;7:1902143.
347. Mabuchi T, Huang SF, Tokumasu T. Nafion ionomer dispersion in mixtures of 1-propanol and water based on the martini coarse-grained model. J Polym Sci A. 2020;58:487–99.
348. Aida T, Meijer EW, Stupp SI. Functional supramolecular polymers. Science (80-). 2012;335:813–7.
349. Sarkar A, Sasmal R, Empereur-Mot C, Bochicchio D, Kompella SVK, Sharma K, et al. Self-sorted, random, and block supramolecular copolymers via sequence controlled, multicomponent self-assembly. J Am Chem Soc. 2020;142:7606–17.
350. Frederix PWJM, Ulijn RV, Hunt NT, Tuttle T. Virtual screening for dipeptide aggregation: toward predictive tools for peptide self-assembly. J Phys Chem Lett. 2011;2:2380–4.
351. Guo C, Luo Y, Zhou R, Wei G. Probing the self-assembly mechanism of diphenylalanine-based peptide nanovesicles and nanotubes. ACS Nano. 2012;6:3907–18.
352. Lee OS, Cho V, Schatz GC. Modeling the self-assembly of peptide amphiphiles into fibers using coarse-grained molecular dynamics. Nano Lett. 2012;12:4907–13.
353. Frederix PWJM, Patmanidis I, Marrink SJ. Molecular simulations of self-assembling bio-inspired supramolecular systems and their connection to experiments. Chem Soc Rev. 2018;47:3470–89.
354. Jung SH, Bochicchio D, Pavan GM, Takeuchi M, Sugiyasu K. A block supramolecular polymer and its kinetically enhanced stability. J Am Chem Soc. 2018;140:10570–7.
355. Moreno-Alcántar G, Aliprandi A, Rouquette R, Pesce L, Wurst K, Perego C, et al. Solvent-driven supramolecular wrapping of self-assembled structures. Angew Chem Int Ed. 2021;60:5407–13.
356. Crespo EA, Schaeffer N, Coutinho JAP, Perez-Sanchez G. Improved coarse-grain model to unravel the phase behavior of 1-alkyl-3-methylimidazolium-based ionic liquids through molecular dynamics simulations. J Colloid Interface Sci. 2020;574:324–36.
357. Huet G, Araya-Farias M, Alayoubi R, Laclef S, Bouvier B, Gosselin I, et al. New biobased-zwitterionic ionic liquids: efficiency and biocompatibility for the development of sustainable biorefinery processes. Green Chem. 2020;22:2935–46.

17590884, 0, Downloaded from https://wires.onlinelibrary.wiley.com/doi/10.1002/wcms.1620 by Cochrane France, Wiley Online Library on [24/11/2022]. See the Terms and Conditions (https://onlinelibrary.wiley.com/terms-and-conditions) on Wiley Online Library for rules of use; OA articles are governed by the applicable Creative Commons License

358. Lee H, Larson RG. Effects of PEGylation on the size and internal structure of dendrimers: self-penetration of long PEG chains into the dendrimer Core. Macromolecules. 2011;44:2291–8.
359. Jeong H, Hwang J, Lee H, Hammond PT, Choi J, Hong J. In vitro blood cell viability profiling of polymers used in molecular assembly. Sci Rep. 2017;7:1–13.
360. Brosz M, Michelarakis N, Bunz UHF, Aponte-Santamaría C, Gräter F. Martini 3 coarse-grained force field for poly(Para-phenylene ethynylene)s. Phys Chem Chem Phys. 2022;24:9998–10010.
361. Wu F, Song Y, Zhao Z, Zhang S, Yang Z, Li Z, et al. Preparation and self-assembly of supramolecular coil-rod-coil triblock copolymer PPO-dsDNA-PPO. Macromolecules. 2015;48:7550–6.
362. Grillo DA, Albano JMR, Mocskos EE, Facelli JC, Pickholz M, Ferraro MB. Mechanical properties of drug loaded diblock copolymer bilayers: a molecular dynamics study. J Chem Phys. 2018;148:214901.
363. Pérez-Sánchez G, Vicente FA, Schaeffer N, Cardoso IS, Ventura SPM, Jorge M, et al. Rationalizing the phase behavior of triblock copolymers through experiments and molecular simulations. J Phys Chem C. 2019;123:21224–36.
364. Vögele M, Holm C, Smiatek J. Coarse-grained simulations of polyelectrolyte complexes: MARTINI models for poly(styrene sulfonate) and poly(diallyldimethylammonium). J Chem Phys. 2015;143:243151.
365. Li C, Iscen A, Sai H, Sato K, Sather NA, Chin SM, et al. Supramolecular–covalent hybrid polymers for light-activated mechanical actuation. Nat Mater. 2020;19:900–9.
366. Friederich P, Fediai A, Kaiser S, Konrad M, Jung N, Wenzel W, et al. Toward Design of Novel Materials for organic electronics. Adv Mater. 2019;31:1808256.
367. Jackson NE. Coarse-graining organic semiconductors: the path to multiscale design. J Phys Chem B. 2021;125:485–96.
368. Mehandzhiyski AY, Zozoulenko I. Computational microscopy of PEDOT:PSS/cellulose composite paper. ACS Appl Energy Mater. 2019;2:3568–77.
369. Modarresi M, Mehandzhiyski A, Fahlman M, Tybrandt K, Zozoulenko I. Microscopic understanding of the granular structure and the swelling of PEDOT:PSS. Macromolecules. 2020;53:6267–78.
370. Lee J, Go EM, Dharmapurikar S, Xu J, Lee SM, Jeong M, et al. Insights into constitutional isomeric effects on donor–acceptor intermolecular arrangements in non-fullerene organic solar cells. J Mater Chem A. 2019;7:18468–79.
371. Delavari N, Gladisch J, Petsagkourakis I, Liu X, Modarresi M, Fahlman M, et al. Water intake and ion exchange in PEDOT:Tos films upon cyclic voltammetry: experimental and molecular dynamics investigation. Macromolecules. 2021;54:6552–62.
372. Rolland N, Modarresi M, Franco-Gonzalez JF, Zozoulenko I. Large scale mobility calculations in PEDOT (poly(3,4-ethylenedioxythiophene)): Backmapping the coarse-grained MARTINI morphology. Comput Mater Sci. 2020;179:109678.
373. Bereau T. Computational compound screening of biomolecules and soft materials by molecular simulations. Model Simul Mater Sci Eng. 2021;29:023001.
374. Newport TD, Sansom MSP, Stansfeld PJ. The MemProtMD database: a resource for membrane-embedded protein structures and their lipid interactions. Nucleic Acids Res. 2019;47:D390–7.
375. Menichetti R, Kanekal KH, Bereau T. Drug-membrane permeability across chemical space. ACS Cent Sci. 2019;5:290–8.
376. Bhatia H, Carpenter TS, Ingólfsson HI, Dharuman G, Karande P, Liu S, et al. Machine-learning-based dynamic-importance sampling for adaptive multiscale simulations. Nat Mach Intell. 2021;3:401–9.
377. Poojari CS, Scherer KC, Hub JS. Free energies of membrane stalk formation from a lipidomics perspective. Nat Commun. 2021;12:6594.
378. Stansfeld PJ, Goose JE, Caffrey M, Carpenter EP, Parker JL, Newstead S, et al. MemProtMD: automated insertion of membrane protein structures into explicit lipid membranes. Structure. 2015;23:1350–61.
379. Corey RA, Song W, Duncan AL, Ansell TB, Sansom MSP, Stansfeld PJ. Identification and assessment of cardiolipin interactions with E. coli inner membrane proteins. Sci Adv. 2021;7:eabh2217.
380. Suárez F, Calvelo M, Tolufashe GF, Muñoz A, Veleiro U, Porto C, et al. SuPepMem: a database of innate immune system peptides and their cell membrane interactions. Comput Struct Biotechnol J. 2022;20:874–881.
381. Ansell TB, Curran L, Horrell MR, Pipatpolkai T, Letham SC, Song W, et al. Relative affinities of protein-cholesterol interactions from equilibrium molecular dynamics simulations. J Chem Theory Comput. 2021;17:6548–58.
382. Bhatia H, Di NF, Moon JY, Zhang X, Chavez JR, Aydin F, et al. Generalizable coordination of large multiscale workflows: challenges and learnings at scale. SC '21: proceedings of the international conference for high performance computing, networking, storage and analysis. Washington, DC: IEEE Computer Society; 2021. p. 1–16.
383. Melo MN, Arnarez C, Sikkema H, Kumar N, Walko M, Berendsen HJC, et al. High-throughput simulations reveal membrane-mediated effects of alcohols on MscL gating. J Am Chem Soc. 2017;139:2664–71.
384. Dutta A, Vreeken J, Ghiringhelli LM, Bereau T. Data-driven equation for drug–membrane permeability across drugs and membranes. J Chem Phys. 2021;154:244114.
385. Frallicciardi J, Melcr J, Siginou P, Marrink SJ, Poolman B. Membrane thickness, lipid phase and sterol type are determining factors in the permeability of membranes to small solutes. Nature Commun. 2022;13:1605.
386. Cardellini A, Jiménez-Ángeles F, Asinari P. Olvera De La Cruz M. a modeling-based design to engineering protein hydrogels with random copolymers. ACS Nano. 2021;15:16139–48.
387. Scott GG, Börner T, Leser ME, Wooster TJ, Tuttle T. Directed discovery of Tetrapeptide emulsifiers. Front Chem. 2022;10:73.
388. Zuckerman DM. Equilibrium sampling in biomolecular simulations. Annu Rev Biophys. 2011;40:41–62.

17590884, 0, Downloaded from https://wires.onlinelibrary.wiley.com/doi/10.1002/wcms.1620 by Cochrane France, Wiley Online Library on [24/11/2022]. See the Terms and Conditions (https://onlinelibrary.wiley.com/terms-and-conditions) on Wiley Online Library for rules of use; OA articles are governed by the applicable Creative Commons License

389. Fathizadeh A, Elber R. A mixed alchemical and equilibrium dynamics to simulate heterogeneous dense fluids: illustrations for Lennard-Jones mixtures and phospholipid membranes. J Chem Phys. 2018;149:072325.
390. Yetukuri L, Huopaniemi I, Koivuniemi A, Maranghi M, Hiukka A, Nygren H, et al. High density lipoprotein structural changes and drug response in Lipidomic profiles following the long-term Fenofibrate therapy in the FIELD substudy. PLoS One. 2011;6:e23589.
391. Yetukuri L, Söderlund S, Koivuniemi A, Seppänen-Laakso T, Niemelä PS, Hyvönen M, et al. Composition and lipid spatial distribution of HDL particles in subjects with low and high HDL-cholesterol. J Lipid Res. 2010;51:2341–51.
392. Moiset G, López CA, Bartelds R, Syga L, Rijpkema E, Cukkemane A, et al. Disaccharides impact the lateral organization of lipid membranes. J Am Chem Soc. 2014;136:16167–75.
393. Baoukina S, Tieleman DP. Direct simulation of protein-mediated vesicle fusion: lung surfactant protein B. Biophys J. 2010;99:2134–42.
394. Kulovesi P, Telenius J, Koivuniemi A, Brezesinski G, Rantamäki A, Viitala T, et al. Molecular organization of the tear fluid lipid layer. Biophys J. 2010;99:2559–67.
395. Koldso H, Shorthouse D, Helie J, Sansom MSP. Lipid clustering correlates with membrane curvature as revealed by molecular simulations of complex lipid bilayers. PLoS Comput Biol. 2014;10:e1003911.
396. Rems L, Tang X, Zhao F, Pérez-Conesa S, Testa I, Delemotte L. Identification of electroporation sites in the complex lipid organization of the plasma membrane. Elife. 2022;11:e74773.
397. Lin X, Gorfe AA, Levental I. Protein partitioning into ordered membrane domains: insights from simulations. Biophys J. 2018;114:1936–44.
398. Su J, Marrink SJ, Melo MN. Localization preference of antimicrobial peptides on liquid-disordered membrane domains. Front Cell Dev Biol. 2020;8:350.
399. Van Eerden FJ, Melo MN, Frederix PWJM, Periole X, Marrink SJ. Exchange pathways of plastoquinone and plastoquinol in the photosystem II complex. Nat Commun. 2017;8:15214.
400. Van Eerden FJ, Van Den Berg T, Frederix PWJM, De Jong DH, Periole X, Marrink SJ. Molecular dynamics of photosystem II embedded in the thylakoid membrane. J Phys Chem B. 2017;121:3237–49.
401. Deeng J, Chan KY, van der Sluis EO, Berninghausen O, Han W, Gumbart J, et al. Dynamic behavior of trigger factor on the ribosome. J Mol Biol. 2016;428:3588–602.
402. Baoukina S, Monticelli L, Amrein M, Tieleman DP. The molecular mechanism of monolayer-bilayer transformations of lung surfactant from molecular dynamics simulations. Biophys J. 2007;93:3775–82.
403. Lin F, Wang R. Hemolytic mechanism of dioscin proposed by molecular dynamics simulations. J Mol Model. 2009;16:107–18.
404. Singharoy A, Maffeo C, Delgado-Magnero KH, Swainsbury DJK, Sener M, Kleinekathöfer U, et al. Atoms to phenotypes: molecular design principles of cellular energy metabolism. Cell. 2019;179:1098–111.
405. Durrant JD, Kochanek SE, Casalino L, Ieong PU, Dommer AC, Amaro RE. Mesoscale all-atom influenza virus simulations suggest new substrate binding mechanism. ACS Cent Sci. 2020;6:189–96.
406. Casalino L, Dommer AC, Gaieb Z, Barros EP, Sztain T, Ahn SH, et al. AI-driven multiscale simulations illuminate mechanisms of SARS-CoV-2 spike dynamics. Int J High Perform Comput Appl. 2021;35:432–51.
407. Bonvin AMJJ. 50 years of PDB: a catalyst in structural biology. Nat Methods. 2021;18:448–9.
408. Luthey-Schulten Z. Integrating experiments, theory and simulations into whole-cell models. Nat Methods. 2021;18:446–7.
409. Arnarez C, Marrink SJ, Periole X. Molecular mechanism of cardiolipin-mediated assembly of respiratory chain supercomplexes. Chem Sci. 2016;7:4435–43.
410. Chavent M, Duncan AL, Rassam P, Birkholz O, Hélie J, Reddy T, et al. How nanoscale protein interactions determine the mesoscale dynamic organisation of bacterial outer membrane proteins. Nat Commun. 2018;9:2846.
411. Reddy T, Shorthouse D, Parton DL, Jefferys E, Fowler PW, Chavent M, et al. Nothing to sneeze at: a dynamic and integrative computational model of an influenza a Virion. Structure. 2015;23:584–97.
412. Reddy T, Sansom MSP. The role of the membrane in the structure and biophysical robustness of the dengue Virion envelope. Structure. 2016;24:375–82.
413. Huber RG, Marzinek JK, Boon PLS, Yue W, Bond PJ. Computational modelling of flavivirus dynamics: the ins and outs. Methods. 2021;185:28–38.
414. Marzinek JK, Holdbrook DA, Huber RG, Verma C, Bond PJ. Pushing the envelope: dengue viral membrane coaxed into shape by molecular simulations. Structure. 2016;24:1410–20.
415. Jefferys EE, Sansom MSP. Computational virology: molecular simulations of virus dynamics and interactions. Adv Exp Med Biol. 2019;1140:201–33.
416. Marzinek JK, Huber RG, Bond PJ. Multiscale modelling and simulation of viruses. Curr Opin Struct Biol. 2020;61:146–52.
417. Wang B, Zhong C, Tieleman DP. Supramolecular organization of SARS-CoV and SARS-CoV-2 Virions revealed by coarse-grained models of intact virus envelopes. J Chem Inf Model. 2022;62:176–86.
418. Pezeshkian W, Grünewald F, Narykov O, Lu S, Wassenaar TA, Marrink SJ, et al. Molecular architecture of SARS-CoV-2 envelope by integrative modeling. bioRxiv. 2021. doi:10.1101/2021.09.15.459697
419. Wang D, Li J, Wang L, Cao Y, Li S, Song C. Toward an atomistic model of SARS-CoV-2. bioRxiv. 2022. doi:10.1101/2022.01.31.478415
420. Bryer AJ, Reddy T, Lyman E, Perilla JR. Full scale structural, mechanical and dynamical properties of HIV-1 liposomes. PLoS Comput Biol. 2022;18:e1009781.

17590884, 0, Downloaded from https://wires.onlinelibrary.wiley.com/doi/10.1002/wcms.1620 by Cochrane France, Wiley Online Library on [24/11/2022]. See the Terms and Conditions (https://onlinelibrary.wiley.com/terms-and-conditions) on Wiley Online Library for rules of use; OA articles are governed by the applicable Creative Commons License

421. Sawa-Makarska J, Baumann V, Coudevylle N, von Bülow S, Nogellova V, Abert C, et al. Reconstitution of autophagosome nucleation defines Atg9 vesicles as seeds for membrane formation. Science (80-). 2020;369:eaaz7714.
422. Jefferies D, Khalid S. To infect or not to infect: molecular determinants of bacterial outer membrane vesicle internalization by host membranes. J Mol Biol. 2020;432:1251–64.
423. Vermaas JV, Mayne CG, Shinn E, Tajkhorshid E. Assembly and analysis of cell-scale membrane envelopes. J Chem Inf Model. 2021;62:602–17.
424. Nemchinova M, Melcr J, Wassenaar TA, Marrink SJ, Guskov A. Asymmetric CorA gating mechanism as observed by molecular dynamics simulations. J Chem Inf Model. 2021;61:2407–17.
425. Barz B, Loschwitz J, Strodel B. Large-scale, dynamin-like motions of the human guanylate binding protein 1 revealed by multi-resolution simulations. PLoS Comput Biol. 2019;15:e1007193.
426. Aho N, Buslaev P, Jansen A, Bauer P, Groenhof G, Hess B. Scalable constant pH molecular dynamics in GROMACS. ChemRxiv. 2022. doi:10.26434/chemrxiv-2022-n025t
427. Carvalho AP, Santos SM, Pérez-Sánchez G, Gouveia JD, Gomes JRB, Jorge M. Sticky-MARTINI as a reactive coarse-grained model for molecular dynamics simulations of silica polymerization. NPJ Comput Mater. 2022;8:49.
428. Müller EA, Jackson G. Force-field parameters from the SAFT-γ equation of state for use in coarse-grained molecular simulations. Annu Rev Chem Biomol Eng. 2014;5:405–27.
429. Kremer K, Grest GS. Dynamics of entangled linear polymer melts: a molecular-dynamics simulation. J Chem Phys. 1990;92:5057–86.
430. Shen KH, Fan M, Hall LM. Molecular dynamics simulations of ion-containing polymers using generic coarse-grained models. Macromolecules. 2021;54:2031–52.
431. Dhamankar S, Webb MA. Chemically specific coarse-graining of polymers: methods and prospects. J Polym Sci A. 2021;59:2613–43.
432. Solano Canchaya JG, Dequidt A, Garruchet S, Latour B, Martzel N, Devémy J, et al. Development of a coarse-grain model for the description of the metal oxide-polymer interface from a bottom-up approach. J Chem Phys. 2019;151:064703.
433. Behbahani AF, Schneider L, Rissanou A, Chazirakis A, Bačová P, Jana PK, et al. Dynamics and rheology of polymer melts via hierarchical atomistic, coarse-grained, and slip-spring simulations. Macromolecules. 2021;54:2740–62.
434. Husic BE, Charron NE, Lemm D, Wang J, Pérez A, Majewski M, et al. Coarse graining molecular dynamics with graph neural networks. J Chem Phys. 2020;153:194101.
435. Nguyen D, Tao L, Li Y. Integration of machine learning and coarse-grained molecular simulations for polymer materials: physical understandings and molecular design. Front Chem. 2022;9:1280.

How to cite this article: Marrink SJ, Monticelli L, Melo MN, Alessandri R, Tieleman DP, Souza PCT. Two decades of Martini: Better beads, broader scope. WIREs Comput Mol Sci. 2022. e1620. https://doi.org/10.1002/wcms.1620

17590884, 0, Downloaded from https://wires.onlinelibrary.wiley.com/doi/10.1002/wcms.1620 by Cochrane France, Wiley Online Library on [24/11/2022]. See the Terms and Conditions (https://onlinelibrary.wiley.com/terms-and-conditions) on Wiley Online Library for rules of use; OA articles are governed by the applicable Creative Commons License